THE PENNSYLVANIA STATE UNIVERSITY

THE GRADUATE SCHOOL

DEPARTMENT OF AEROSPACE ENGINEERING

THERMODYNAMIC EFFECTS ON DEVELOPED CAVITATION IN WATER AND FREON 113

Master of Science Thesis

by

Michael L. Billet

Thesis Advisor
J. William Holl
Professor of Aerospace Engineering

March 1970

Research Sponsored

by

The National Aeronautics and Space Administration

Grant NGL 39-009-001

NASA Lewis Research Center
Cleveland, Ohio
Liquid, Rocket Technology

Werner R. Britsch

PLEASE SIGN DOCUMENT RELEASE FORM AND INDICATE ACTION TO BE TAKEN

Return to
John Cruickshank
254 ERB MS 5-5

RECEIVED
NASA STI FACILITY
INPUT BRANCH
MAY 1970

N70-27540
(ACCESSION NUMBER) (THRU)
156 1
(PAGES) (CODE)
CR-109840 33
(NASA CR OR TMX OR AD NUMBER) (CATEGORY)
FACILITY FORM 602

Reproduced by
NATIONAL TECHNICAL
INFORMATION SERVICE

PRECEDING PAGE BLANK NOT FILMED.

TABLE OF CONTENTS

TABLE OF CONTENTS (Cont.)

LIST OF TABLES

LIST OF FIGURES

LIST OF FIGURES (Cont.)

LIST OF FIGURES (Cont.)

LIST OF FIGURES (Cont.)

LIST OF FIGURES (Cont.)

NOMENCLATURE

a	center of ellipse
A	area
B	B-factor $= \dfrac{\text{vapor volume}}{\text{liquid volume}}$
C	specific heat
D	cavity diameter
F	force
Fr	Froude number (Eq. 62)
K	thermal conductivity
$\bar{h}$	heat transfer coefficient
L	length of cavity
m	semi-major axis of ellipse
M	mass
n	semi-minor axis of ellipse
Nn	Nusselt number (Eq. 62)
P	pressure
Pr	Prandtl number (Eq. 62)
$\dot{q}$	heat transfer rate
Q	net amount of heat transferred
Q_f	volume flow rate
Re	Reynolds number (Eq. 62)

NOMENCLATURE (Cont.)

S	entropy
t	time
T	temperature
V	velocity
V	volume
λ	latent heat of evaporation
μ	dynamic viscosity
ν	kinematic viscosity
ρ	density
σ	cavitation number
α	thermal diffusivity
δ	liquid thickness

Subscripts

B	blocked
C	corrected, cavity
exit	exit conditions
L	liquid
U	unblocked
V	vapor
W	wall
X	unknown

NOMENCLATURE (Cont.)

1	initial
2	final
5,7,0	location of pressure taps in test section
∞	infinity
$\perp$	perpendicular

CHAPTER I

INTRODUCTION

1.1 Origin and Importance of Investigation

The subject of a fully developed cavity and the various similarity laws which predict the various parameters that affect the cavity have been under study by many researchers (1, 2, 3). Their research has largely been divided into two types of cavity flows: 1) ventilated cavities, and 2) vaporous cavities. However, these cavities have one similar characteristic in that the cavity shape is a single-valued function of the cavitation number based on the cavity pressure.

The rear of these cavities is a complex and often highly turbulent region of flow where the contents of the cavity are carried or entrained away. However, in the case of vaporous cavitation where the cavity contains mostly vapor, the loss of vapor is immediately made up by the evaporation from the walls of the cavity. On the other hand, a continual supply of gas is needed to form a ventilated cavity.

In recent years, developed vaporous cavitation has become increasingly more important due to the need to design pumps and other turbomachines for operation in cryogenics. The fluid properties of these liquids inherently affect the vaporization process which supplies vapor to the cavity. This fluid property effect is given the term "thermodynamic effect," and is defined to be the effect of variations in liquid temperature on the cavitation number.

This thermodynamic effect, however, will occur in any liquid and will become more significant as the temperature is increased, resulting in the cavity temperature being lower than the bulk temperature of the fluid. This reduced temperature and correspondingly reduced cavity pressure can seldom be predicted from fluid to fluid. Thus, more understanding is needed of the mechanics of developed cavitation to develop similarity relations for use in the design of pumps and turbomachinery.

1.2 Previous Investigations

One of the first theoretical and experimental investigations into the variation of cavitation number with temperature has been conducted by Stahl and Stepanoff (4). In their investigation, the B-factor method for predicting thermodynamic effects was developed with particular emphasis on pump applications. Later, other researchers, such as Salemann (5), Spraker (6), and Hammitt (7), also studied the effect of fluid temperature variation on the performance characteristics of pumps.

Recently, NASA has undertaken a program to determine various cavitation characteristics and the thermodynamic behavior of different fluids in an effort to obtain improved design criteria to aid in the prediction of cavitating pump performance. Their extensive work has been carried out in a venturi section of a cavitation tunnel employing various fluids by Gelder, Ruggeri, and Moore (9, 10, 11) and Hord, Edmonds, and Millhisen (8). In the theoretical work by Gelder, Ruggeri, and Moore, reasonable agreement with experimental results was found, using a modified B-factor method. During the experimental investigation, both temperature and pressure measurements were taken within the vaporous cavitation regime, and Freon 114 was the primary test fluid. Thus, their work is of most importance because it parallels the investigation presented in this thesis, and a discussion is presented in Chapters III and IV.

1.3 Statement of Problem

Presently, existing theories which deal with the problems of fluid property effects on vaporous cavitation have been developed using a thermostatic or B-factor approach. However, in this investigation, it was attempted to present a dynamic theory based on entrainment theories which can account for the physics of the vaporization process.

In developing the entrainment theory, some of the variables which were investigated experimentally were: 1) velocity, 2) model size, 3) liquid temperature, 4) different fluids, 5) cavity length, and 6) cavity geometry. Along with these variables, certain assumptions had to be investigated in order to develop a cavity model accounting for dynamic effects, and these are: 1) to establish a single pressure indicative of the cavity, 2) to define cavity stability, 3) to relate similarities between an entrained cavity and a natural cavity for a fixed cavitation number, and 4) to establish a single relationship between cavity geometry and cavitation number.

1.4 General Scope

The experimental portion of this investigation was divided into two main phases: 1) water testing, including an air entrainment study, a cavity geometry study, and a temperature study through a range of 80° F to 300° F, and 2) Freon 113 testing including a cavity temperature and pressure study through a range of 80° F to 190° F. The water phase was used mostly to develop the theory and the Freon phase was applied as a check.

The primary model used in the Freon and water study is basically the same as developed by L. E. Buddenbaum (14). It is an 0.24-inch zero-caliber-ogive with three pressure taps, three air injection ports, and when measuring cavity temperatures, fitted with two thermocouples. As a secondary model, an 0.50-inch zero-caliber-ogive with one pressure tap and three air injection ports was used in water to determine model geometric similarity laws. Also, for both models, three basic ratios of cavity length to model diameter were examined. They were an (L/D) of 2.08, 3.65, and 5.21, corresponding to cavity lengths for the primary model of 0.500 inch, 0.875 inch, and 1.25 inches respectively.

Cavitation numbers were obtained for each cavitation state over a temperature range of 80° F to 300° F in water and of 50° F to 190° F in Freon 113. This testing was conducted in the NASA ultra-high-speed water tunnel where the nominal velocities of 37 fps, 64 fps, and 120 fps were used.

CHAPTER II

DESCRIPTION OF THE EXPERIMENTAL INVESTIGATION

2.1 Water Tunnel

This experimental investigation of developed cavitation in water and in Freon 113 on zero-caliber-ogives was conducted in the NASA-sponsored high-speed, high-pressure, high-temperature water tunnel at The Pennsylvania State University. The tunnel is a recirculating system having a circular 1.5-inch internal diameter test section. The present drive system consists of an 150 hp, 3600 rpm induction motor driving a six-speed truck transmission through a fabricated right angle gear box. The transmission has rpm values of 315, 558, 952, 1690, and 2400, and corresponding unblocked velocity values of 45, 76, 132, 234, and 332 fps. A detailed description of earlier versions of this tunnel and supporting facilities is given in References 12 and 13.

2.2 Modifications Required for High Temperature Water Capabilities

At the conclusion of testing conducted by L. E. Buddenbaum, the tunnel motor-gearbox drive system was disassembled to check the shafts, seals, and bearings. From this inspection, the impeller shaft was found to be cracked, and thus, the shaft and its mated bearing were replaced. Also, at that time, various pressure manifold values and a by-pass section of pipe were replaced so that the leaks could be eliminated.

The largest modification to the existing facility necessary for the very high temperature study was the addition of a 40 kw immersion heater, Figure 1. The new heater was needed to replace the old 14 kw heater which was worn out and did not have the capability to heat the water to temperatures in excess of 300° F. The new heater was installed in the by-pass system at the same location as the previous one.

2.3 Modifications Required for High Temperature Freon 113 Capabilities

The primary experimental investigation was conducted using Freon 113 in the NASA tunnel. The major modifications to the tunnel for the Freon conversion are: 1) Freon filter system, and 2) Freon storage system. The Freon filter system, Figure 1, was installed in the tunnel by-pass system as shown in Figure 2. This system consists of a special primary Freon filter which is used to remove water from the Freon, and a secondary after filter which is a particle trap. This enabled the tunnel to be converted to Freon without removing the small amount of residual water in the system after careful draining. The Freon storage system is shown in Figures 3 and 4. This system consists of a 150 gallon, 125 psia, galvanized tank, an Allis-Chalmers pump, and the pipe and valves necessary to fill and drain the tunnel. Also, due to the excessive amount of air in the Freon, it was necessary to construct a distiller. The purpose of the distiller was to condense the boiling Freon vapors and to release the air escaping from the Freon.

2.4 Safety Equipment

Special safety precautions have been taken with the Freon system due to the volatility of the liquid at room temperature. These include a 125 lb. safety valve on the Freon storage tank, a 400 lb. safety valve in the Freon filter system, a halide meter, and a fan. The purpose of the fan was to keep a steady circulation around the tunnel because the Freon vapors are heavier than air. Also, the halide meter monitors the concentration of Freon in the air so that the 800 ppm limit set by du Pont could be avoided.

2.5 Automatic Data Recording System

The NASA tunnel was converted to a new data recording system which has the capabilities to record both temperatures and pressures upon command. The concept for the data collecting system, Figure 5, is to select certain pressures and temperatures and send the results to a computer for rapid reduction. This system consists of a 48 station, 1000 psi Scanivalve, Figure 6, two Pace variable reluctance transducers, Figure 7, and their carrier-demodulators, Figure 8, a Hewlett-Packard integrating digital voltmeter, and a dual channel scanivalve drive.

The Pace transducers in the system are A-C variable-reluctance type providing multirange capability with the use of interchangeable diaphragms. This eliminated the need to have several individual pressure transducers. These transducers have the range of ± 1, ± 5, ± 25, ± 100, ± 500 psi, gauge and differential, and the instrument is easily disassembled for replacement of diaphragm. However, under the tunnel running conditions, the transducers were arranged for the ± 25 and ± 500 psi ranges. The measurements taken from the transducers are well within accuracy requirements set forth to be ± 0.02 in the 0-50 psi range, and ± 0.05 psi in the 50-200 psi range.

The transducers are calibrated with a special dead weight calibrator, Figure 9. This consists of a piston of known diameter which is rotated to reduce friction, and various pressure levels are attained by adding various combinations of weights to the circular platform.

2.6 Models

The primary model used in this study is basically the same as developed by L. E. Buddenbaum from his high temperature testing. It is a 0.24-inch zero-caliber-ogive with three pressure taps, three air injection ports, two thermocouple ports, and a thermocouple mounted in the support sting. This model was fabricated from stainless steel and is shown in Figure 10.

The pressure taps are located 120° apart, and are 0.020-inch diameter holes drilled into three 0.065-inch diameter stainless steel tubes running along the surface of the model. Also, they are located 0.150, 0.425, and 0.825 inches from the front edge of the model in coordination with cavity sizes 0.500, 0.875, and 1.25 inches. Thus, the taps are located along the various cavities in such a way that the axial pressure gradient can be calculated.

Air injection into the cavity formed by the model is accomplished with three ports, 120° apart, located in line with the first pressure tap. The ports are drilled into a central cavity located in the hollow model to form the supply reservoir. Symmetry in the injection was selected as the most feasible after studying many papers on entrainment.

After completion of entrainment testing, the two thermocouples were installed in the model. One thermocouple is located midway between pressure taps 1 and 2, and the other is in the same vertical plane as tap 2. The wires for the sensors are run through the hollow center of the model.

2.7 Measurement of Tunnel Velocity and Pressure

Pressure measurements used for determining tunnel velocity were measured by means of a high pressure transducer. The taps needed were connected to a common scanivalve which selected each tap for the transducer. The transducer used had a 0-500 psi range, and the output was displayed on an integrating digital voltmeter.

A 0-400 psia Heise gauge which was connected to a converging part of the settling section was employed for the maintenance of a constant tunnel pressure level while pressure distribution and velocity determination tests were being performed.

2.8 Measurement of Model Temperature and Cavity Pressure

Cavity pressures were measured by means of a ± 100 psi Pace transducer through a similar system as used for the tunnel pressures. That is, the taps are fed into a lower pressure scanivalve, the output goes to a low pressure transducer, and the voltage output of the transducer was displayed on an integrating digital voltmeter.

Temperature determination inside the cavity and for the free stream was accomplished with copper constantan thermocouples fabricated by means of a helium atmosphere arc welder. Two thermocouples were installed in the nose and another was located in the tunnel leg to measure the free stream temperature.

The thermocouple wires for the model were extended through the model mounting plugs and were connected to a central input scanner, after being subjected to an ice-bath reference junction (see reference 14 for assembly procedure). The input scanner is basically an automatic switchbox which outputs the signal to an integrating voltmeter. Thus, in order to measure directly the absolute value of the temperature, the thermocouples were calibrated through the system. Also, periodically during testing, reference points for temperature calibration were taken.

2.9 Measurement of Cavity Area and Flow Rate for Ventilated Cavities

The profile shapes of the natural and entrained cavities were photographed for each set of stable test conditions; that being a specified cavity length, pressure and velocity. The exposure time was chosen in such a manner that a long time average of the cavity shape could be obtained without impairing the clarity of the cavity profile. Thus, the cavity shape was measured by projecting lines on the photographic pictures and measuring the position of the upper and lower edges of the cavity relative to the horizontal reference line drawn through the center of the cavity. These measurements were obtained at various axial positions from the edges of the model to a point established as the end of the cavity. Then, these measurements were converted to actual distance by a mathematical equation established by a reference frame to account for the distortion of the tunnel test section. Finally, the measured points were fitted to an ellipse and then the various areas could easily be calculated.

The method for obtaining the experimental conditions for ventilated cavities was first to set the free stream velocity and pressure without cavitation, and then vary the air flow into the formed cavity from maximum to minimum to establish the limits for which a stable cavity could be maintained. The air flow was then adjusted to form at least four different cavities within this range.

A nitrogen tank was used as the supply source for the cavity and the flow rate was measured by a calibrated flowmeter, Gilmont volumetric flowmeter - size no. 4, Figure 11.

2.10 Data Collection and Reduction

The procedure of data collection required two persons: an operator to establish the required cavitating condition, and a data recorder to read and record the digital output of the system. During the tests, the operator adjusted the tunnel pressure and temperature until a specified cavity length and free stream temperature was established. This cavity length was defined by lines scribed on the model's surface. After stabilization of the cavity, the recorder started the input scanner, and then the tunnel pressure, model cavity temperatures, and model cavity pressures were recorded automatically in rapid succession. Thus, one data point consists of about ten different measurements.

In reducing the experimental data, the manner is outlined in Appendix A for calculating the experiment or uncorrected cavity number, and is given by:

$$\sigma' = \frac{P_{2u} - P_v}{P_o - P_{2u}} \quad C_{P2u} + C_{P2u} - 1.00 \quad , \qquad (A.9)$$

where C_{P2u} was obtained from unblocked cavitation data given by Figure 12.

To compare the results with other experiments, the cavitation number had to be corrected for the area blockage created by the model in the NASA tunnel. Appendix B defines the correct cavitation number to be:

$$\sigma = \sigma'/N \quad , \tag{B.1}$$

where N is a correction factor based on similar tests in the 12-inch water tunnel. Also, N depends only on the ratio of cavity cross section versus test section velocity, and is given by:

Model: 0.24-inch diameter ogive

Cavity	N
I	1.10
II	1.23
III	1.32

CHAPTER III

ANALYTICAL STUDIES

3.1 General Description

For the case of developed cavitation, many investigators have shown that the forward section of the cavity is quite stable, and that the cavity is sustained by a flow of vapor entering the wall and being carried out the rear of the cavity. Thus, it was suspected that the growth behavior would be a function of this vaporization and entrainment process. Therefore, a theory is developed to include the dynamics of the cavity.

The cavitation number for such a cavity can be expressed as:

$$\sigma = \frac{P_\infty - P_c}{\frac{1}{2} \rho V_\infty^2} , \tag{1}$$

where $P_c \approx P_v + P_G - \Delta P_v$,

or finally,

$$\sigma = \frac{P_\infty - P_v}{\frac{1}{2} \rho V_\infty^2} + \frac{P_G}{\frac{1}{2} \rho V_\infty^2} - \frac{\Delta P_v}{\frac{1}{2} \rho V_\infty^2} , \tag{2}$$

where

$\frac{P_\infty - P_v}{\frac{1}{2} \rho V_\infty^2} \doteq$ cavitation number based on vapor pressure at bulk temperature,

$$\frac{P_G}{\frac{1}{2}\rho V_\infty^2} = \text{contribution due to noncondensable gas, and}$$

$$\frac{\Delta P_v}{\frac{1}{2}\rho V_\infty^2} = \text{contribution due to the thermodynamic effect.}$$

The effect of air content in Equation (2) is known and experimenters (15, 16) have shown that the effect of the undissolved gas pressure P_G can be significant for cavity flows. However, its effect can be approximated, Reference 17, to be some fraction of the saturation gas pressure, given as:

$$P_G = k\,\alpha\,\beta, \tag{3}$$

where

k = empirical factor,

α = air content concentration, and

β = Henry's Law constant.

Therefore, in order to reduce the effect of P_G, the air content was reduced before each test, and because the tests were conducted in a fluid above its boiling point, the gas content cannot be measured with any accuracy.

As temperature increases beyond the boiling point of the fluid, the dimensionless vapor pressure depression term of the Equation (2) becomes more important. Previous investigations into the theory of thermodynamic scale effects on the cavitation have derived expressions for the difference in vapor pressure across the cavity wall, ΔP_v. To obtain this simple expression, a Taylor series expansion for the vapor pressure difference is applied:

$$\Delta P_v = \frac{dP_v}{dT} \Delta T + \frac{d^2P_v}{dT^2} \frac{(\Delta T)^2}{2!} + \ldots \tag{4}$$

and, taking only the first term as an approximation, becomes:

$$\Delta P_v \approx \frac{dP_v}{dT} \Delta T . \tag{5}$$

Now, using the Clausius-Clapeyion relationship for dP_v/dT yields:

$$\frac{dP_v}{dT} \cong \frac{\rho_v \lambda}{T (1 - \rho_v/\rho_L)} , \tag{6}$$

and the thermodynamic effect term becomes:

$$\frac{\Delta P_v}{\frac{1}{2} \rho V_\infty^{\ 2}} = \frac{\dfrac{\rho_v \lambda \Delta T}{T (1 - \rho_v/\rho_L)}}{\frac{1}{2} \rho V_\infty^{\ 2}} \tag{7}$$

Presently, two theoretical methods of predicting the temperature difference are presented, and are 1) the quasi-static or modified B-factor theory, and 2) the entrainment theory.

3.2 Development of the Modified B-Factor Theory

One of the first theoretical treatments of thermodynamic effects on cavitation was given by Stahl and Stepanoff in Reference 4. In their paper, the local reduction in vapor pressure was a function of fluid and vapor properties, and a thermal cavitation parameter B. The parameter B was defined as the ratio of the volume of vapor to the volume of liquid passing through a zone where the local pressure had been reduced below the bulk vapor pressure of the liquid.

The conventional equation for the B-factor theory is given by:

$$\frac{\Delta P_v}{\rho_L} = \frac{\lambda^2 \cdot B}{T_\infty C_{P_L}} \left(\frac{\rho_v}{\rho_L} \right)^2 , \qquad (8)$$

where

ρ_v = density of vapor,

ρ_L = density of liquid,

C_{P_L} = specific heat of the liquid,

λ = latent heat of vaporization,

$B = \dfrac{\text{volume of vapor}}{\text{volume of liquid}}$,

T_∞ = bulk temperature, and

ΔP_v = local reduction in vapor pressure.

The detailed derivation of Equation (8) is given by Seidel in Reference 17; however, it is important to understand the limitations on the development.

In general, the pressure depressions are a function of fluid properties as well as the complicated geometry, velocities and heat- and mass-transfer mechanisms involved. However, by simplifying assumptions to the energy, momentum and continuity equation, the derivation of Equation (8) is reduced to solving a problem in thermostatics, which Acosta and Hollander (18) state as: "An insulated cylinder with a tightly fitted piston is completely filled with a unit mass of saturated liquid. The piston is then slowly withdrawn until a certain given volume of the vapor is formed. The pressure of the resulting mixture is then to be determined," where the basic assumptions made are:

1) the flow is frictionless, steady and irrotational,
2) the vaporization process is adiabatic and frictionless and the fluid is in equilibrium,
3) the process is steady and one-dimensional.

Since the process is one of constant entropy, the entropy of the final state is given by:

$$S_2 = S_{2_L} + x\,(S_v - S_L)_2 \quad , \tag{9}$$

where

S_2 = entropy at end of process,

S_{2_L} = liquid entropy at end of process,

x = mass of vapor/total mass, and

S_v = entropy of vapor,

and the final-initial entropies can be equated as:

$$S_{L_1} = S_{L_2} + x\,(S_v - S_L)_2$$

or

$$S_{L_1} - S_{L_2} = x\,(S_v - S_L)_2 \quad . \tag{10}$$

The second law of thermodynamics can be used to solve for $(S_v - S_L)$, and is:

$$ds = \left.\frac{dQ}{T}\right|_{\text{reversible}} = \lambda/T = S_v - S_L \tag{11}$$

Finally, Equations (10) and (11) can be substituted into the first law of thermodynamics for a liquid given by:

$$\begin{aligned} Tds &= du + pdv \\ &= du \approx CpdT \end{aligned} \tag{12}$$

and yielding:

$$\begin{aligned} S_{L_1} - S_{L_2} &= C_{P_L} \ln (T_1/T_2) \\ &= x\, \lambda_2/T_2 \end{aligned} \tag{13}$$

Equation (13) can be simplified mathematically by expanding $\ln (T_1/T_2)$ into a geometric series for $\ln \left[1 + \frac{(T_1 - T_2)}{T_2} \right]$ and neglecting the higher order terms. This will give the equation for ΔT, as:

$$\Delta T = T_1 - T_2 \left(\frac{x\lambda_2}{C_{P_L}}\right) \quad , \tag{14}$$

where $x = \dfrac{\text{mass of vapor}}{\text{total mass}}$

Now, the vapor to liquid volume ratio B can be introduced in order to solve for the quantity x. Thus, from definition:

$$B = \frac{\text{volume of vapor formed}}{\text{volume of liquid}}$$

$$B = \frac{M_v \cdot \rho_L}{M_L \cdot \rho_v} \tag{15}$$

and

$$X = \frac{M_v}{M_v + M_L} = \frac{M_v/M_L}{M_v/M_L + 1} \quad . \tag{16}$$

Thus, substituting Equation (15) into Equation (16) yields:

$$X = \frac{B}{\rho_L/\rho_v + B} \tag{17}$$

and assuming that $\rho_L/\rho_v \gg B$, Equation (17) reduces to:

$$X = B \cdot (\rho_v/\rho_L) \tag{18}$$

Finally, the equation for the temperature depression using the B-factor theory is obtained by substituting Equation (18) into Equation (14) which yields:

$$\Delta T = B \cdot (\rho_v/\rho_L) \cdot \lambda/C_{P_L} \tag{19}$$

This equation is in agreement with Equation (8), the Clausius-Clapeyion equation for ΔT. Useful predictions from the above equation are difficult due to the inability to calculate the ratio of vapor to liquid volume for a given flow condition. The vapor volume can be easily obtained from the dimensions of the cavity; however, the liquid volume is a function of many variables and cannot be easily estimated, unless some physical assumptions are made. Recently, Gelder, Ruggeri, and Moore (19) have developed a method for predicting the variables which affect the liquid volume and some of their ideas will be discussed.

In their paper, it was assumed that the vapor volume is proportional to the product of cavity length and cavity thickness, and also the liquid volume is proportional to the cavity length and thickness of the liquid layer supplying the heat of vaporization. Thus, the equation could have the form:

$$B = \text{constant} \cdot f\,(D_m/\delta) \quad , \tag{20}$$

where

D_m = cavity maximum diameter, and

δ = thickness of liquid layer.

From experimental results, Appendix C, the ratio of maximum cavity diameter to model diameter is solely a function of the cavitation number which in turn is a function of the geometry (L/D). Therefore, the maximum cavity diameter in Equation (20) can be changed to:

$$B = \text{constant } f\,(L/D),\ (D/\delta) \ ; \tag{21}$$

however, some theoretical heat analysis is needed to define (δ).

Consider a small differential element of thickness (δ) and differential area ΔA traveling along the cavity wall for which the heat of vaporization is supplied. An energy balance for the element would be given by applying the first law of thermodynamics for a liquid:

$$\frac{\Delta Q}{\Delta A} = \rho_L \cdot \frac{\Delta V}{\Delta A} \cdot (C_{P_L} \Delta T)$$

$$= \rho_L \cdot \delta \cdot C_{P_L} \cdot \Delta T \quad , \tag{22}$$

and over the whole cavity, Equation (22) becomes:

$$Q/A = \rho_L \cdot \delta \cdot C_{P_L} \cdot (T_\infty - T_{exit}) \quad , \tag{23}$$

where T_{exit} is the temperature of the particle after it leaves the cavity wall. Also, the amount of heat needed to supply the cavity with vapor is given by:

$$Q/A = \lambda \rho_v \cdot \frac{Q_f}{A} \cdot t = \lambda \cdot \rho_v \cdot V_\perp \cdot t \quad , \tag{24}$$

where

$V_\perp$ = vapor velocity perpendicular to area A,

Q_f = volume flow rate, and

t = time that it takes the element to travel along the cavity wall.

Thus, the total heat conduction is equal to Equation (24) and can be stated:

$$k \left\{ \frac{T_\infty - T_w}{\delta} \right\} \cdot t = Q/A$$

$$= \lambda \cdot \rho_v \cdot V_\perp \cdot t \quad . \tag{25}$$

Now, setting Equations (23) and (25) equal, the value of δ becomes:

$$\rho_L \cdot \delta \cdot C_{P_L} \cdot (T_\infty - T_{exit})$$

$$= k \left\{ \frac{T_\infty - T_W}{\delta} \right\} \cdot t \tag{26}$$

or

$$\delta^2 = \frac{(T_\infty - T_W) \cdot}{T_\infty - T_{exit}} \cdot t \cdot \alpha \quad , \tag{27}$$

where α = thermal diffusivity. However, for a given flow rate, Equation (27) has two independent variables, δ and $(T_\infty - T_W)$ / $(T_\infty - T_{exit})$; therefore a restriction is needed. Assume the function $(T_\infty - T_W)$ must be a multiple of $(T_\infty - T_{exit})$; i.e., $T_\infty - T_W = k$ $(T_\infty - T_{exit})$. Thus, the fluid layer thickness becomes a function of the following variables:

$$\delta^2 = \text{constant} \cdot \alpha \cdot t$$

$$= \text{constant} \cdot (\alpha \cdot L/V_\infty)^{\frac{1}{2}}$$

or, in more empirical terms:

$$\delta = \text{constant } f \; (\alpha \cdot L/V) \; . \tag{28}$$

Therefore, B is shown to be a function of the following variables:

$$B = \text{constant} \cdot f \; (L/D), \; \left(\frac{DV_\infty}{\alpha} \right) \quad , \tag{29}$$

and using a reference value for B, the constant can be evaluated resulting in:

B predicted

$$= B_{ref} \cdot \frac{(\alpha_{ref})^{l}}{\alpha} \cdot \left[\frac{(L/D)}{(L/D)_{ref}} \right]^{m} \cdot \left(\frac{D}{D_{ref}} \right)^{n} \cdot \left(V_\infty / V_{\infty_{ref}} \right)^{p} , \qquad (30)$$

where l, m, n, p are coefficients which must be determined experimentally.

The purpose of Equation (30) is to predict the cavitating performance of a model from fluid to fluid and from one temperature to another. Also, any single experiment may be chosen to provide the reference data. However, with the use of various types of models such as the venturi section versus an ogive, the exponents appear to change.

3.3 Development of the Entrainment Theory

The cavitated region which is uniformly developed with its leading edge at a fixed axial location is continuously supplied with vapor from the cavity walls. Despite some fluctuation near the rear of the cavity where the vapor is entrained away, under steady flow conditions, this natural cavity is quite stable, having a constant shape. Thus, this type of developed cavitation has the characteristic that the cavity geometry is a single-valued function of the cavitation number based on cavity pressure.

The vapor supply for such a cavity is inherently due to a change of liquid state to the vapor state at the wall of the cavity.

This change of state requires energy in the form of heat. The rate at which heat is transferred must be given by:

$$\dot{q} \quad = \quad \lambda \, \dot{m}_v \quad , \tag{31}$$

where

$\dot{q}$ = rate of heat transfer,

λ = latent heat of vaporization, and

$\dot{m}_v$ = mass flow rate of vapor,

and $\dot{m}_v$ can be expressed as:

$$\dot{m}_v \quad = \quad \rho_v \, V_v \, A_v \quad = \quad \rho_v \cdot Q_v \quad , \tag{32}$$

where

ρ_v = density of vapor,

V_v = velocity of vapor leaving the cavity,

A_v = average-sectional area of vapor flow, and

Q_v = volume flow rate.

Now, a new variable can be defined as:

$$C_Q \quad = \quad \frac{Q_v}{d^2 \; V_\infty} \quad , \tag{33}$$

where C_Q is the entrainment coefficient, and this can be substituted into Equation (31) yielding:

$$\dot{q} \quad = \quad \rho_v \cdot C_Q \cdot d^2 \cdot V_\infty \cdot \lambda \tag{34}$$

From the theory of heat conduction, the heat flux is proportional to the temperature gradient independent of the various mechanisms of convection and is given by:

$$\bar{q}/A = -k \frac{\partial T}{\partial y} , \quad (35)$$

where k is the thermal conductivity, and $\partial T/\partial y$ is the temperature gradient in the liquid normal to the wall at the liquid vapor interface. If the details of the flow and heat transfer process were known for this convective flow situation, the temperature distribution within the fluid could be determined and the heat transfer rate at the wall calculated from Equation (35). However, for this flow situation, there is very little information available regarding the velocity and temperature patterns. In this case, it is then convenient to define a surface coefficient of heat transfer $\bar{h}$, by the following equation:

$$\bar{h} = \frac{\dot{q}/A}{T_\infty - T_w} = k \left(\frac{\partial T/\partial y}{T_\infty - T_w} \right)_{wall} , \quad (36)$$

where T_w is the cavity wall temperature, and T_∞ is the temperature of the free stream liquid. In this equation, the heat transfer coefficient is a function of fluid properties, including velocity, and may depend on the surface of the cavity wall.

Now, solving Equation (36) for $\dot{q}/A$ and substituting the equation into Equation (34), the temperature difference $T_\infty - T_w$ becomes:

$$(T_\infty - T_w)\,\bar{h} = \dot{q}/A_{wall} = k\,\frac{\partial T}{\partial y}\,\text{wall}$$

$$= \lambda \cdot \frac{M_V}{A_w} = \rho_v \cdot \frac{C_Q}{A_w} \cdot d^2 \cdot V_\infty \cdot \lambda \quad , \qquad (37)$$

or finally:

$$(T_\infty - T_w) = \frac{C_Q}{\bar{h}} \cdot \frac{d^2}{A_w} \cdot V_\infty \cdot (\lambda \cdot \rho_v) \quad , \qquad (38)$$

where $T_\infty - T_w = \Delta T$ = temperature depression,

C_Q = entrainment coefficient,

$\bar{h}$ = surface coefficient of heat transfer,

V_∞ = velocity of liquid at infinity,

λ = latent heat of evaporization, and

ρ_v = density of the vapor.

The main contribution of Equation (38) is the dynamic approach to the estimation of thermodynamic effects based upon the effect of entrainment. The form of the equation is in agreement with the equation proposed by Acosta-Parkin in the discussion of Reference 1. Also, the equation predicts the absolute value eliminating the need for a reference point. However, for a certain cavitating surface, the entrainment coefficient, surface coefficient of heat transfer and geometric similarity coefficient must be known. These coefficients are a function of liquid, liquid temperature, flow velocity, cavity length and model scale, and must be determined empirically before Equation (38) becomes useful.

3.4 Theoretical and Empirical Comparisons

As developed in the previous section, the expression for the difference in temperature across the cavity wall for the B-factor theory was:

$$\Delta T \quad = \quad B \cdot (\rho_V/\rho_L) \cdot \frac{\lambda}{C_{P_L}} \quad , \tag{19}$$

where $B \quad = \quad \dfrac{\text{volume of vapor formed}}{\text{volume of liquid forming the vapor}}$

Also, the coefficients in Equation (30) used for predicting B were solved empirically by Moore and Ruggeri (19) from data obtained from tests conducted on a venturi section. The workable expression developed for B was given by:

$$B_{pre} \quad = \quad B_{ref} \left(\frac{\alpha_{ref}}{\alpha} \right) \left(\frac{V_\infty}{V_{\infty_{ref}}} \right)^{0.8} (D/D_{ref})^{0.2} \left\{ \frac{L/D}{(L/D)_{ref}} \right\}^{0.3} \tag{39}$$

and therefore:

$$\Delta T \quad = \quad \text{constant } (1/\alpha) \, (V_\infty)^{0.8} \, (D)^{0.2} \, (L/D)^{0.3} \, (\rho_V/\rho_L) \cdot \frac{\lambda}{C_{P_L}} \, . \tag{40}$$

From an entrainment point of view, the theory predicting the thermodynamic effect was given by:

$$\Delta T \quad = \quad \frac{C_Q}{\bar{h}} \cdot \frac{d^2}{A_W} \cdot V_\infty \cdot (\lambda \cdot \rho_V) \quad , \tag{38}$$

where:

C_Q = volume flow rate coefficient,

$\bar{h}$ = heat transfer coefficient,

d = model diameter,

A_w = area of heat transfer,

V_∞ = velocity at infinity,

λ = latent heat of evaporization, and

ρ_v = density of vapor.

Also, in spite of many difficulties, an analysis of water testing data obtained with two different diameter zero-caliber-ogives was conducted to determine the coefficients C_Q, d^2/A_w, and $\bar{h}$. The following empirical relationships as derived in the appendices were developed for the ogive over the variables tested:

$$\bar{h} \approx \text{constant} \cdot Re^{0.35} \cdot Pr^{0.45} \cdot Fr^{-0.40} \cdot (K_L/L) \qquad (41)$$

$$C_Q \approx \text{constant} \cdot (Fr)^{-0.75} (L/D)^{0.98} \qquad (42)$$

$$d^2/A_w \approx \text{constant} \cdot (L/D)^{-1.23} \qquad (43)$$

Thus, the above can be substituted into Equation (38), yielding:

$$\Delta T \approx \text{constant} \cdot \frac{(L/D)^{-0.25} \cdot V_\infty \cdot (\lambda \cdot \rho_v)\ (L)}{Re^{0.35}\ Pr^{0.45}\ Fr^{0.35}\ (K_L)}, \qquad (44)$$

In order to compare the B-factor theory, Equation (40), to the entrainment theory, Equation (44), some consideration must be given to the conditions under which the empirical portions of both theories were derived. For instance, the empirical parameters for determining

B in the B-factor theory were obtained from test data using a venturi section, and the coefficients to determine $\bar{h}$, C_Q, and d^2/A_w in the entrainment theory were obtained from test data using a zero-caliber-ogive model. Therefore, a third equation was derived by solving the empirical parameters for determining B in the B-factor theory from test data using a zero-caliber-ogive model. The results for the three conditions are:

B-factor Theory Based on Venturi Section

$$\Delta T \cong \text{constant } (1/\alpha)\ (V_\infty)^{0.8}\ (D)^{0.2}\ (L/D)^{0.3}\ (\rho_V/\rho_L) \cdot \frac{\lambda}{C_{P_L}} \tag{40}$$

B-factor Theory Based on Zero-Caliber-Ogive

$$\Delta T \cong \text{constant } (1/\alpha)^{0.60}\ (V_\infty)^{0.3}\ (D)^{0.33}\ (L/D)^{0.58}\ (\rho_V/\rho_L) \cdot \frac{\lambda}{C_{P_L}} \tag{45}$$

Entrainment Theory Based on Zero-Caliber-Ogive

$$\Delta T \cong \text{constant } (1/\alpha)\ (V_\infty)^{0.55} \cdot (D)^{0.3} \cdot (L/D)^{0.33}$$

$$(\rho_V/\rho_L)^{0.58} \cdot (1/\mu)^{0.9} \cdot \left(\frac{\lambda}{C_{P_L}}\right)^{0.10} \tag{46}$$

Now, the three results can be compared on the basis of cavitation similarity parameters. For instance, if the velocity was varied and all other factors remained constant, the results would be:

entrainment (ogive)

$$\Delta T \quad (V_\infty) \quad \cong \quad \text{constant} \cdot V^{0.30}$$

B-factor (ogive)

$$\Delta T \quad (V_\infty) \quad \cong \quad \text{constant} \cdot V^{0.30}$$

B-factor (venturi)

$$\Delta T \quad (V_\infty) \quad \cong \quad \text{constant} \cdot V^{0.80}$$

and for cavity length and model diameter:

entrainment (ogive)

$$\Delta T \quad (L) \quad \cong \quad \text{constant} \cdot L^{0.58}$$

$$\Delta T \quad (D) \quad \cong \quad \text{constant} \cdot (1/D)^{0.25}$$

B-factor (ogive)

$$\Delta T \quad (L) \quad \cong \quad \text{constant} \cdot L^{0.58}$$

$$\Delta T \quad (D) \quad \cong \quad \text{constant} \cdot (1/D)^{0.25}$$

B-factor (venturi)

$$\Delta T \quad (L) \quad \cong \quad \text{constant} \cdot (L)^{0.3}$$

$$\Delta T \quad (D) \quad \cong \quad \text{constant} \cdot (1/D)^{0.10}$$

From these results, some general conclusions can be drawn concerning the variables of cavity length, velocity, model diameter, and geometry, and these are:

1) The scaling factors of cavity length, velocity and model diameter agree both qualitatively and quantitatively for the entrainment and B-factor theories empirically based on zero-caliber-ogive results.

2) The scaling factors agree only qualitatively when comparing the B-factor theory based on the venturi section versus the B-factor theory based on the ogive.

3) In all cases, the temperature depression increases with cavity length and velocity and decreases slightly with model diameter.

Finally, the last variable to consider is temperature. To compare the effect of free stream temperature on the temperature depression, the B-factor equation based on venturi section reduces to:

$$\Delta T \cong \text{constant} \quad (\rho_V/\rho_L) \cdot \frac{\lambda}{C_{P_L}} \cdot (1/\alpha) \quad ,$$

the B-factor equation based on ogive model reduces to:

$$\Delta T \cong \text{constant} \quad (\rho_V/\rho_L) \cdot \frac{\lambda}{C_{P_L}} \cdot (1/\alpha)^{0.6} \quad ,$$

and the entrainment equation based on ogive model reduces to:

$$\Delta T \cong \text{constant} \quad (\rho_V/\rho_L)^{0.9} \cdot \frac{\lambda}{C_{P_L}} \cdot \left(\frac{1}{\mu_L}\right)^{-0.10} \cdot (1/\alpha)^{0.55}$$

From these equations, the trends of the thermodynamic variables are in qualitative agreement; however, for the entrainment results, the viscosity appears as a variable and the thermal diffusivity is less important.

CHAPTER IV

EXPERIMENTAL RESULTS

4.1 Comparisons of Experimental Results and Theoretical Predictions

The objective of the experimental investigation was to obtain the temperature depressions for various flow conditions. Plots showing this variation for Freon 113 and water, for speeds of 64 and 120 ft/sec, and cavity lengths of 0.500, 0.875, and 1.25 inch are given in Figures 28 through 39. These figures also show curves derived from the theoretical considerations for comparison.

In order to apply the entrainment theory or the B-factor theory as in the figures, a series of initial tests had to be conducted. Each test served to solve one of the variables of the entrainment theory, and can be summarized as follows:

1. Entrainment tests - Appendix E, the flow coefficient (C_Q) was solved as a function of non-dimensionable variables by creating a specific cavity with air injection.

2. Photographic tests - Appendix C and F, photographs were taken of both entrained and natural cavities to establish geometric similarity and to solve for the area coefficient (d^2/A_w) as a function of non-dimensional coefficients.

3. <u>Temperature depression measurement in water</u> - the heat transfer coefficient, Appendix G, was solved as a function of non-dimensional coefficients by measuring the temperature depression in water for various flow coefficients.

Then, the B-factor theory, Equations (40 and 44), and the entrainment theory, Equation (45), can be applied knowing the following reference points:

Velocity - 64 ft/sec

Cavity length - 0.875 inch

Model diameter - 0.24 inch

Temperature - 260° F, in water

Temperature depression - 1.6° F

The temperature depressions in the figures were obtained by extrapolating the measured cavity-temperature profile, Appendix H. This was accomplished by measuring the temperatures at various points inside the cavity. The results of one measuring station are shown in Figure 40, and the total cavity-temperature profile is shown in Figure 41. The profile was then extended to the nose of the model and that depression was plotted.

From the data, it can be seen that, in most cases, there is a significant departure from the two theories as shown in Section 3.3. However, this might be from 1) the difference in geometry from which each theory was derived (i.e., a venturi section versus a zero-cailber-ogive), and/or 2) the effect of air content in the cavity. This effect of air content on the cavity temperature depression has been measured in some degree, Figure 42; however, most of the tests were conducted in Freon 113 in which some of the air was removed. The procedure for removing the air was to boil the Freon in the tunnel and condense the escaping vapors in a distiller. In summary, the maximum temperature difference obtained in Freon 113 due to air content was the order of a degree or less, and the effect of air decreased as the temperature increased.

In conjunction with the measured temperatures, the pressures inside the cavity were also measured. From these pressures, a minimum cavity pressure was established, Appendix I, and the cavitation numbers based on this minimum pressure were plotted for various flow conditions, Figures 43 through 48. The results agree with previous experimenters and are as follows:

1. the cavitation number based on minimum cavity pressure is independent of temperature for a given flow state, and
2. the cavitation numbers for a specified geometry and velocity are identical for Freon 113 and water.

More important than the cavitation numbers are the conditions under which the measured pressures and pressure corresponding to measured temperatures in the cavity can compare. Figures 49 and 50 indicated that these pressures are not in agreement. The temperature depressions obtained from the cavity temperature measurements are, for the most part, greater than those derived from the measured cavity pressures. This trend can be partially explained by the presence of non-condensable gas in the fluid. The partial pressure of the gas in the cavity increases the cavity pressure.

4.2 Cavity Flow Characteristics

Agreement has been found between the scaling factors for the B-factor and entrainment theories based on the zero-caliber-ogive, even though the B-factor theory is a conduction model and the entrainment theory is a convection model. This agreement was partially the result that the heat transfer coefficient in the entrainment theory was independent of velocity for the velocities encountered in the experiment. Therefore, more investigation into the cavity flow characteristics is needed to understand why the B-factor model predicts the proper trends.

The B-factor theory has been specialized to developed cavitation by appropriate assumptions in the theory, and some of these cases have been compared with the experimental results in this investigation. One of the important assumptions is that the liquid thickness can be expressed as:

$$\delta = (\alpha \cdot t)^{\frac{1}{2}} \tag{47}$$

where

α = thermal diffusivity, and

$t \cong L/V$ - time traveled along the cavity.

On the other hand, using one-dimensional energy considerations, Equations (31) and (35), another relationship can be obtained for δ:

$$\delta = \frac{K_L \cdot \Delta T}{\lambda \cdot \rho_v \cdot \dot{V}_\perp} \tag{48}$$

where $\dot{V}_\perp = \dfrac{\text{volume flow rate of vapor}}{\text{area of heat transfer}}$

Thus, the volume flow rate has been measured along with the area of the cavity wall, and the liquid thickness (δ) was calculated directly. The numerical results are summarized in the following table:

	Water Equation		Freon 113 Equation	
	(47)	(48)	(47)	(48)
V = 120 ft/sec L = 1.25 in W-T = 250° F F-T = 150° F	4.81×10^{-4} inch	1.65×10^{-4} inch	2.29×10^{-4} inch	6.1×10^{-5} inch
V = 120 ft/sec L = 0.875 in W-T = 250° F F-T = 150° F	4.03×10^{-4} inch	1.45×10^{-4} inch	1.91×10^{-4} inch	5.85×10^{-5} inch
V = 64 ft/sec L = 0.875 in W-T = 250° F F-T = 150° F	5.50×10^{-4} inch	1.60×10^{-4} inch	2.62×10^{-4} inch	8.6×10^{-5} inch
V = 64 ft/sec L = 0.875 in W-T = 300° F F-T = 200° F	5.54×10^{-4} inch	1.86×10^{-4} inch	2.43×10^{-4} inch	7.8×10^{-5} inch

Although the magnitude of the layer thickness varies, both equations predict the same trends under various flow conditions, and are summarized as follows:

1. The average liquid thickness increases with increasing cavity length and decreases as free stream velocity is increased.

2. The average liquid thickness increased with increasing temperature in water, but decreased with increasing temperature in Freon 113.

However, if Equation (47) is replaced by Equation (27) derived in the theory as:

$$\delta^2 = \frac{T_\infty - T_W}{T_\infty - T_{exit}} \cdot t \cdot \alpha \tag{27}$$

where $t \cong L/V$ - time traveled along the cavity, and the assumption that $(T_\infty - T_W) / (T_\infty - T_{exit})$ can be approximated by a constant is applied, the equation for the liquid thickness reduces to:

$$\delta \cong 3.1 \; (L/V \cdot \alpha)^{\frac{1}{2}} \tag{49}$$

which predicts the thickness within a reasonable error. Therefore, applying $(\alpha \cdot L/V)^{0.5}$ as a scaling factor for predicting temperature depression seems to be a good selection.

Also, in a paper by Eisenburg and Pond (2), the velocity of vapor across the cavity wall was estimated by the following equation:

$$V_\perp = \frac{\Delta T}{\lambda \cdot \rho_v} \cdot \sqrt{\frac{K_L \cdot C_{P_L} \cdot \rho_L}{t}} \tag{50}$$

All of the quantities in Equation (50) were measured experimentally and the results were compared to the entrainment rates obtained for the zero-caliber-ogive. Some of the results are:

	Water		Freon 113	
	Calculated	Measured	Calculated	Measured
V = 120 ft/sec L = 1.25 in W-T = 250° F F-T = 150° F	0.093 ft/sec	0.270 ft/sec	0.096 ft/sec	0.270 ft/sec
V = 120 ft/sec L = 0.875 in W-T = 250° F F-T = 150° F	0.090 ft/sec	0.240 ft/sec	0.095 ft/sec	0.240 ft/sec
V = 64 ft/sec L = 0.875 in W-T = 250° F F-T = 150° F	0.063 ft/sec	0.128 ft/sec	0.064 ft/sec	0.128 ft/sec
V = 64 ft/sec L = 0.875 in W-T = 300° F F-T = 200° F	0.059 ft/sec	0.128 ft/sec	0.064 ft/sec	0.128 ft/sec

Thus, the measured vapor wall velocities agree qualitatively and somewhat quantitatively to the calculated velocities. Both results indicate that the vapor volume flow rate inside the cavity is independent of fluid temperature and of fluid used. Therefore, the assumption that the entrainment coefficient is a function of velocity and geometry seems to be valid.

Finally, the rate at which vapor is entrained away was calculated directly from the measured ventilated cavity flow rates, and the measured cavity cross-sectional areas. The results are:

Velocity - 64 ft/sec

Cavity Length / Model Diameter	Exit Velocity
2.08	1.7 ft/sec
3.65	2.3 ft/sec
5.21	2.5 ft/sec

The average exit velocity of the vapor is very small and the difference in fluid velocity across the cavity wall can be approximated by free stream velocity. Thus, the concept of a re-entrant jet of fluid seems quite possible. The liquid at the end of the cavity wall has enough momentum to overcome the vapor and enter the cavity. In fact, when the fluid velocity becomes very high, the re-entrant jet has been observed to reach the model nose.

CHAPTER V

SUMMARY

5.1 Summary of Results

A theoretical and experimental investigation has been conducted into thermodynamic effects in water at temperatures from 80° F to 290° F and in Freon 113 at temperatures from 75° F to 190° F. Also, the dynamics of the steady-state cavity have been investigated in the NASA High-Speed Fluid Tunnel.

The tunnel was designed for high temperature capabilities with the addition of a larger heater. Also, due to the number of temperature pressure taps for the experimentation, a new digital read-out system was designed and developed. Finally, for Freon 113 testing, a closed loop storage system was constructed and the tunnel by-pass system was redesigned to accommodate special Freon filters.

A theory of thermodynamic effects on cavitation has been developed from a dynamic approach called the entrainment theory. It has been compared with a previously developed quasi-static theory, the B-factor theory, and found to be similar in form to the thermodynamic effect. However, comparisons of the two theories with experimentally determined temperature depressions obtained as functions of temperature, velocity, cavity length, and fluid properties seem to indicate that there exists a definite geometric effect. This implies that the B-factor equation developed from venturi testing will not predict the temperature depression for a zero-caliber-ogive, and so forth.

Conclusions have been drawn from this investigation, and recommendations for further study have been made.

5.2 Conclusions

The following conclusions were derived from the experimental portion of the investigation:

1. The temperature depressions within the developed cavity increased with free stream temperature, cavity length, and velocity.
2. The temperature depression profile within the developed cavity increased approaching the model nose.
3. The measured cavity pressures were, for the most part, greater than the vapor pressure corresponding to the measured cavity temperature. At least part of this difference is attributed to the presence of noncondensable gases.
4. The B-factor theory based on empirical coefficients by Gelder, Ruggeri, and Moore does not appear to predict temperature depressions accurately for different geometries; i.e., venturi section versus zero-caliber-ogive.

5. Conclusions concerning the corrected cavitation number based on minimum cavity pressure are:

   a) The cavitation number remained constant with temperature.

   b) The cavitation number remained constant or increased very slightly for a fixed geometry with an increase in velocity.

   c) The cavitation number decreased with increasing cavity length.

6. The cavitation number based on vapor pressure decreased with increasing velocity and temperature.

7. Conclusions concerning the measured entrained flow coefficient are:

   a) For a given velocity and model diameter, as the flow coefficient increased, the cavity size increased and the corresponding cavitation number decreased.

   b) The entrainment coefficient decreased for a constant cavitation number and, hence, (L/D) as velocity increases.

   c) No appreciable change in entrainment coefficient was found for a fixed cavity shape and velocity as temperature was increased.

   d) The flow coefficient increased with increasing model diameter.

8. Conclusions concerning the shape of a cavity formed by a zero-caliber-ogive are:
   a) The size of the cavity increases with increasing model nose diameter and is independent of free stream velocity.
   b) The proportions of the cavity are solely dependent upon the cavitation number.
   c) For a given cavitation number, the shape defined by the length of the cavity under natural cavitation conditions and the shape of the cavity under entrained conditions are identical.
   d) The shape of the cavity can be approximated by an elliptical equation for the range of Froude numbers encountered.

The following conclusions were derived from the theoretical portion of the investigation:

1. The temperature depression predicted by the B-factor theory based on empirical coefficients obtained in water is in agreement with experimental results in water and Freon 113 for the zero-caliber-ogive.
2. In the empirical portion of the entrainment theory, the heat transfer coefficient became independent of velocity.
3. The theoretical results agree qualitatively with experimental results for both theories; however, only the entrainment theory agrees in a quantitative way.

4. Because the vapor cavity formed is a function of geometry, the empirical coefficients in the B-factor theory will vary for different geometries.

5.3 Recommendations for Further Study

1. Further research on thermodynamic effects is necessary in order to establish the influence of cavity geometry.
2. The effect of noncondensable gas on cavity flows should be systematically investigated.
3. A method for measuring the gas content at water and Freon temperatures above their boiling points must be developed.
4. It is also recommended that the following modifications be made to the thermocouple measuring system:
   a) the free stream and cavity thermocouples should be coupled so that the temperature difference can be read directly, and
   b) a resistance thermometer be purchased so that the absolute free stream temperature can be read accurately.
5. A two-dimensional test section should be designed and constructed for the NASA tunnel so that probes for temperature and pressure measurement could be inserted into the developed cavity.

REFERENCES

1. Holl, J. W., and Wislicenus, G. F., "Scale Effects on Cavitation," Trans. ASME, Series D, Journal of Basic Engineering, Vol. 83, 1961, pp. 385-398.

2. Eisenberg, P., and Pond, H., "Water Tunnel Investigations of Steady State Cavities," Carderock, Md., David Taylor Model Basin, October 1948, DTMB Report 668.

3. Waid, R. L., "Cavity Shapes for Circular Disks at Angles of Attack," Pasadena, California, Hydrodynamics Laboratory, California Institute of Technology, September 1957, Report E-73.4.

4. Stahl, H. A., and Stepanoff, A. J., "Thermodynamic Aspects of Cavitation in Centrifugal Pumps," Trans. ASME, Vol. 78, 1956, pp. 167-173.

5. Salemann, V., "Cavitation and NPSH Requirements of Various Liquids," Trans. ASME, Series D, Journal of Basic Engineering, Vol. 81, 1959, pp. 167-173.

6. Spraker, W. A., "The Effects of Fluid Properties of Cavitation in Centrifugal Pumps," Trans. ASME, Series D, Journal of Basic Engineering, Vol. 87, 1965.

7. Hammitt, F. G., "Observation of Cavitation Scale and Thermodynamic Effects in Stationary and Rotating Components," Trans. ASME, Series D, Journal of Basic Engineering, Vol. 85, 1963.

8. Hord, J., Edmonds, D. K., and Millhiser, D. R., "Thermodynamic Depressions Within Cavities and Cavitation Inception in Liquid Hydrogen and Liquid Nitrogen," NASA CR-72286, March 1968.

9. Moore, R. D., and Ruggeri, R. S., "Prediction of Thermodynamic Effects of Developed Cavitation Based on Liquid-Hydrogen and Freon 114 Data in Scaled Venturis," NASA TW-D-4899, November 1968.

10. Gelder, T. F., Ruggeri, R. S., and Moore, R. D., "Cavitation Similarity Considerations Based on Measured Pressure and Temperature Depression in Cavitating Regions of Freon 114," NASA TND-3509, July 1966.

REFERENCES (Cont.)

11. Gelder, T. F., Moore, R. D., and Ruggeri, R. S., "Incipient Cavitation of Freon-114 in a Tunnel Venturi," NASA TND-2662, February 1965.

12. Holl, J. W., and Treaster, A. L., "Cavitation Hysteresis," ASME Transactions, Journal of Basic Research, Series D, March 1966, pp. 199-212.

13. Holl, J. W., "Cavitation Research Facilities at the Ordnance Research Laboratory of The Pennsylvania State University," presented at the Symposium on Cavitation Research Facilities and Techniques, Fluids Engineering Conference, ASME, Philadelphia, Pennsylvania, May 18-20, 1964.

14. Buddenbaum, L. E., "Thermodynamic Effects on Developed Cavitation on Zero-Caliber-Ogives in Water at Temperatures from 80° F to 260° F," M. Engrg. Report, The Pennsylvania State University, March 1968.

15. Holl, J. W., "An Effect of Air Content on the Occurrence of Cavitation," ASME Transactions, Journal of Basic Engineering, Vol. 82, Series D, No. 4, December 1960, pp. 941-446.

16. Brennen, C., "The Dynamic Balances of Dissolved Air and Heat in Natural Cavity Flows," Journal of Fluid Mechanics, Vol. 37, Part 1, 1969, pp. 115-127.

17. Seidel, Gerald S., "An Investigation of Thermodynamic Effects on Cavitation in Water from 80° F to 180° F on Hemispherical-Nosed Bodies," M. S. Thesis, The Pennsylvania State University, June 1966.

18. Acosta, A. J., and Hollander, A., "Remarks on Cavitation in Turbomachines," Hydromechanics Laboratory, California Institute of Technology, Report 79.3, October 1959.

19. Moore, R. D., and Ruggeri, R. S., "Prediction of Thermodynamic Effects of Developed Cavitation Based on Liquid-Hydrogen and Freon 114 Data in Scaled Venturis," NASA TN-D-4899, November 1968, p. 14.

REFERENCES (Cont.)

20. Swanson, W. M., and O'Neill, J. P., "The Stability of an Air-Maintained Cavity Behind a Stationary Object in Flowing Water," Hydrodynamics Laboratory, California Institute of Technology, Report No. M24.3, September 5, 1951.

21. Reichardt, H., "The Laws of Cavitation Bubbles at Axially Symmetrical Bodies in a Flow," MAP Reports and Translations, August 15, 1956, Report No. 776.

22. Cox, R. N., and Clayden, W. A., "Air Entrainment at the Rear of a Steady Cavity," Cavitation in Hydrodynamics, Proceedings of a Symposium held at the National Physical Laboratory, September 14-17, 1955, Report 12.

23. Kreith, Frank, Principals of Heat Transfer, 2nd Ed., International Textbook Company, Scranton, Pennsylvania, 1965, pp. 445-448.

24. Kreith, Frank, Principals of Heat Transfer, 2nd Ed., International Textbook Company, Scranton, Pennsylvania, 1965, pp. 453-466.

25. Langhaar, Henry, Dimensional Analysis and Theory of Models, John Wiley & Sons, Inc., New York, 1951.

APPENDIX A

DATA REDUCTION

In this investigation, the standard stainless steel test section and the pressure tap nomenclature provided by Seidel in Reference 17 were employed. However, the taps utilized to determine the cavitation number differ from previous investigators due to the excessive amount of blockage created by the large cavity formed by the blunt nosed ogive.

From the definition of the cavitation number based on cavity pressure:

$$\sigma = \frac{P_\infty - P_c}{\frac{1}{2}\rho V_\infty^2} \tag{A.1}$$

and Bernoulli's equation given by:

$$P_o - P_\infty = \frac{1}{2}\rho V_\infty^2 \quad , \tag{A.2}$$

the pressures needed to establish the cavitation number are:

$$\sigma = \frac{P_\infty - P_c}{P_o - P_\infty} \quad , \tag{A.3}$$

where P_∞ = static pressure in the plane of the model nose,

P_c = cavity pressure, and

P_o = total or dynamic pressure.

The model is instrumented so that the pressure inside the cavity can be easily measured, and the stagnation pressure can be measured by the pressure tap at station 0. This tap (P_o) is located in the straight settling section upstream to the nozzle and, as stated by Seidel, the pressure at station 0 was found to equal the stagnation pressure.

However, the model projected upstream past the tap at station 7 which in previous tests was selected as the reference free stream static pressure. Therefore, a tap at station 2 was selected as the unblocked reference station because it is located one test section diameter upstream of the model nose. Thus, in order to determine the pressure in the cavitation plane at station 7, the measured pressure at station 2 must be corrected to account for the pressure difference existing between stations 2 and 7.

The uncorrected cavitation number as defined by Equation (A.1) can be written using the pressure tap numbers as:

$$\sigma' = \frac{P_{7u} - P_c}{P_o - P_{7u}} \tag{A.4}$$

where P_{7u} = unblocked static pressure in the plane of the model, tap number 7,

P_o = stagnation pressure, tap number 0, and

P_c = cavity pressure.

Now Equation (A.4) can be rearranged into:

$$\sigma = \frac{P_{2u} - P_{2u} + P_{7u} - P_c}{P_o - P_{7u}}$$

$$= \frac{P_{2u} - P_c}{P_o - P_{7u}} - \frac{(P_2' - P_{7u})}{P_o - P_{7u}} \qquad (A.5)$$

where P_{2u} is the pressure tap located upstream of the model nose. Also, the equation can be reduced to:

$$\sigma' = \frac{P_{2u} - P_o}{P_o - P_{7u}} + \frac{P_o - P_{2u}}{P_o - P_{7u}} - 1,$$

or finally:

$$\sigma' = \frac{P_{2u} - P_o}{P_o - P_{2u}} \cdot \left\{ \frac{P_o - P_{2u}}{P_o - P_{7u}} \right\} + \frac{P_o - P_{2u}}{P_o - P_{7u}} - 1, \qquad (A.6)$$

The pressure coefficient at any station X is defined as:

$$C_{P_X} = \frac{P_{stag} - P_x}{\frac{1}{2} \rho V_\infty^2} \qquad (A.7)$$

or, for this case:

$$C_{P_X} = \frac{P_o - P_x}{P_o - P_{7u}} . \qquad (A.8)$$

Thus, Equation (A.8) can be substituted into Equation (A.6) yielding:

$$\sigma' = \frac{P_{2u} - P_c}{P_o - P_{2u}} \cdot C_{P_{2u}} + C_{P_{2u}} - 1. \qquad (A.9)$$

During the actual testing, P_{2u}, P_c, and P_o were measured and the pressure coefficient values for $C_{P_{2u}}$ were obtained from Figure 12.

APPENDIX B

TUNNEL BLOCKAGE CORRECTION

In order to compare the results obtained in the NASA tunnel to other facilities, the effect of tunnel blockage had to be determined. The ratio of the model diameter to test section diameter in the NASA tunnel is $\frac{0.24}{1.50}$ and, thus, the velocity field will be perturbed due to the interference of the walls on the model. This blockage could have three major effects: 1) the velocity in the vicinity of the model could be increased affecting the cavitation number, 2) the cavity geometry could be distorted due to the rapidly changing pressure gradients along the blocked area, and 3) the rate at which vapor is carried from the cavity could be altered because of the changing gradients along the cavity wall.

Therefore, an identical test series was conducted in an unblocked condition in the 12-inch water tunnel using the same ogive where the model diameter to tunnel diameter ratio is $\frac{0.24}{12.0}$. In this test series, using the identical flow conditions as obtained in the NASA tunnel, the cavitation number, the cavity entrained flow rate, and the cavity dimensions were measured for various flow conditions.

Thus, the results of the unblocked-blocked test series can be compared and, in summary:

1. for similar flow conditions of velocity and (L/D), the entrainment flow coefficient (C_Q) is identical for the blocked and unblocked cases,
2. the geometry of the cavity, Appendix C, is also identical for the two cases under similar flow conditions, and
3. the cavitation numbers differed by a constant, solely a function of (L/D), Figure 13.

Therefore, the only blocked-unblocked correction factors for the 0.24-inch ogive are for the various cavity-cavitation numbers and are:

Cavity 1, L = 0.500 inch

N = 1.10

Cavity 2, L = 0.875 inch

N = 1.23

Cavity 3, L = 1.25 inch

N = 1.32

where $$N = \frac{\text{Uncorrected Cavitation Number}}{\text{Corrected Cavitation Number}} \tag{B.1}$$

APPENDIX C

PHOTOGRAPHIC MEASUREMENT OF CAVITY SIZES

The profile shapes of the natural and entrained cavities were photographed for each set of stable test conditions; i.e., velocity, cavity length, and temperature. The exposure time was chosen such that a long time average of the cavity shape could be obtained without impairing the clarity of the cavity profile. Figures 14 and 15 are typical examples of photographs of natural and entrained cavities for a given flow condition. The dark background makes the cavity profile stand out in silhouette.

The cavity shape was measured by projecting lines on the photographic pictures and measuring the position of the upper and lower edges of the cavity relative to the horizontal reference line drawn through the center of the cavity. Then, these measurements were converted to actual distance by a mathematical equation established by a reference frame to account for the distortion of the tunnel test section. The results of cavity 2, L = 0.875 inch, speeds 40, 67, 120 fps, are shown in Figures 16, 17, and 18 for natural and entrained cavities. Also, the cavity shape was fitted to an ellipse and the comparisons can be noted in the figures.

The cavity shape data for various velocities and cavity lengths as noted by Waid (3) can be analyzed for the characteristic dimensions such as maximum cavity diameter, and the cavity half length denoted as the distance from the leading edge to the axial point where the maximum cavity diameter occurs. Dimensionless forms of these results are presented in Figures 19 and 20 as functions of cavitation number, independent of both model size and free stream velocity. The following conclusions are made about the shape of a cavity formed by a zero-caliber-ogive:

1) For a given cavitation number, the shape is independent of free stream velocity.
2) For a given cavitation number, the shape defined by the length of the cavity under natural cavitation conditions and the shape of the cavity under entrained conditions are identical, within a small experimental error.
3) The proportions of the cavity are solely dependent upon the cavitation number.
4) The shape of the cavity can be approximated by an elliptical equation for the range of Froude numbers encountered in this investigation.
5) The size of the cavity is directly proportional to the nose diameter.

These conditions exist for the ranges of variables encountered in the NASA tunnel and the 12-inch water tunnel for the 0.24- and 0.50-inch zero-caliber-ogive and are in agreement with the results reported by Waid, Reference 3.

APPENDIX D

POLYNOMIAL REPRESENTATIONS OF THE PHYSICAL PROPERTIES OF WATER AND FREON 113

For the reduction of data, nine thermodynamic properties of working fluid were curve fitted by the use of polynomials. Of these nine properties, seven were chosen as independent variables, and, for water, these are:

1) latent heat of evaporation
2) liquid thermal conductivity
3) vapor pressure
4) kinematic viscosity
5) thermal diffusivity
6) density of liquid
7) density of vapor,

and for Freon 113, these are:

1) latent heat of evaporation
2) liquid thermal conductivity
3) vapor pressure
4) dynamic viscosity
5) liquid heat capacity

6) density of liquid

7) density of vapor

These properties are listed in the following tables, and all polynomials are given in the form:.

$$f(x) = a_0 + a_1x + a_2x^2 + \ldots + a_nx^n$$

TABLE 1

PHYSICAL PROPERTIES OF WATER

1) $f(x)$ = latent heat of evaporation

x = temperature - $^{\circ}F$

valid range: 50 to 300° F

units: Btu/ $\frac{lb - sec^2}{in}$

$a_0 = 0.42008 \times 10^{6}$
$a_1 = 0.2187 \times 10^{3}$
$a_2 = 0.31145 \times 10^{-1}$
$a_3 = 0.19905 \times 10^{-3}$
$a_4 = 0.29806 \times 10^{-6}$

2) $f(x)$ = liquid thermal conductivity

x = temperature - $^{\circ}F$

valid range: 50 to 300° F

units: Btu/in - sec - $^{\circ}F$

$a_0 = 0.65793 \times 10^{-5}$
$a_1 = 0.30025 \times 10^{-7}$
$a_2 = -0.15183 \times 10^{-9}$
$a_3 = 0.77712 \times 10^{-12}$
$a_4 = -0.19221 \times 10^{-14}$
$a_5 = 0.18536 \times 10^{-17}$

3) $f(x)$ = vapor pressure

x = temperature - $^{\circ}F$

valid range: 50 to 300° F

units: lb/in^2

$a_0 = 0.75335 \times 10^{-1}$
$a_1 = 0.65231 \times 10^{-2}$
$a_2 = 0.10236 \times 10^{-3}$
$a_3 = 0.17362 \times 10^{-5}$
$a_4 = 0.78075 \times 10^{-8}$
$a_5 = 0.47494 \times 10^{-10}$
$a_6 = -0.35612 \times 10^{-13}$
$a_7 = 0.57462 \times 10^{-17}$

4) $f(x)$ = kinematic viscosity

x = temperature - $^{\circ}$F

valid range: 50 to 300° F

units: in^2/sec

$a_0 = 0.45038 \times 10^{-2}$
$a_1 = 0.71226 \times 10^{-4}$
$a_2 = 0.507829 \times 10^{-6}$
$a_3 = 0.11875 \times 10^{-8}$
$a_4 = 0.53696 \times 10^{-11}$
$a_5 = 0.41227 \times 10^{-13}$
$a_6 = 0.97242 \times 10^{-16}$
$a_7 = 0.81121 \times 10^{-19}$

5) $f(x)$ = thermal diffusivity

x = temperature - $^{\circ}$F

valid range: 50 - 300° F

units: in^2/sec

$a_0 = 0.17949 \times 10^{-3}$
$a_1 = 0.58709 \times 10^{-6}$
$a_2 = -0.53350 \times 10^{-8}$
$a_3 = 0.24478 \times 10^{-10}$
$a_4 = 0.62563 \times 10^{-13}$
$a_5 = 0.61034 \times 10^{-16}$

6) $f(x)$ = density of liquid

x = temperature - $^{\circ}$F

valid range: 50 - 300° F

units: $\frac{lb - sec^2}{in^4}$

$a_0 = 0.93446 \times 10^{-4}$
$a_1 = 0.12941 \times 10^{-7}$
$a_2 = 0.21040 \times 10^{-9}$
$a_3 = 0.40362 \times 10^{-12}$
$a_4 = 0.40563 \times 10^{-15}$

7) $f(x)$ = density of vapor

x = temperature - $^{\circ}$F

valid range: 50 - 300° F

units: $\frac{lb - sec^2}{in^4}$

$a_0 = 0.25426 \times 10^{-10}$
$a_1 = 0.56520 \times 10^{-11}$
$a_2 = 0.18195 \times 10^{-12}$
$a_3 = 0.17299 \times 10^{-14}$
$a_4 = 0.15136 \times 10^{-16}$
$a_5 = 0.37683 \times 10^{-19}$

TABLE 2

PHYSICAL PROPERTIES OF FREON 113

1)	$f(x)$	= latent heat of evaporation	a_0 =	0.7257×10^{2}
			a_1 =	0.15243×10^{0}
	x	= temperature - $^{\circ}$F	a_2 =	0.20793×10^{-2}
	valid range:	$50 - 260^{\circ}$ F	a_3 =	0.24599×10^{-4}
	units:	Btu/lb_m	a_4 =	0.15211×10^{-6}
			a_5 =	0.49195×10^{-9}
			a_6 =	0.18981×10^{-8}
2)	$f(x)$	= liquid thermal conductivity	a_0 =	0.10231×10^{-5}
			a_1 =	0.18981×10^{-8}
	x	= temperature - $^{\circ}$F		
	valid range:	$50 - 350^{\circ}$ F		
	units:	Btu/sec - in - $^{\circ}$F		
3)	$f(x)$	= vapor pressure	a_0 =	0.33066×10^{2}
	$\log_{10}(fx)$	$= a_0 + a_1 x^{-1} + a_2 \log_{10}(x) + a_3 x$	a_1 =	-0.43310×10^{4}
			a_2 =	-0.92635×10^{1}
	x	= temperature - $^{\circ}$R	a_3 =	0.20539×10^{-2}
	valid range:	$50 - 300^{\circ}$ F		
	units:	lb/in^2		

4) $f(x)$ = dynamic viscosity

x = temperature - ^{o} F

valid range: 50 - 300^{o} F

units: lb/sec - in

$a_0 = 0.67229 \times 10^{-4}$
$a_1 = -0.54011 \times 10^{-6}$
$a_2 = 0.19505 \times 10^{-8}$
$a_3 = 0.251147 \times 10^{-11}$
$a_4 = 0.52724 \times 10^{-13}$
$a_5 = 0.18411 \times 10^{-15}$
$a_6 = 0.21638 \times 10^{-18}$

5) $f(x)$ = liquid heat capacity

x = temperature - ^{o} F

valid range: 50 - 260^{o} F

units: Btu/lb_m - ^{o} F

$a_0 = 0.26161 \times 10^{0}$
$a_1 = -0.27963 \times 10^{-2}$
$a_2 = 0.55381 \times 10^{-4}$
$a_3 = -0.51461 \times 10^{-6}$
$a_4 = 0.25985 \times 10^{-8}$
$a_5 = -0.67648 \times 10^{-11}$
$a_6 = 0.71158 \times 10^{-14}$

6) $f(x)$ = density of liquid

x = temperature - ^{o} F

valid range: 50 - 350^{o} F

units: lb_m/in^3

$a_0 = 0.59925 \times 10^{-1}$
$a_1 = -0.41238 \times 10^{-4}$
$a_2 = -0.36806 \times 10^{-7}$

7) $f(x)$ = density of vapor

x = temperature - ^{o} F

valid range: 50 - 300^{o} F

units: lb_m/in^3

$a_0 = -0.28237 \times 10^{-4}$
$a_1 = 0.37254 \times 10^{-5}$
$a_2 = -0.80744 \times 10^{-7}$
$a_3 = 0.13063 \times 10^{-8}$
$a_4 = -0.10270 \times 10^{-10}$
$a_5 = 0.48679 \times 10^{-13}$
$a_6 = -0.12079 \times 10^{-15}$
$a_7 = 0.12307 \times 10^{-18}$

APPENDIX E

DETERMINATION OF THE ENTRAINMENT COEFFICIENT

In order to apply the entrainment theory for various flow conditions, a relationship for estimating the flow coefficient must be obtained. One of the first experimental investigations into the factors that affect air entrainment was conducted at the California Institute of Technology in 1951 by Swanson and O'Neill (20). They noted that the rate required to maintain a constant cavity size was determined largely by the process at which the air flow was entrained away. Thus, the flow regime for a ventilated cavity was divided into two classes: 1) cavity flows with a re-entrant jet, and 2) cavity flows with trailing twin vortices.

It was experimentally found that, for the twin vortices regime, as the supply of air was decreased, the cavity size decreased only slightly over a large range of air supply rates until a certain minimum rate of air supply was reached. At the point, the re-entrant jet forms and a slight decrease in the air supply led to a rapid reduction in the size of the cavity. This is a significant result because the flow regime defines the parameters which affect the entrainment coefficient.

For the case of the ogive with the cavity sizes and velocities obtained in the NASA tunnel, the entrainment coefficients measured as in Figure 21 were all in the re-entrant jet regime. In this regime, O'Neill states that the reciprocal of the Froude number tends to be a significant parameter. Also, a further generalization is made by Reichardt (21) by employing the maximum cavity diameter and the Froude number as the important parameters.

From the experimental results, maximum cavity diameter/model diameter versus cavitation number, Figure 18, and cavity length/model diameter versus maximum cavity diameter/model diameter, Figure 22, show that the cavitation number can be expressed as a function of cavity length/model diameter. Therefore, the flow coefficient defined as:

$$C_Q \equiv \frac{Q}{d^2 V_\infty} \tag{E.1}$$

was solved as a function of the dimensionless group

$$C_Q \sim \frac{1}{\left(\dfrac{V_\infty}{\sqrt{gL}}\right)} \cdot (L/D) \tag{E.2}$$

for the regime encountered testing the 0.24- and 0.50-inch zero-caliber-ogive.

To obtain the experimental values of the flow coefficient, the primary test series for the two ogives was conducted in the 12-inch water tunnel. The equipment used can be seen in Figure 11, and the procedure for measuring the volumetric flow rate was as follows: 1) establish a pressure in the tunnel above the model incipient cavitation number, 2) adjust the throttle valve between the air supply tank and the ball flowmeter so that a certain cavity length appeared which was determined by a line scribed on the model, and 3) read the flowmeter, pressure at the flowmeter, and the necessary tunnel and cavity pressures to establish the cavitation number of the prescribed cavity. With this information and a theory of correlation based on a dimensionless combination of Stoke's law and flow coefficients, it was relatively simple to calculate the volumetric flow rate at the conditions which existed at the flowmeter. Then, this resultant flow rate could be corrected to cavity conditions, and the flow coefficient could be calculated. Finally, this procedure was applied to various cavity lengths, velocities, model diameters, and water temperatures.

The results of the entrainment tests are shown in Figures 23, 24, 25, and 26 and, in summary, are as follows:

1) For a given velocity and model diameter, as the flow coefficient increased, the cavity size increased and the corresponding cavitation number decreased.

2) The entrainment coefficient decreased for a constant cavitation number and, hence, (L/D) as velocity increases.

3) No appreciable change in entrainment coefficient was found for a fixed cavity shape and velocity as temperature was increased to 200° F in water.

4) For a given velocity and cavitation number as (L/D), the flow coefficient increased with increasing model diameter.

These results are in qualitative agreement with the results of Swanson and O'Neill (20), and Cox and Claydon (22).

Finally, the non-dimensional form for predicting the flow coefficient for the regime encountered in this investigation can be derived from the data is approximated by:

$$C_Q \approx k\left(\frac{1}{Fr}\right)^{0.75} (L/D)^{0.98} \qquad (E.3)$$

This result is in qualitative agreement with the conclusion by Brennen (16) that the volume rate of entrainment was dependent only on cavitation number or (L/D) and tunnel velocity.

APPENDIX F

SURFACE-VOLUME RELATIONSHIPS FOR NATURAL AND ENTRAINED CAVITIES

The analytical equation describing the cavity profile must meet the requirements of being tangent to the nose surface at the point of flow separation, and parallel to the free stream direction at the point of maximum diameter. To satisfy these requirements, the analytic cavity shape should be in the quasi-elliptical form:

$$\frac{X^2}{m^2} + \frac{Y^2}{m^2} + \frac{(z - a)^2}{n^2} = 1 \ , \qquad \text{(F.1)}$$

where the cavity is oriented as shown in Figure 57.

To use Equation (F.1), photographs of entrained cavities and natural cavities were taken, and the parameters such as the center of the cavity, the maximum cavity diameter, and length of the cavity were measured. From these results, plots of a/d versus cavitation number, Figure 20, and of d_m/d versus cavitation number, Figure 19, were established with the result that the shape of the cavity is independent of free stream velocity for a given cavitation number. Also, even more important is the result that both the entrained and natural cavities for the 0.24- and 0.50-inch ogive coincide on the same curve.

Now, by specifying a specific cavitation number, the elliptical equation of the cavity can be solved analytically, and the results of several cavities are shown in Figures 16, 17, and 18. Also, on these figures, actual measured points for entrained and natural cavities are shown. It can be seen that the results correlate within a reasonable experimental error.

Finally, when using the entrainment theory for predicting the temperature depression inside a cavity, the approximate area of the cavity must be known. To do this, an integration was conducted over the cavity formed by the zero-caliber-ogive.

From Figure 58, we can say:

$$\Delta A_k \approx (\Delta S)_k \cos\theta$$

or

$$\Delta S_k \approx \frac{1}{\cos\theta_k} \Delta A_k \tag{F.2}$$

From the equation of the surface:

$$F(x,y,z) = \frac{X^2}{m^2} + \frac{Y^2}{m^2} + \frac{(z-a)^2}{n^2} - 1 = 0, \tag{F.3}$$

the gradient can be obtained and is:

$$\text{grad } F = \frac{\partial F}{\partial X}\vec{i} + \frac{\partial F}{\partial Y}\vec{j} + \frac{\partial F}{\partial Z}\vec{k}$$

$$= 2x/m^2\,\vec{i} + 2y/m^2\,\vec{j} + 2(z-a)/n^2\,\vec{k}\ . \tag{F.4}$$

Now, the unit vector normal to the surface of the ellipse can be solved:

$$\vec{N} = \frac{\frac{2x}{m^2}\vec{i} + \frac{2y}{m^2}\vec{j} + \frac{2(z-a)}{n^2}\vec{k}}{\left\{\frac{4x^2}{m^4} + \frac{4y^2}{m^4} + \frac{4(z-a)^2}{n^4}\right\}^{\frac{1}{2}}} \tag{F.5}$$

and finally:

$$\cos\theta = \vec{n}\cdot\vec{i} =$$

$$\frac{2x/m^2}{\left\{\frac{4x^2}{m^4} + \frac{4y^2}{m^4} + \frac{4(z-a)^2}{n^4}\right\}^{\frac{1}{2}}} \tag{F.6}$$

Thus, Equation (F.2) becomes:

$$\Delta S_k = \left\{\frac{x^2/m^4 + y^2/m^4 + \frac{(z-a)^2}{n^2}}{x^2/m^2}\right\}^{\frac{1}{2}} (\Delta A)_k, \tag{F.7}$$

and over the entire area, we have:

$$S = \int_{z_1}^{z_2}\int_{y_1}^{y_2} f\,(y,\,z)\,dydz = \iint_R \Delta S_k \tag{F.8}$$

To integrate Equation (8), the variable x must be replaced by:

$$x = \left\{ \left[1 - y^2/m^2 - \frac{(z-a)^2}{n^2}\right] m^2 \right\}^{\frac{1}{2}} \tag{F.9}$$

and finally the integral becomes:

$$S = 4\frac{m}{n} \int_0^L \int_0^{m\left[1 - \frac{(z-a)^2}{n^2}\right]^{\frac{1}{2}}} \left\{ \frac{n^4 - (z-a)^2 (n^2 - m^2)}{m^2 n^2 - n^2 y^2 - m^2 (z-a)^2} \right\}^{\frac{1}{2}} dydz \tag{F.10}$$

Equation (F.10) can be integrated by substitution by variables and then integrating by parts. After this, the answer becomes:

$$S = \pi m \frac{(n^2 - m^2)^{\frac{1}{2}}}{n^2} \left\{ (L-a)\sqrt{n^4 - \frac{(L-a)^2}{n^2 - m^2} (n^2\ m^2)} \right.$$

$$+ \frac{n^4}{n^2 - m^2} \sin^{-1} \left\{ \frac{(L-a)\ (n^2 - m^2)}{n^2} \right\}^{\frac{1}{2}} + a\sqrt{n^4 - \frac{a^2 (n^2 - m^2)}{n^2 - m^2}}$$

$$\left. - \frac{n^4}{(n^2 - m^2)} \sin^{-1} \left[-a\frac{(n^2 - m^2)}{n^2} \right]^{\frac{1}{2}} \right\} \tag{F.11}$$

for all $m \neq n$.

Similarly, the volume of the cavity can be calculated from the integral:

$$\text{Volume} = 4 \int_0^L \int_0^{m\left[1 - \frac{(z-a)^2}{n^2}\right]^{\frac{1}{2}}} \int_0^{m\left[1 - y^2/m^2 - \frac{(z-a)^2}{n^2}\right]^{\frac{1}{2}}} dydz \tag{F.12}$$

and the result is:

$$\text{Volume} = \pi \left\{ m^2 L - m^2/n^2 \; \frac{(L - a)^3}{3} + \frac{m^2}{n^2} \; \frac{(-a)^3}{3} \right\} \quad . \qquad (F.13)$$

From these relationships for cavity volume and cavity surface area, the average cavity cross-sectional flow area can be calculated and also the ratio (d^2/A_w) could be plotted, Figure 27.

APPENDIX G

SOLUTION OF THE HEAT TRANSFER COEFFICIENT

To evaluate the rate of heat transfer by convection between a fluid-gas boundary, the following equation is normally applied:

$$\dot{q}_{surface} = A_w \bar{h} (T_\infty - T_w) \tag{G.1}$$

This equation seems quite simple; however, the simplicity is misleading because the above equation is a definition of the average unit thermal convective conductance rather than a law of heat transfer by convection. Thus, the coefficient is actually a complicated function of the fluid flow, the thermal properties of the fluid medium, and the geometry of the system.

Of the major methods available for the evaluation of convective-heat-transfer coefficient, dimensional analysis is mathematically simple and has found the widest range of application. However, the chief limitation of this method is that results obtained by it are incomplete and inadequate without experimental data.

Now, from the description of the convective-heat transfer process, it is reasonable to expect that the physical quantities listed below are pertinent to the problem.

1. cavity length, [L] = L

2. thermal conductivity of the fluid, $[\frac{ML}{t^3 \cdot T}] = k_L$

3. velocity of the fluid, [L/t] = V_∞

4. density of the fluid, $[M/L^3] = \rho_L$

5. viscosity of the fluid, $[\frac{M}{L \cdot t}] = M_L$

6. specific heat at constant pressure, $[\frac{L^2}{t^2 \cdot T}] = C_P$

7. heat-transfer coefficient, $[\frac{M}{t^3 \cdot T}] - \bar{h}$

8. buoyancy force, $[\frac{M - L}{t^2}] - F$

where M = mass

L = length

t = time

T = temperature

There are eight physical quantities and four primary dimensions. Thus, it can be estimated that the number of dimensionless groups required to correlate the data will be the number of variables minus the number of primary dimensions or four dimensionless groups, Reference 25. From previous results in the field of convective heat transfer, the functional relationship can be written as:

$$Nu = f\ (Re, Pr, Fr), \tag{G.2}$$

where

$$Nu = \frac{\bar{h}L}{k_L} = \text{Nusselt number}$$

$$Re = \frac{VL\rho_L}{\mu_L} = \text{Reynolds number,}$$

$$Pr = \frac{C_p\mu_L}{k_L} = \text{Prandtl number, and}$$

$$Fr = V/\sqrt{gL} = \text{Froude number.}$$

This case in which the Froude number is included in the heat transfer coefficient has occurred frequently in the literature for the case of liquid flow over a large spherical volume.

Now it remains that the powers of Reynolds number, Prandtl number and Froude number be solved by correlation of experimental data. To do this, the expression for h derived by simple heat balance in the entrainment theory must be used. The derived expression is:

$$\bar{h} = \frac{\frac{\dot{q}_{surface}}{A_w}}{\Delta t}$$

$$= \frac{\lambda \cdot C_Q \cdot V_\infty \cdot d^2 \cdot \rho_v}{\Delta t \cdot A_w} \tag{G.3}$$

Using this equation and the temperature depressions measured in water and Freon 113 where velocity, cavity length, and temperature were variables, the trends in the heat transfer coefficient can be established and, hence, the exponents can be estimated. In summary, the heat transfer coefficient must have the following properties:

for water

1. As the cavity length increases, the heat transfer coefficient decreases for a given temperature and velocity.
2. The heat transfer coefficient decreases slightly as temperature increases for a given cavity length and velocity.
3. No significant change in the coefficient was found for increasing velocity for a given temperature and cavity length.

for Freon 113

1. The coefficient decreases as cavity length increases for a given velocity and temperature.
2. Again, no significant velocity effect was found for a given temperature and cavity length.
3. The heat transfer coefficient decreases very slightly as temperature increases for a given cavity length and velocity,

and thus, for the coefficients, we have:

$$h_c = 150.0 \left(\frac{k_L}{L'} \right) (Re)^{0.35} (Pr)^{0.45} (Fr)^{-0.40} \tag{G.4}$$

From the above equation, it can be seen that the real function of the Froude number in the above case was to reduce the importance of the velocity effect and, hence, the Reynolds number. Also, the power on the Prandtl number indicates that the dependence is increased.

This effect of large Prandtl and little Reynolds number dependence differs somewhat from the standard type of convection heat transfer coefficient such as:

$$h_c = 0.036 \frac{(k_L)}{L} (Re)^{0.8} (Pr)^{0.33} \tag{G.5}$$

which is for turbulent flow over a flat plate; however, the trend in temperature and cavity length is in agreement with Equation (G.4). Therefore, if the physics of the problem is basically correct, it seems that the regime of heat transfer which compares favorably to the solved results is nucleate boiling with forced convection (23).

The system which is used to describe this regime consisted of a vertical annulus containing an electrically heated stainless steel tube placed centrally in tubes of various diameters. Then, the temperature difference between the heating surface and the bulk of the fluid was measured for various velocities and pressure. The results noted that the onset of boiling caused by increasing the heat flux depends on the velocity of the liquid and the degree of subcooling below its saturation temperature at the prevailing pressure. At lower pressures, the boiling point at a given velocity is reached at lower heat fluxes. An increase in velocity increases the effectiveness of forced convection, decreased the surface temperature at a given heat flux, and thereby delays the onset of boiling. However, it was found experimentally that, in the boiling region, the heat transfer coefficient, $\bar{h} = \frac{\mathring{q}/A}{\Delta T}$, is practically independent of the fluid velocity.

Although very little theoretical work has been done with this case, some for the major variables involved for film forced convection vaporization, which is similar in nature, can be expressed as given in Reference 24 as:

$$\bar{h} = \text{constant} \left\{ \frac{k_L^{\,3} \, (\rho_L)^2 \, g\lambda}{L \, \mu_L \, \Delta T} \right\}^k , \tag{G.6}$$

where k is around 0.25. Thus, if nucleate boiling with forced convection is more representative of this case, the Re, Pr, and Fr representation is incorrect, and Equation (G.4) should be written as:

$$h_c = 150.0 \left\{ \frac{k_L^{\,0.55} \, g^{0.18} \, \rho_L^{\,0.35} \, C_P^{\,0.45}}{L^{0.47} \, \mu_L^{\,-0.10}} \right\} , \tag{G.7}$$

keeping in mind that ΔT was eliminated as a variable.

In summary, the heat transfer coefficient obtained from experimental results and the assumptions made in the entrainment theory seem to be similar in nature to those obtained in either film forced convection vaporization or nucleate boiling with forced convection regime. However, at this time, the non-dimensional variables Re, Pr, and Fr in the entrainment theory will be retained.

APPENDIX H

EXTRAPOLATION OF TEMPERATURE DEPRESSIONS FROM MEASURED DATA

The temperature depression profile in the cavitated region was determined by first measuring the depressions at various stations, then a "best-fit" curve was drawn through the data points. Thus, the maximum depression, which experimenters have shown occurs at the nose of the model, was obtained by extending the profile curve. Then, the "transferred" temperature depression, that being the predicted depression at the nose, was plotted on the curves.

In general, Figures 51 and 52 represent a typical temperature data scatter for a particular tap location. From this, a weighted average was established for each group of temperatures. These averages were plotted on a temperature depression versus non-dimensional thermocouple distance location plot where the non-dimensional thermocouple is defined as the distance of the thermocouple from the nose divided by the cavity length. Then a straight line was drawn through the tap results and extended to the nose, Figures 53 and 54, where the maximum temperature depression was obtained.

APPENDIX I

DETERMINATION OF THE MINIMUM CAVITY PRESSURE

Pressure measurements were obtained at four locations along the cavity to determine 1) the point of minimum pressure, 2) the pressure profile inside the cavity, and 3) the fluctuations of the pressures at several locations. The pressures were measured through the pressure ports on the model surface, fed into a transducer, and read by an integrating voltmeter. Thus, the transducer responded almost instantaneously and the voltmeter integrated over various set time periods.

In general, the measured pressure and temperature depression were not in thermodynamic equilibrium; the pressures inside the cavity fluctuated greatly, as shown in Figure 55. However, as the thermodynamic effect became significant, the cavity pressures became more stable and a definite pressure pattern was formed, Figure 56. In this case, the pressure was lowest at the nose of the cavity, remained constant at a slightly higher pressure through the mid-section, and rapidly increased at the end of the cavity. This was found for both water and Freon 113 cavities.

To study this in some detail, four pressure taps were located equally along the center line for the cavity length of 0.875 inch, with the first one being at the nose and the last one at the end of the cavity. The results of the pressures were:

1) The lowest pressure inside the cavity; has high frequency, small oscillatory pressures.
2) In most cases, the next lowest pressure inside cavity; has low frequency, quite substantial oscillatory pressures.
3) Slightly above average pressure of tap no. 2; has very constant pressure with little oscillations.
4) Highest pressure inside cavity; has high amplitude, low frequency oscillations.

These results seem to indicate that some kind of process was taking place in the region of the cavity before mid-point. This process might have been due to rapidly varying pressure gradients and increasing flow area which occurred after the small forward section of the cavity. The rapid change of pressure at the end of the cavity was due to the cavity length variations caused by bubble collapse.

Finally, the forward tap was chosen as the model representative of the cavity, and the cavitation numbers were based on this tap. Also, this tap turned out to be a good selection because the cavitation number for a fixed geometry became independent of temperature.

TABLE I

PHYSICAL PROPERTIES OF WATER

T	P_v	α	ρ_v	ρ_L	ν_L	K_L	λ	C_P	μ
^oF	lb/in^2	in^2/sec	$\frac{lb\text{-}sec^2}{in^4}$	$\frac{lb\text{-}sec^2}{in^4}$	in^2/sec	$\frac{Btu}{in\text{-}sec\text{-}^oF}$	$\frac{Btu}{lb\text{-}sec^2/in}$	$\frac{Btu}{\frac{^oF\text{-}lb\text{-}sec^2}{in}}$	$\frac{lb\text{-}sec}{in^2}$
80	0.507	0.226×10^{-3}	0.238×10^{-8}	0.933×10^{-4}	0.134×10^{-2}	0.814×10^{-5}	0.403×10^{6}	0.385×10^{3}	0.125×10^{-6}
100	0.949	0.234	0.428	0.930	0.106	0.837	0.398	0.385	0.984×10^{-7}
120	1.69	0.240	0.737	0.926	0.869×10^{-3}	0.855	0.393	0.385	0.804
140	2.89	0.245	0.122×10^{-7}	0.921	0.735	0.872	0.389	0.385	0.677
160	4.74	0.250	0.193	0.915	0.634	0.885	0.388	0.386	0.580
180	7.51	0.254	0.298	0.909	0.554	0.896	0.381	0.387	0.503
200	11.53	0.258	0.446	0.902	0.488	0.905	0.376	0.388	0.440
220	17.19	0.262	0.648	0.895	0.435	0.911	0.370	0.389	0.389
240	24.97	0.265	0.918	0.887	0.394	0.915	0.366	0.390	0.349
260	35.43	0.266	0.127×10^{-6}	0.878	0.364	0.917	0.360	0.392	0.320
280	49.20	0.267	0.173	0.870	0.340	0.918	0.355	0.394	0.295
300	67.01	0.268	0.232	0.860	0.317	0.919	0.350	0.397	0.272

T = Temperature

P_v = Vapor Pressure

α = Thermal Diffusivity

ν_L = Kinematic Viscosity

K_L = Liquid Thermal Conductivity

C_{P_L} = Liquid Heat Capacity

μ = Dynamic Viscosity

λ = Latent Heat of Evaporation

ρ_L = Density of Liquid

ρ_v = Density of Vapor

TABLE II

PHYSICAL PROPERTIES OF FREON 113

T	P_V	α	ρ_V	ρ_L	ν_L	K_L	λ	C_P	μ
^{o}F	lb/in^2	in^2/sec	lb/in^3	lb/in^3	in^2/sec	$\frac{Btu}{sec\text{-}in\text{-}^{o}F}$	Btu/lb	$\frac{Btu}{lb\text{-}^{o}F}$	$\frac{lb}{sec\text{-}in}$
60	4.37	0.752×10^{-4}	0.862×10^{-4}	0.573×10^{-1}	0.730×10^{-3}	0.909×10^{-6}	0.672×10^{2}	0.211	0.418×10^{-4}
80	6.90	0.719	0.131×10^{-3}	0.564	0.642	0.871	0.659	0.215	0.362
100	10.48	0.682	0.194	0.554	0.570	0.833	0.645	0.220	0.316
120	15.39	0.646	0.278	0.544	0.511	0.795	0.629	0.226	0.278
140	21.94	0.612	0.388	0.534	0.463	0.757	0.613	0.231	0.248
160	30.44	0.579	0.529	0.524	0.423	0.720	0.596	0.237	0.222
180	41.23	0.547	0.707	0.513	0.389	0.681	0.577	0.242	0.199
200	54.67	0.515	0.927	0.502	0.359	0.644	0.556	0.249	0.180

T = Temperature

P_V = Vapor Pressure

α = Thermal Diffusivity

K_L = Liquid Thermal Conductivity

C_{P_L} = Liquid Heat Capacity

μ = Dynamic Viscosity

λ = Latent Heat of Evaporation

ρ_L = Density of Liquid

ρ_V = Density of Vapor

ν_L = Kinematic Viscosity

TABLE III

UNCORRECTED CAVITATION NUMBERS FOR

0.24-INCH ZERO OGIVE IN WATER

Velocity ft/sec	Temp. °F	Cavity in.	Reynolds Number x 10^6	Prandtl Number	Froude Number	Uncorrected Cavitation Number* Average
64	150	0.500	0.590	2.74	57.9	0.475
64	200	0.500	0.825	1.88	57.9	0.480
64	250	0.500	1.06	1.42	57.9	0.486
64	300	0.500	1.27	1.18	57.9	0.482
120	150	0.500	1.06	2.74	103.6	0.508
120	200	0.500	1.48	1.88	103.6	0.520
120	250	0.500	1.91	1.42	103.6	0.495
120	300	0.500	2.27	1.18	103.6	0.510
64	150	0.875	1.03	2.74	43.7	0.384
64	200	0.875	1.44	1.88	43.7	0.380
64	250	0.875	1.86	1.42	43.7	0.388
64	300	0.875	2.22	1.18	43.7	0.382
120	150	0.875	1.85	2.74	78.4	0.392
120	200	0.875	2.59	1.88	78.4	0.394
120	250	0.875	3.33	1.42	78.4	0.382
120	300	0.875	3.97	1.18	78.4	0.390
64	150	1.25	1.48	2.74	36.6	0.314
64	200	1.25	2.06	1.88	36.6	0.320
64	250	1.25	2.66	1.42	36.6	0.324
64	300	1.25	3.17	1.18	36.6	0.318
120	150	1.25	2.64	2.74	65.6	0.342
120	200	1.25	3.69	1.88	65.6	0.338
120	250	1.25	4.76	1.42	65.6	0.332
120	300	1.25	5.68	1.18	65.6	0.334

* Based upon minimum cavity pressure

TABLE IV

UNCORRECTED CAVITATION NUMBERS FOR

0.24-INCH ZERO OGIVE IN FREON 113

Velocity	Temp.	Cavity	Reynolds Number	Prandtl Number	Froude Number	Uncorrected Cavitation Number*
ft/sec	°F	in.	x 10^6			
64	75	0.500	0.608	9.05	57.9	0.485
64	125	0.500	0.807	7.81	57.9	0.478
64	175	0.500	1.01	7.11	57.9	0.470
64	225	0.500	1.23	6.87	57.9	-
120	75	0.500	1.09	9.05	103.6	0.516
120	125	0.500	1.45	7.81	103.6	0.507
120	175	0.500	1.82	7.11	103.6	0.514
120	225	0.500	2.19	6.87	103.6	-
64	75	0.875	1.06	9.05	43.7	0.380
64	125	0.875	1.41	7.81	43.7	0.388
64	175	0.875	1.78	7.11	43.7	0.380
64	225	0.875	2.15	6.87	43.7	-
120	75	0.875	1.91	9.05	78.4	0.405
120	125	0.875	2.53	7.81	78.4	0.386
120	175	0.875	3.18	7.11	78.4	0.395
120	225	0.875	3.84	6.87	78.4	-
64	75	1.25	1.52	9.05	36.6	0.328
64	125	1.25	2.01	7.81	36.6	0.334
64	175	1.25	2.54	7.11	36.6	0.330
64	225	1.25	3.06	6.87	36.6	-
120	75	1.25	2.72	9.05	65.6	0.335
120	125	1.25	3.61	7.81	65.6	0.340
120	175	1.25	4.55	7.11	65.6	0.334
120	225	1.25	5.48	6.87	65.6	-

* Based upon minimum cavity pressure

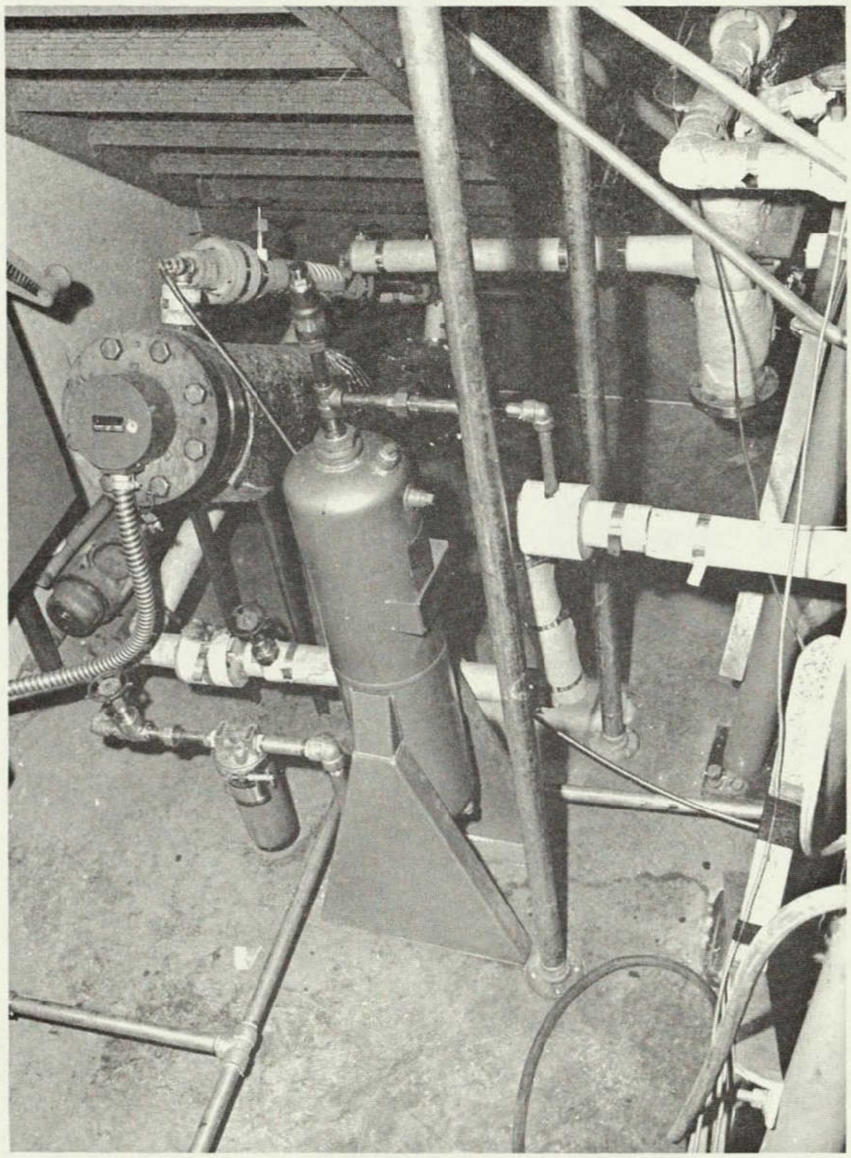

Figure 1 View of 40 KW Immersion Heater

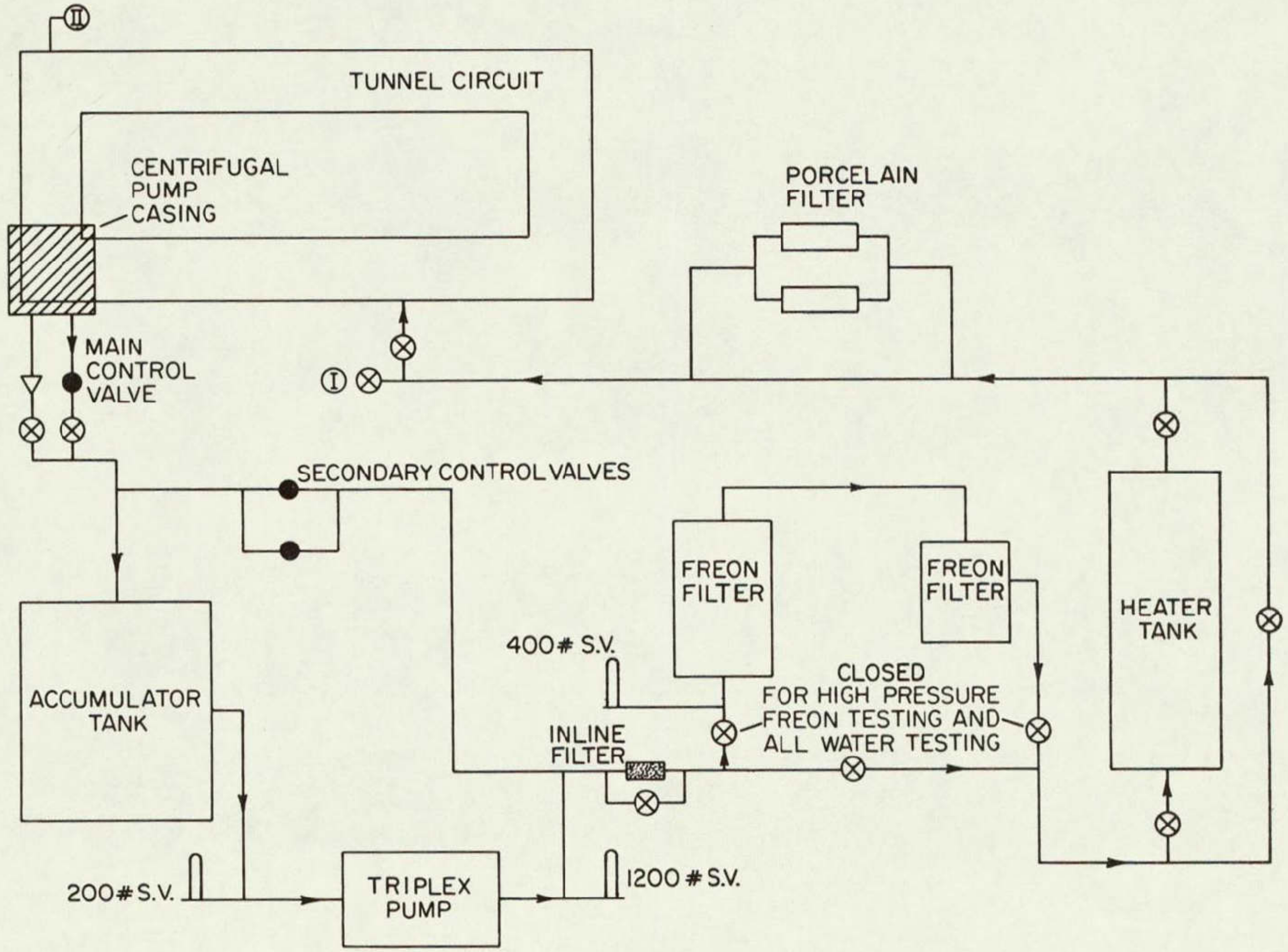

Figure 2 Schematic of Tunnel By-Pass System

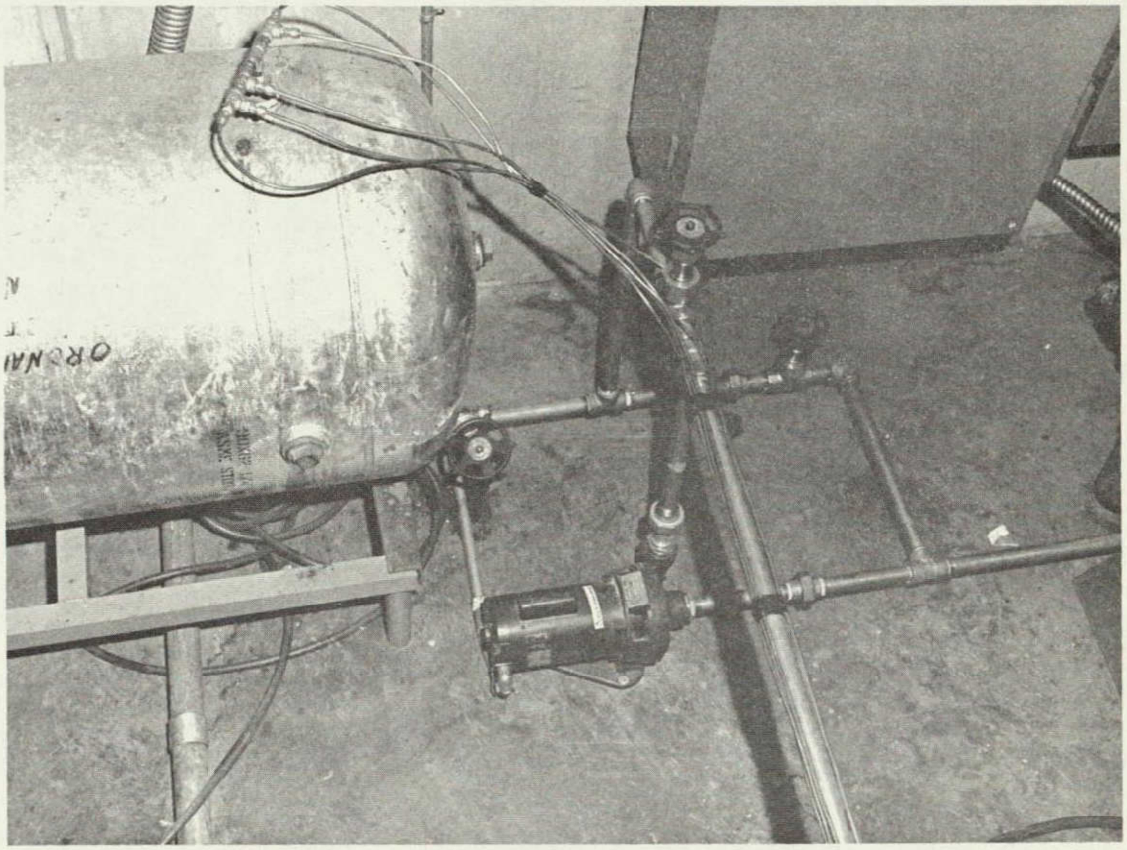

Figure 3 View of Freon Supply and Storage System

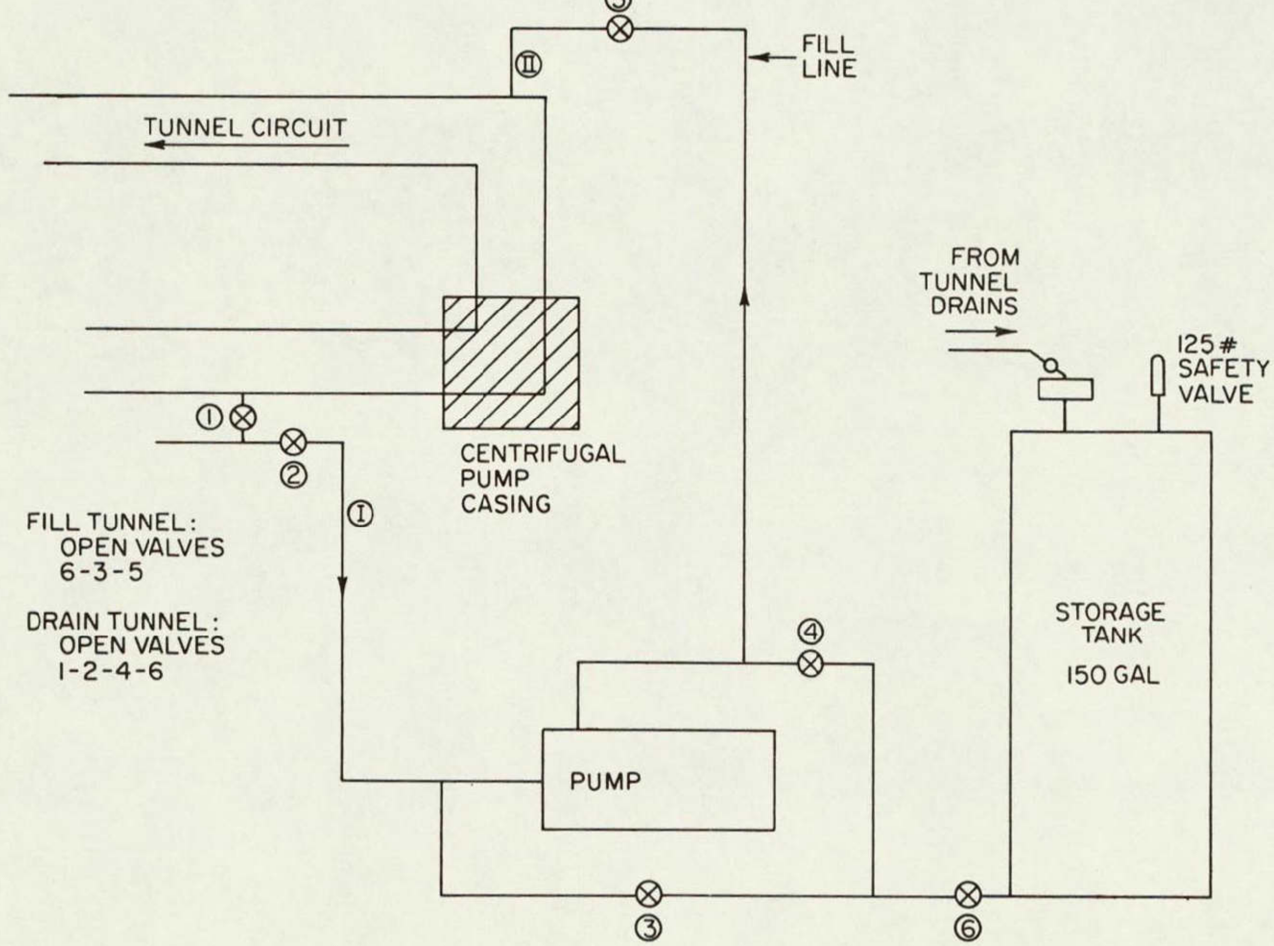

Figure 4 Schematic of Freon Supply and Storage System

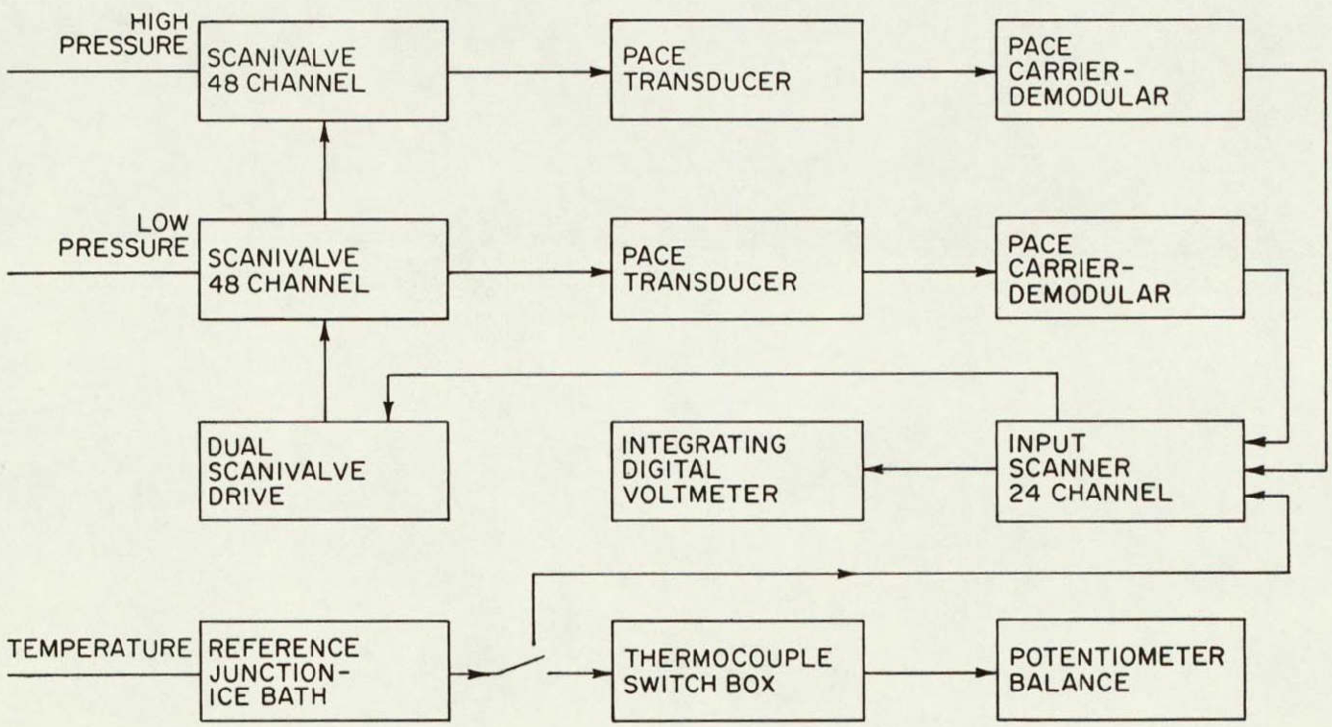

Figure 5 Schematic of Present Data Recording System

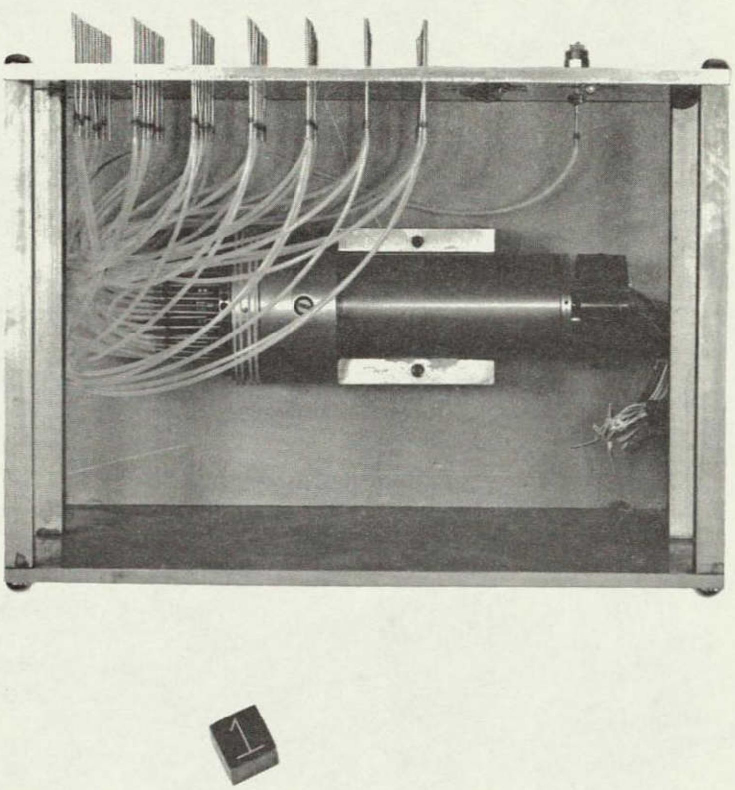

Figure 6 View of 1000 psi-48 Channel Scanivalve

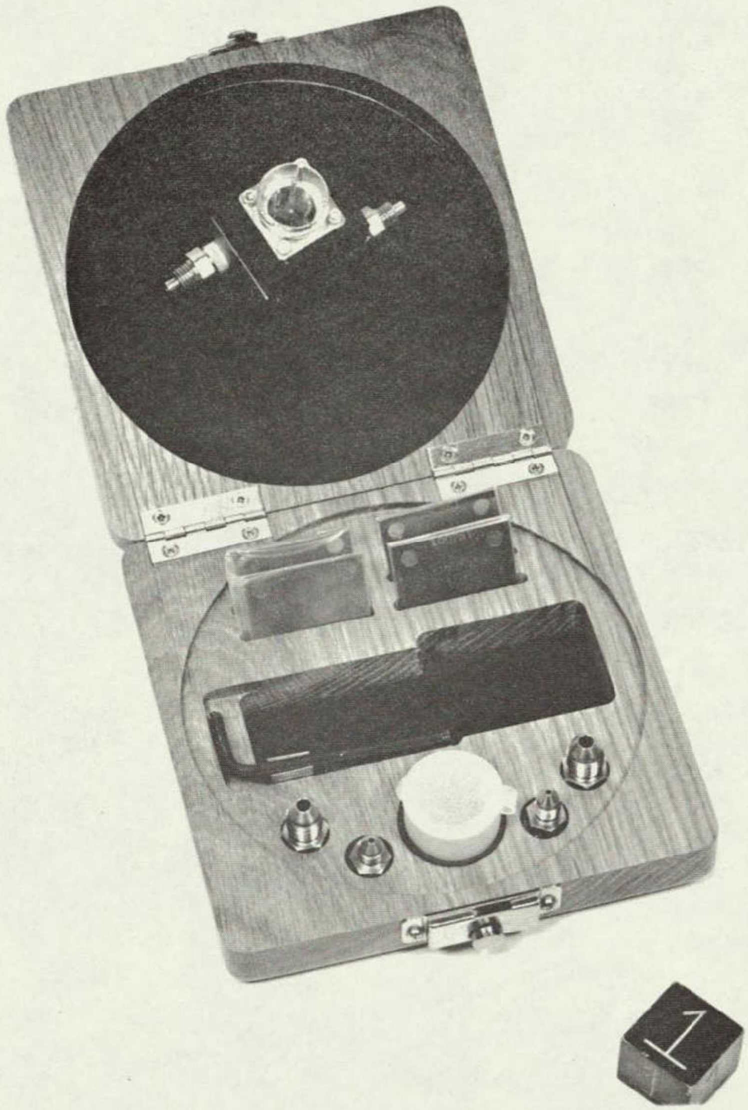

Figure 7 View of Pace Transducer and Pressure Diaphragms

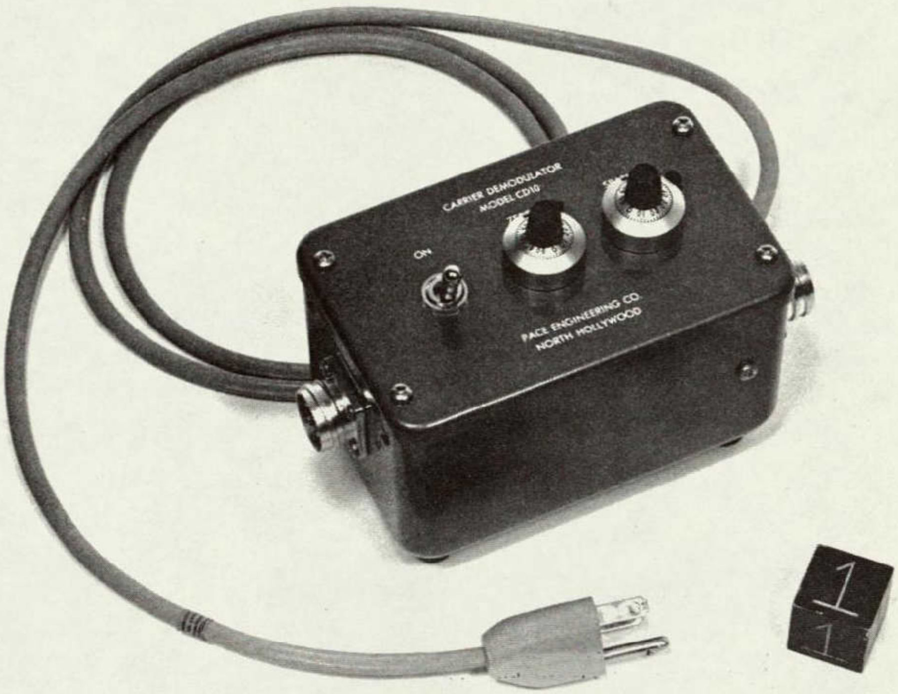

Figure 8 Pace Carrier-Demodulator for Transducer

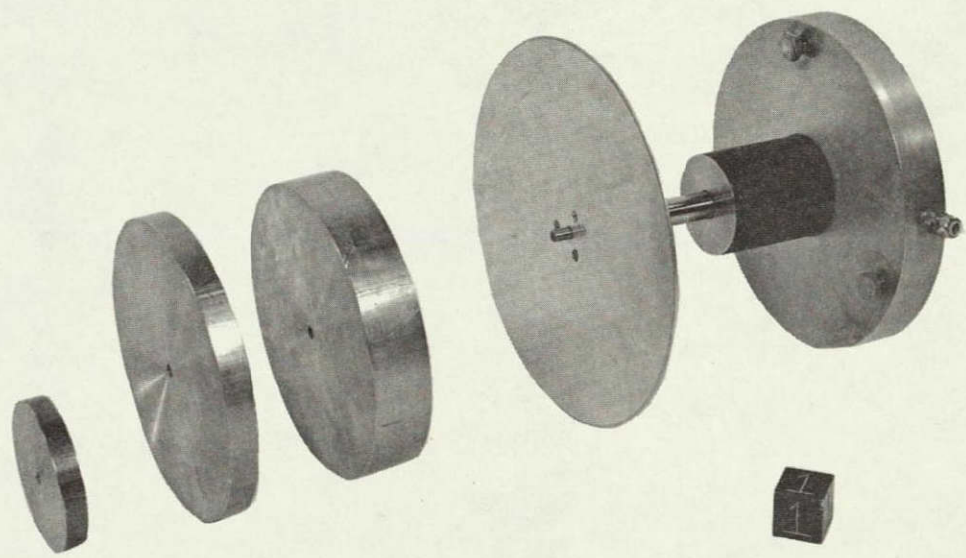

Figure 9 High Pressure Transducer Calibrator and Weights

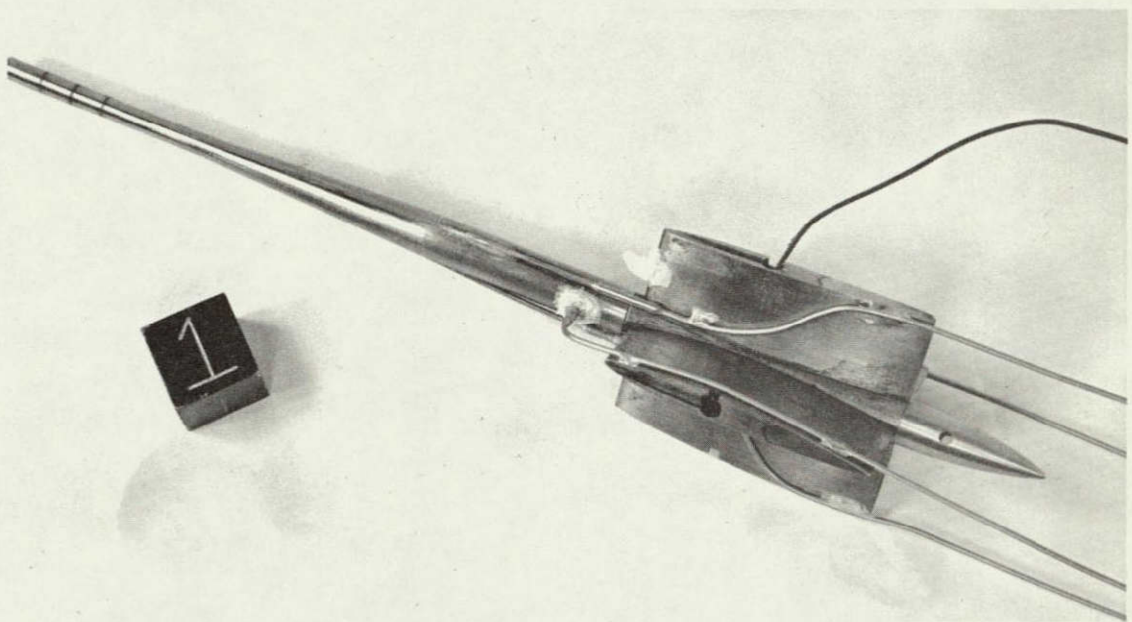

Figure 10 0.24-Inch Diameter Zero-Caliber-Ogive Model

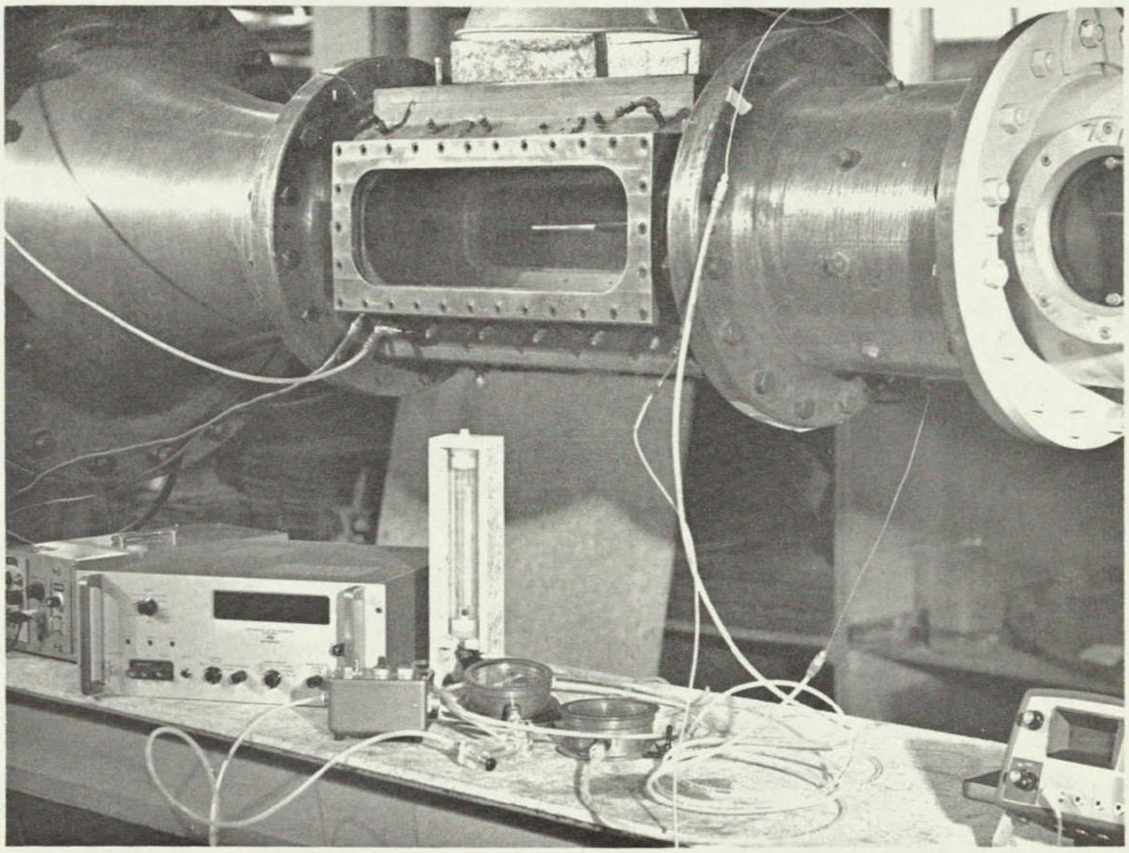

Figure 11 View of Flowmeter Used for Air Entrainment Test in 12-Inch Water Tunnel

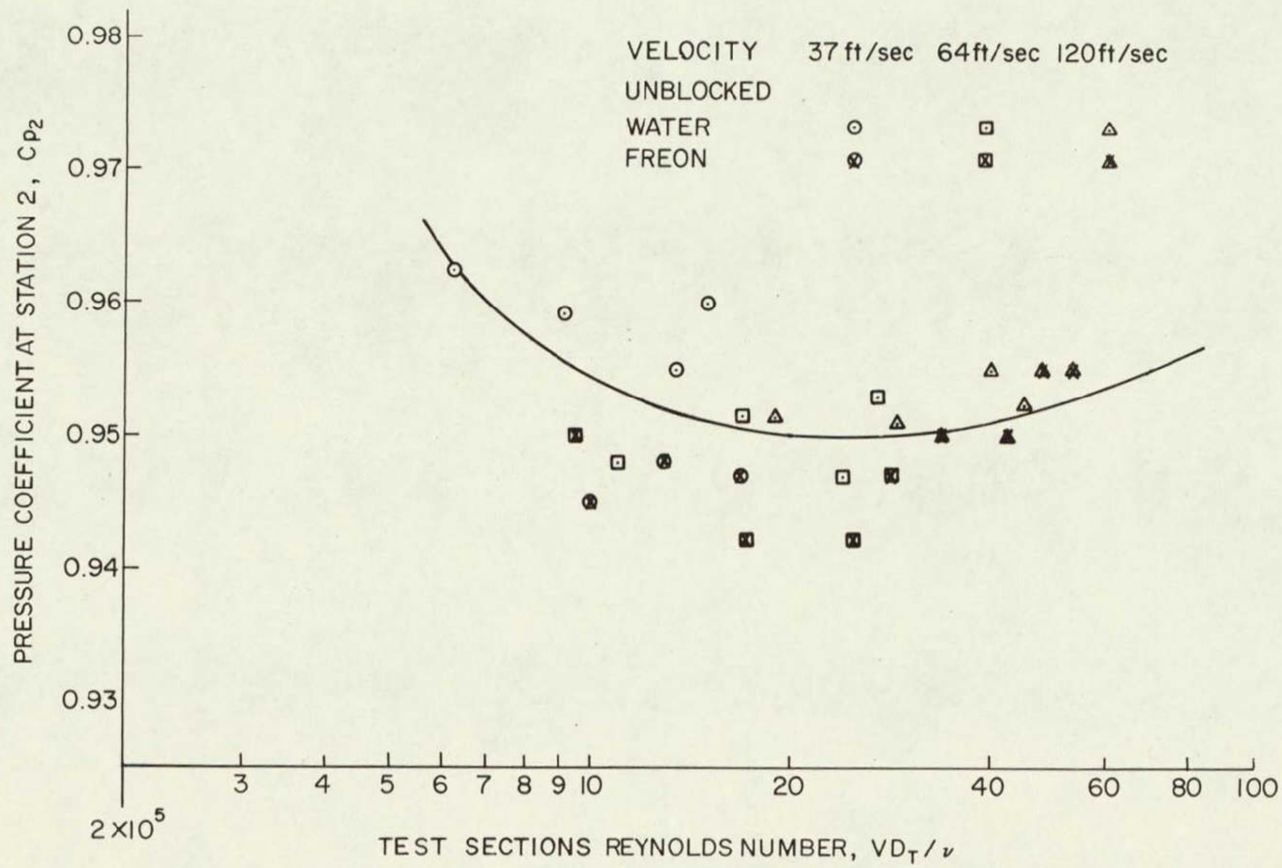

Figure 12 Tunnel Pressure Coefficient ($C_{P_{2u}}$) Versus Test Section Reynolds Number

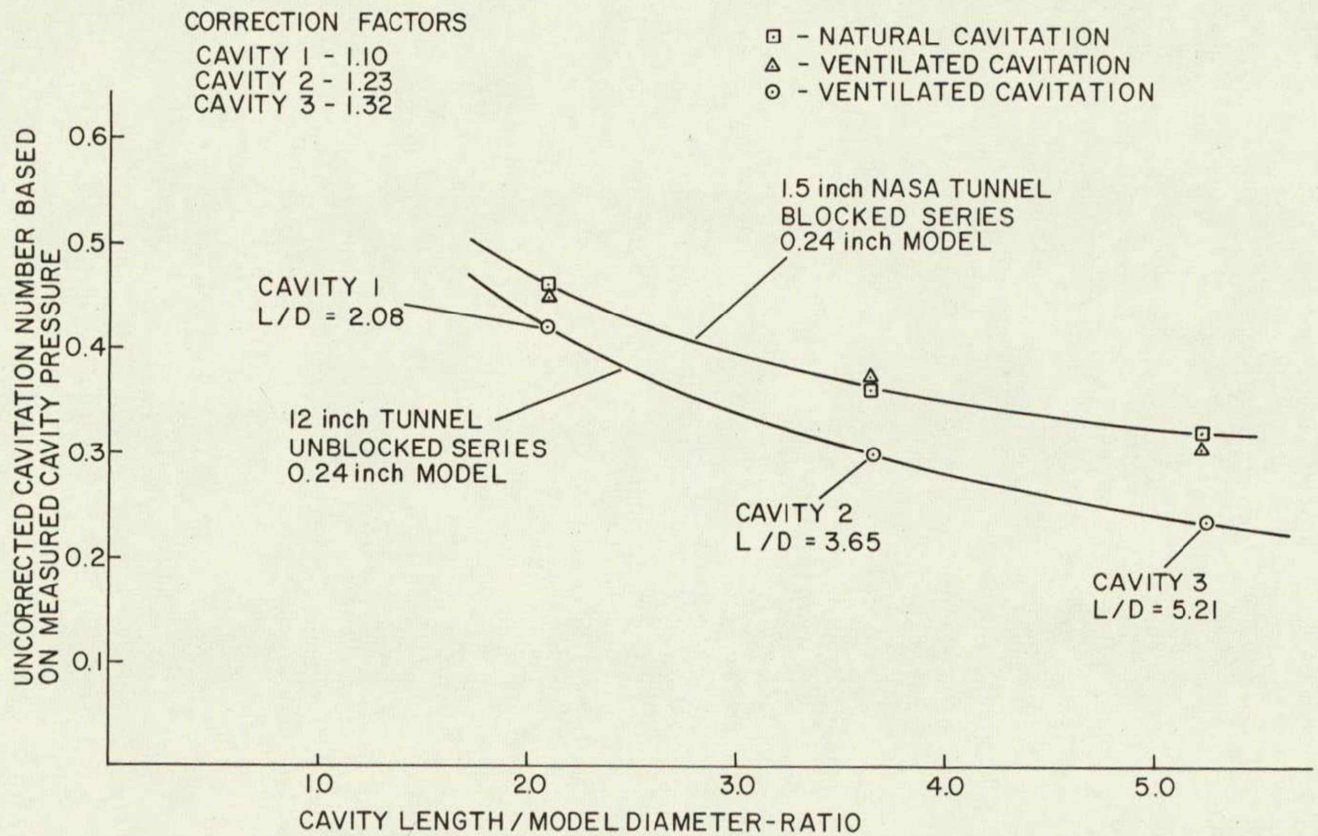

Figure 13 Blockage Correction Coefficients

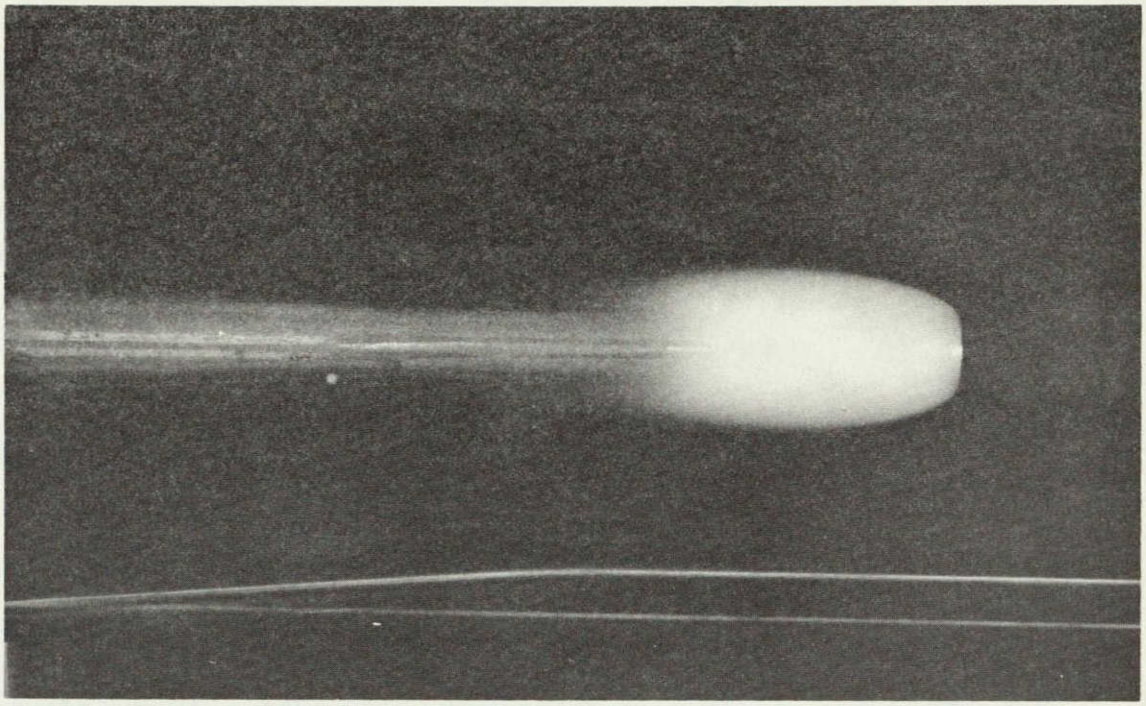

Figure 14 Natural Developed Cavity for 0.24-Inch Zero-Caliber-Ogive

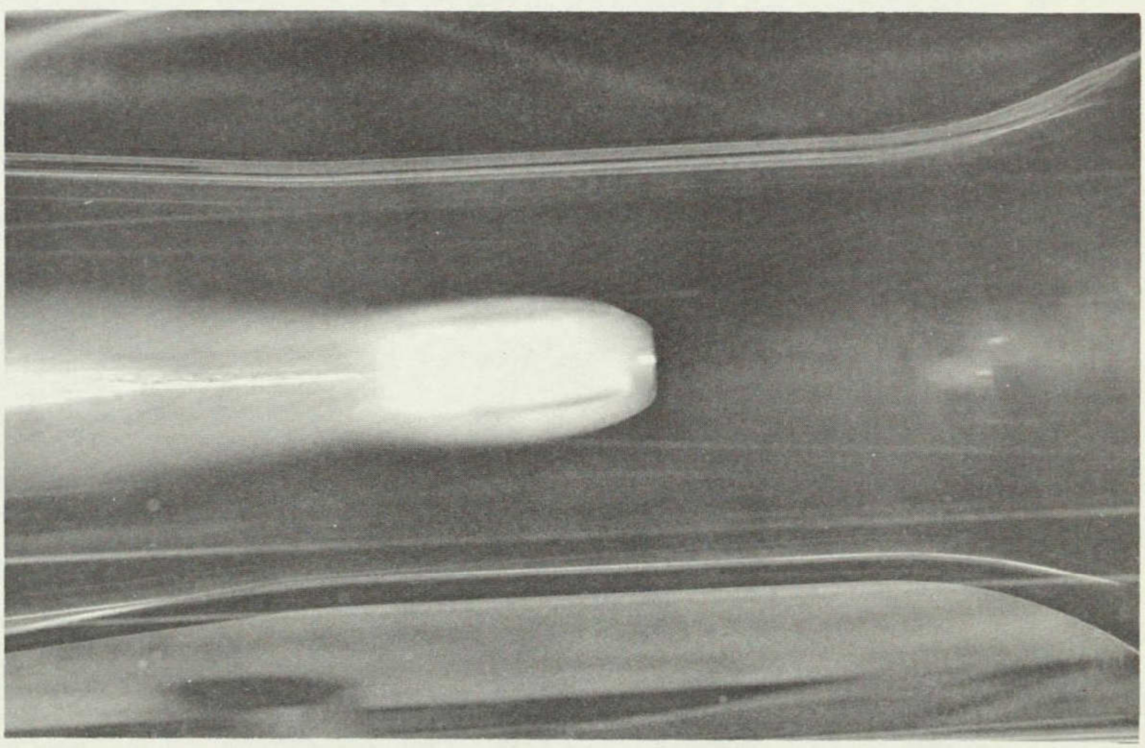

Figure 15 Entrained Developed Cavity for 0.24-Inch Zero-Caliber-Ogive

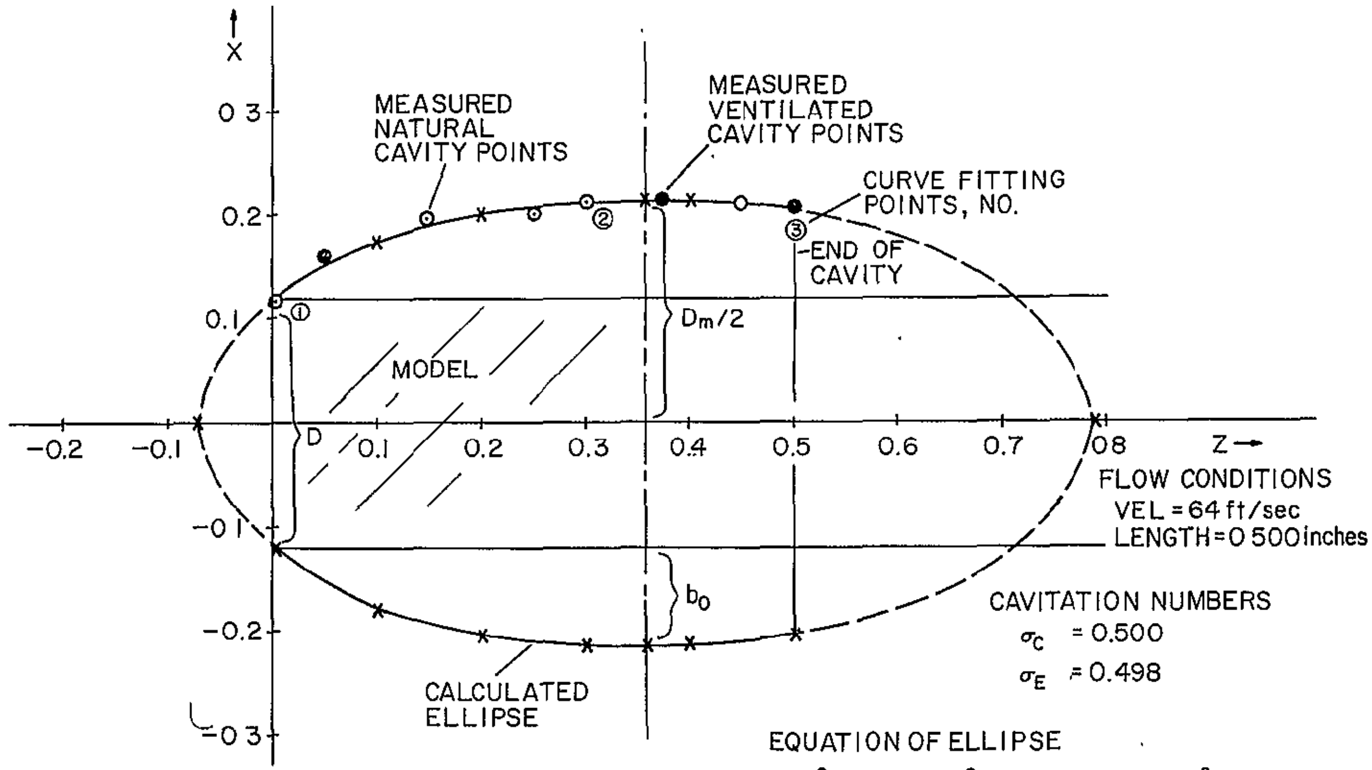

EQUATION OF ELLIPSE

$$\frac{X^2}{(0.217)^2} + \frac{Y^2}{(0.217)^2} + \frac{(Z-0.359)^2}{(0.431)^2} = 1$$

CAVITY PARAMETERS

$$\frac{D_m}{D} = \frac{0.217}{0\ 120} = 1.81$$

$$\frac{b_o}{D} = \frac{0.097}{0\ 240} = 0\ 404$$

$$\frac{A}{D} = \frac{0.359}{0.240} = 1.49$$

Figure 16 Mathematical Representation of a Developed Cavity; Velocity = 64 ft/sec, Length = 0.500 inch

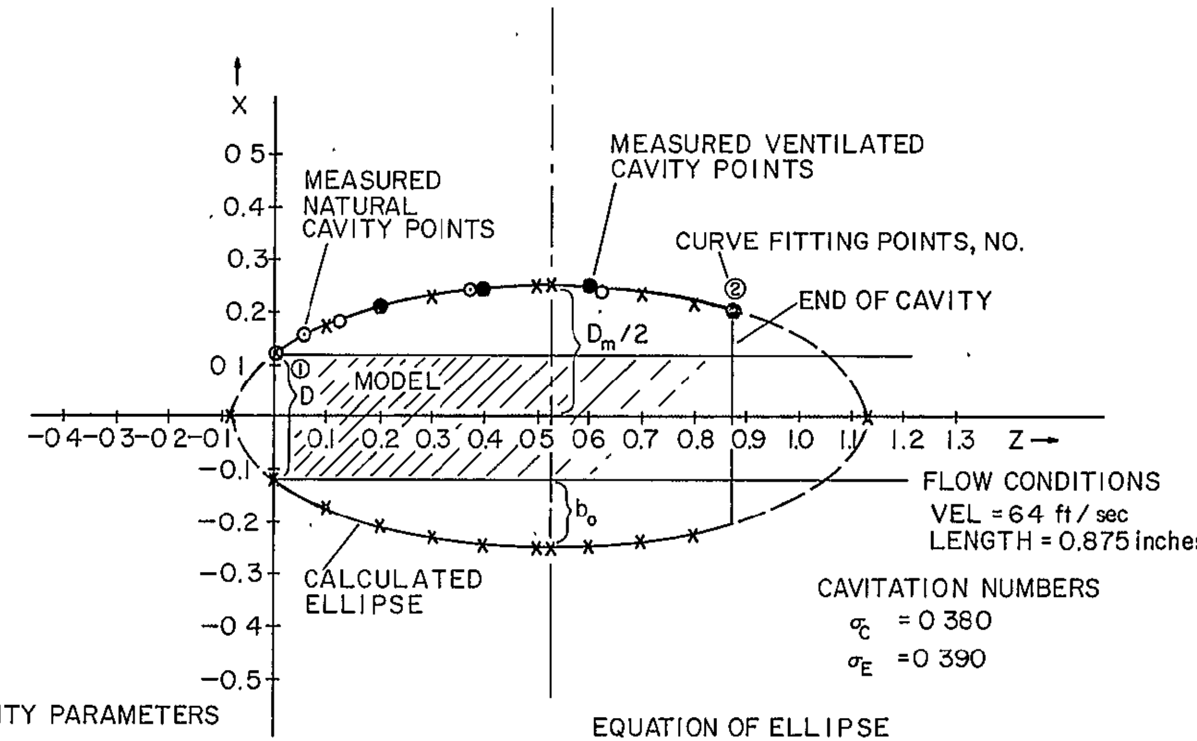

CAVITY PARAMETERS

$$\frac{D_m}{D} = \frac{0.250}{0.120} = 2.08$$

$$\frac{b_o}{D} = \frac{0.130}{0.240} = 0.542$$

$$\frac{A}{D} = \frac{0.529}{0.240} = 2.21$$

EQUATION OF ELLIPSE

$$\frac{X^2}{(0.250)^2} + \frac{Y^2}{(0.250)^2} + \frac{(Z-0.529)^2}{(0.603)^2} = 1$$

Figure 17 Mathematical Representation of a Developed Cavity; Velocity = 64 ft/sec, Length = 0.875 inch

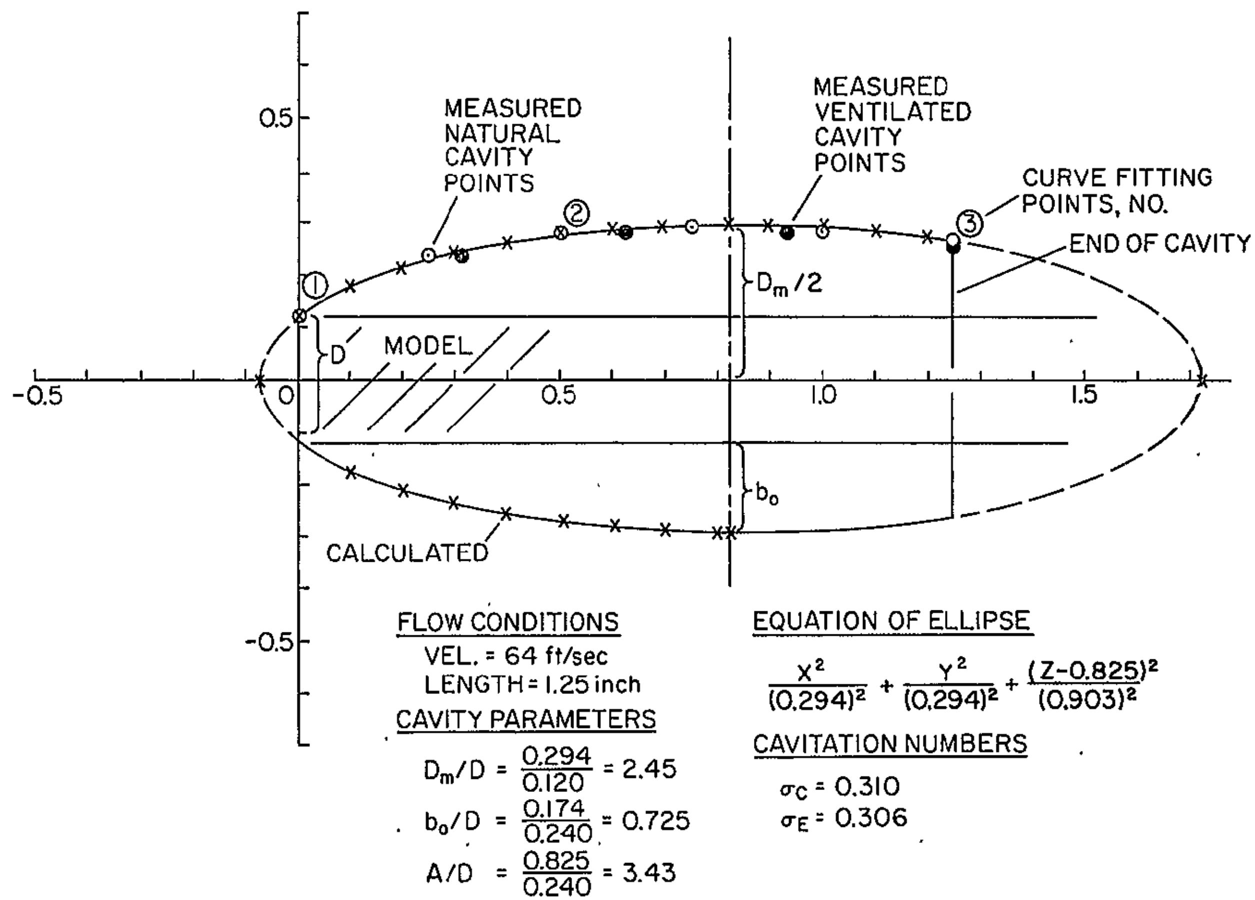

Figure 18 Mathematical Representation of a Developed Cavity; Velocity ≐ 64 ft/sec, Length = 1.25 inch

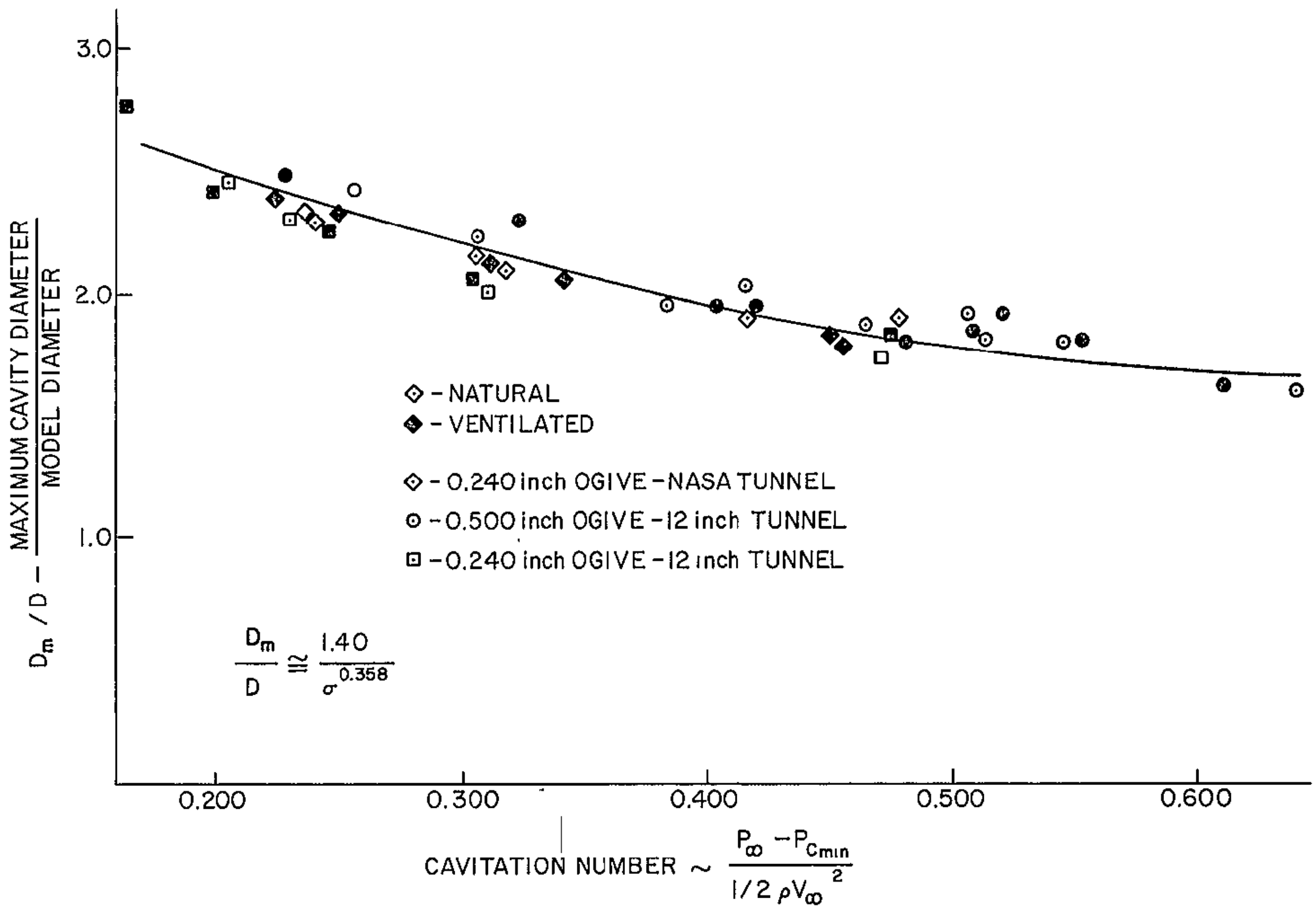

Figure 19 Ratio of Maximum Cavity to Model Diameter Versus Corrected Cavitation Number

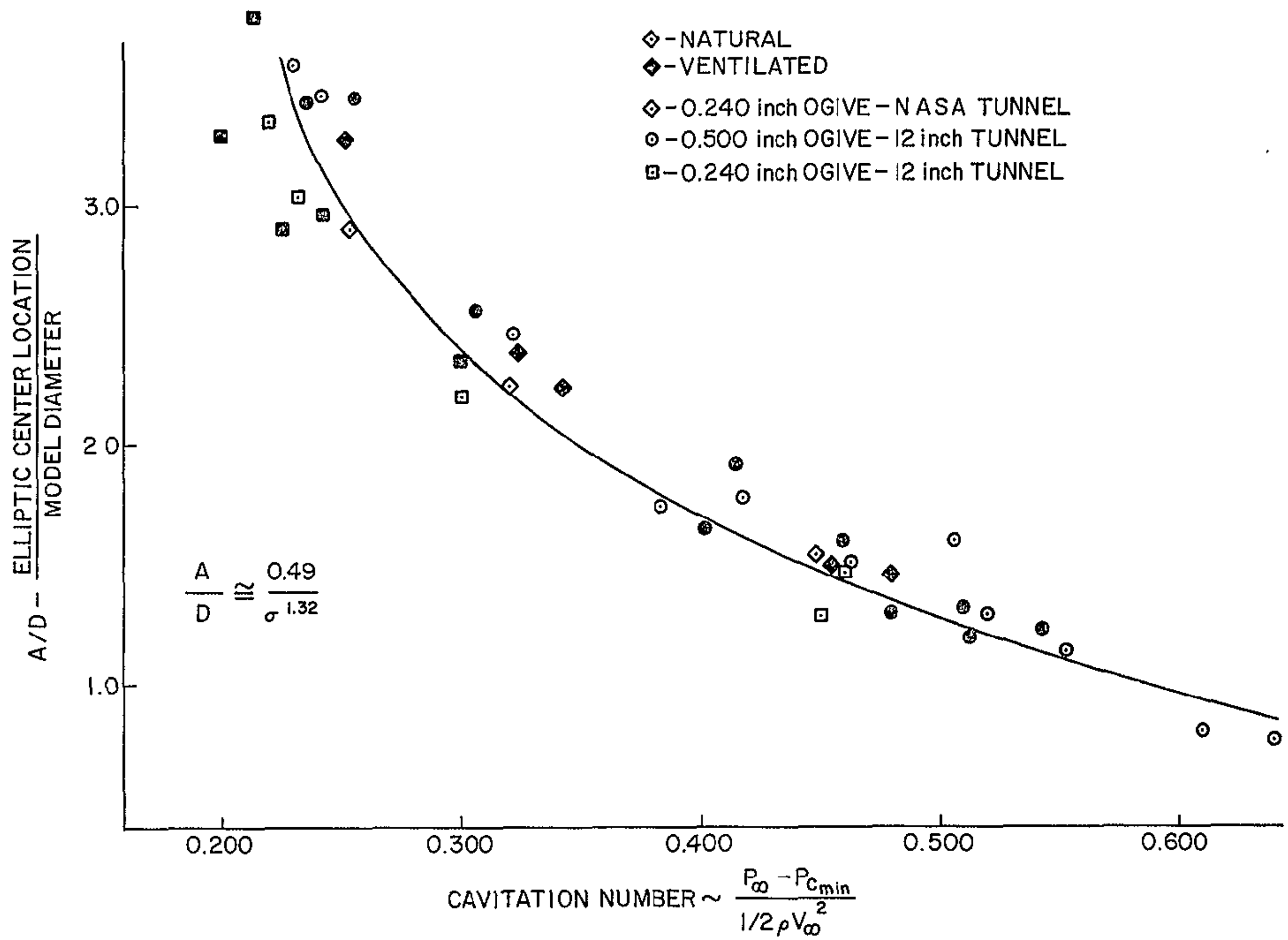

Figure 20 Ratio of Position of Maximum Cavity to Model Diameter Versus Corrected Cavitation Number

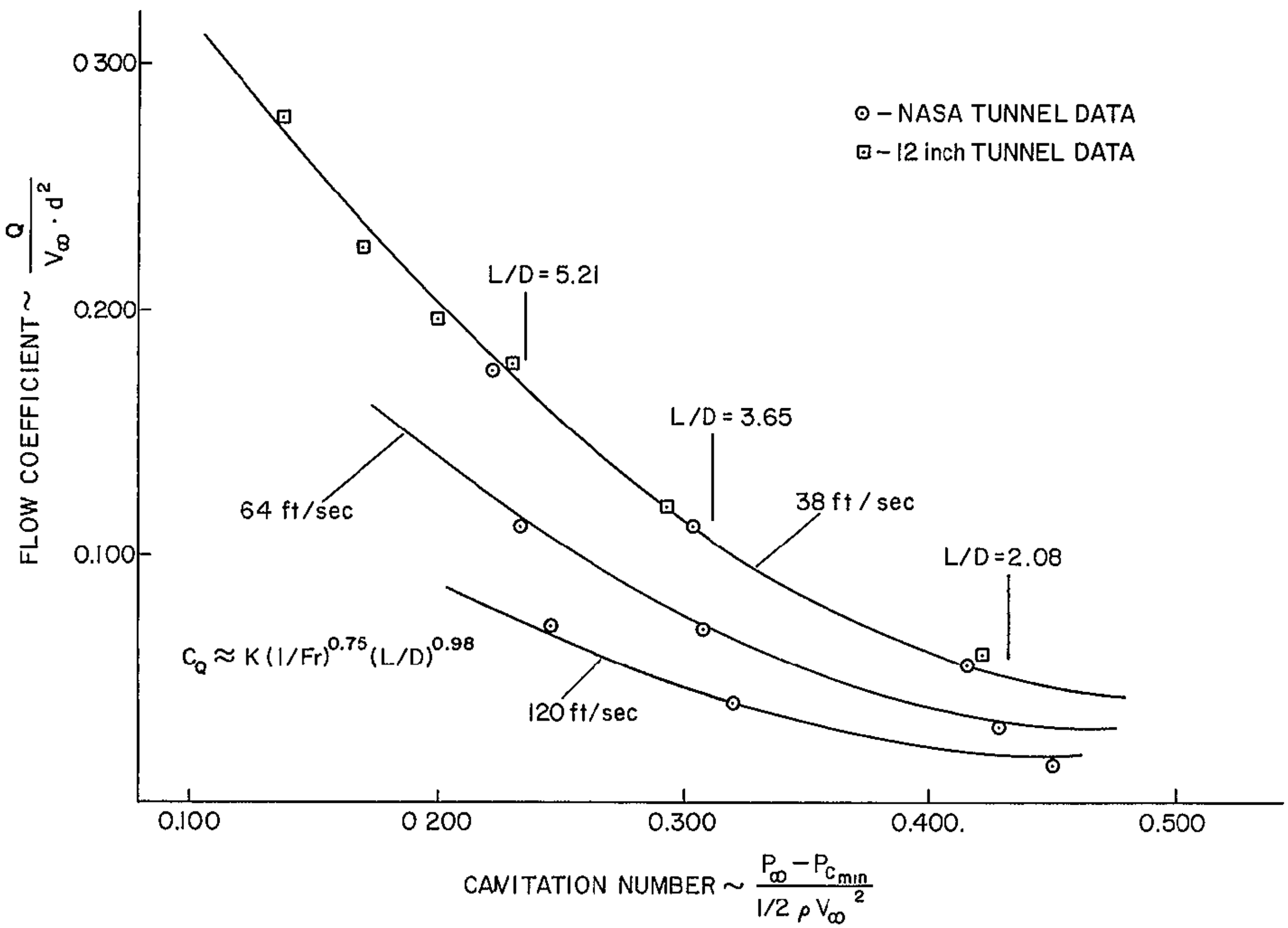

Figure 21 Flow Coefficient Versus Corrected Cavitation Number for the 0.24-Inch Zero-Caliber-Ogive in the NASA Tunnel

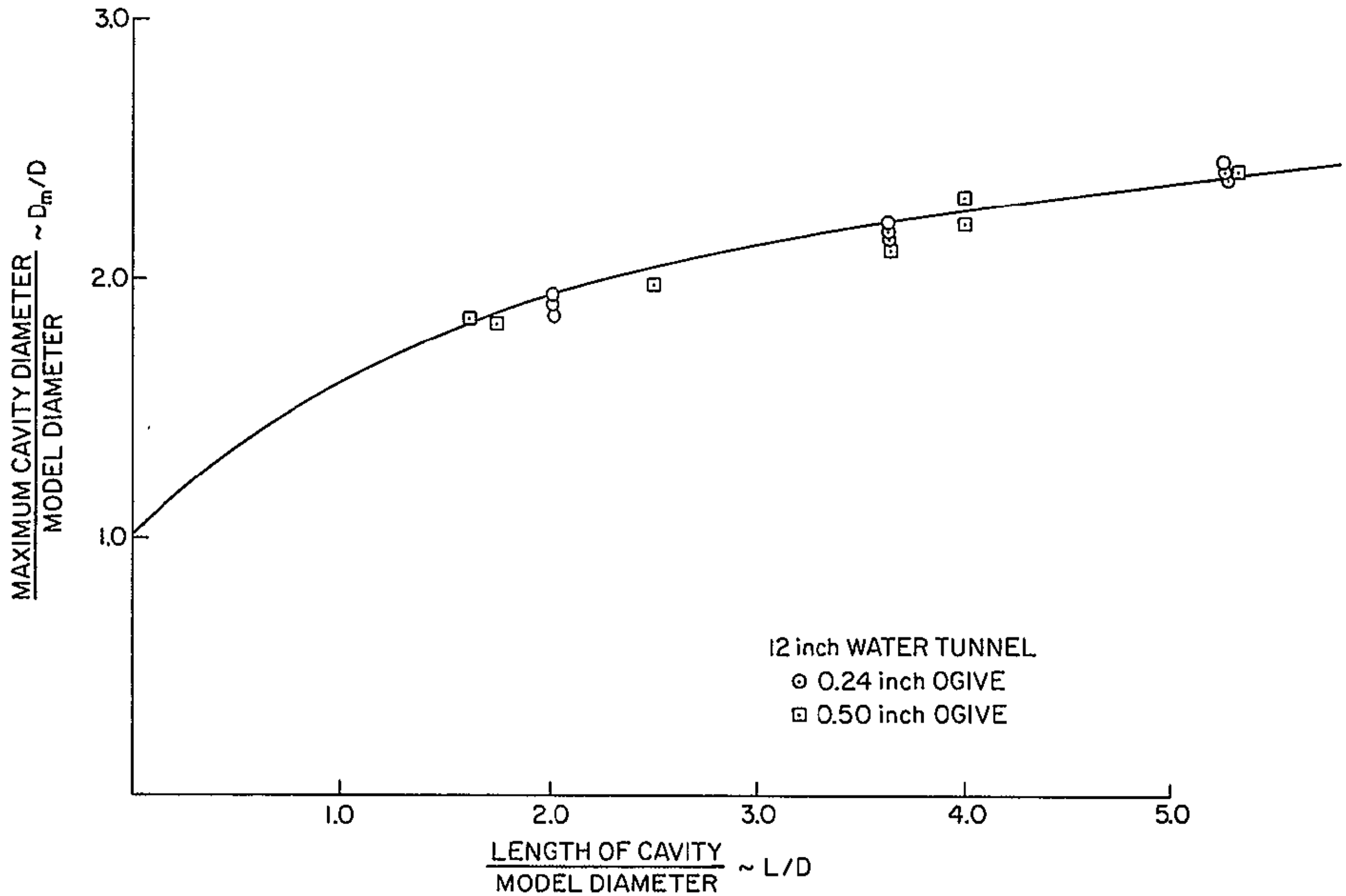

Figure 22   Ratio of Cavity Length to Model Diameter Versus the Ratio of Maximum Cavity to Model Diameter

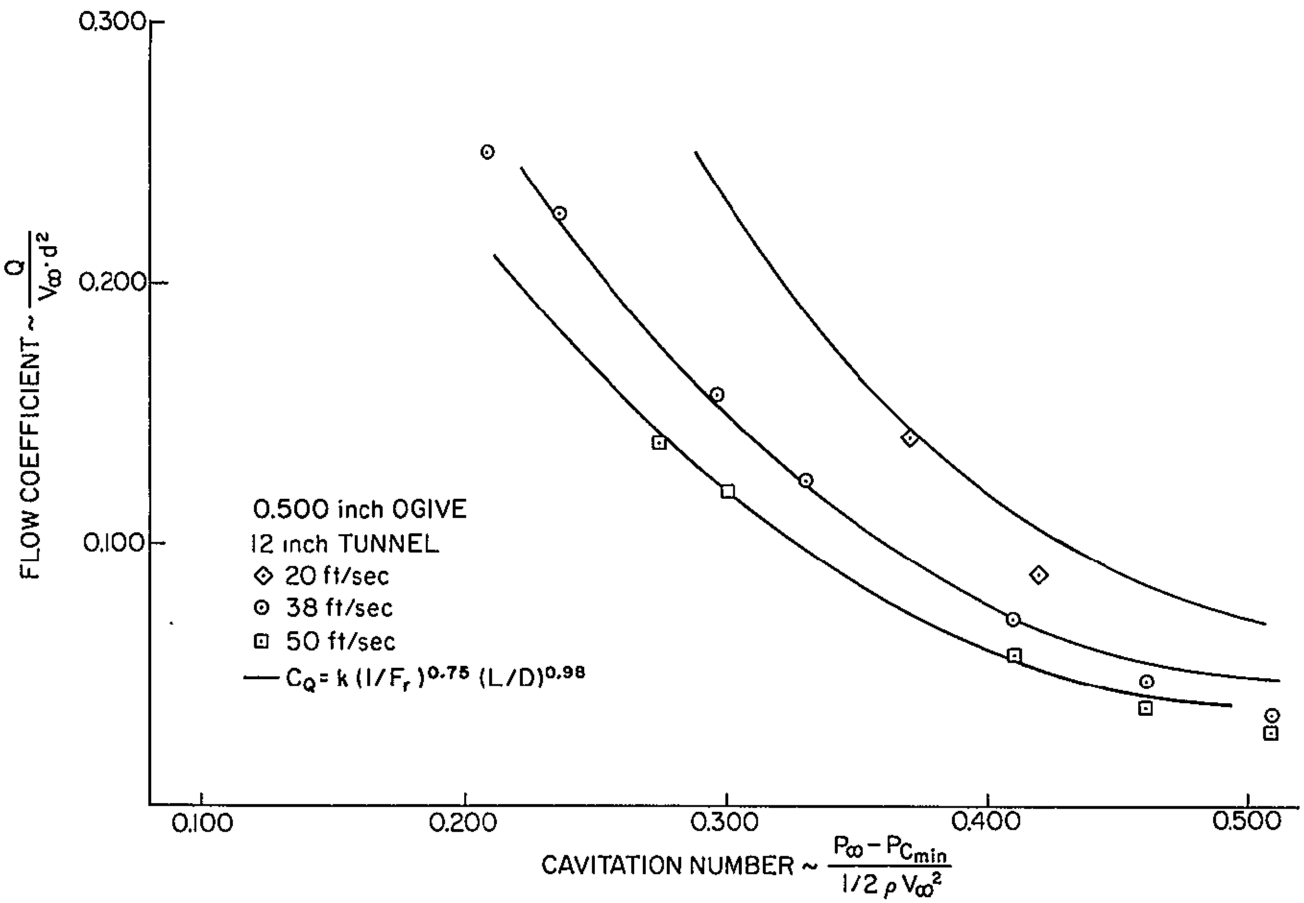

Figure 23 Flow Coefficient Versus Cavitation Number for the 0.50-Inch Zero-Caliber-Ogive in the 12-Inch Water Tunnel

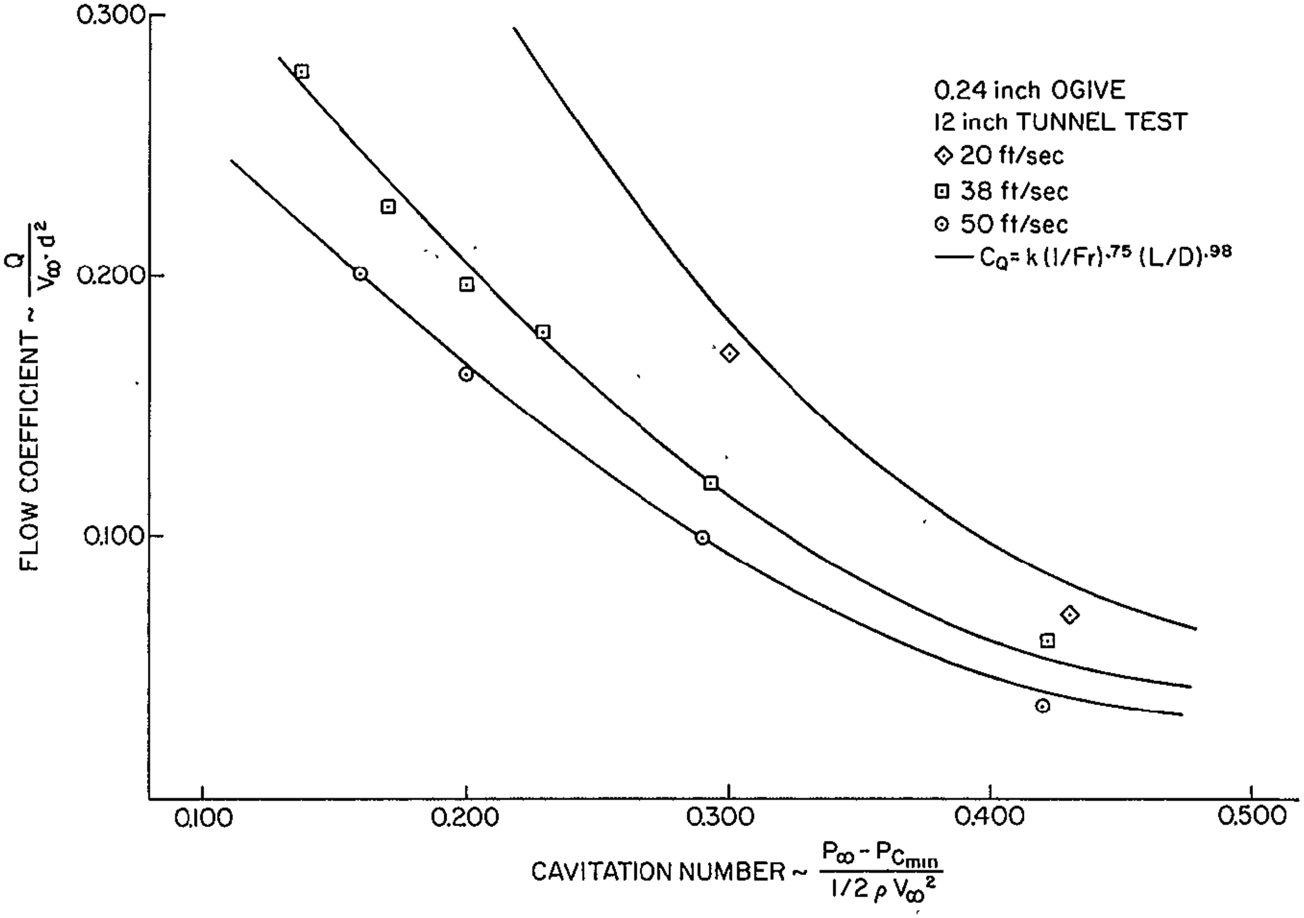

Figure 24 Flow Coefficient Versus Cavitation Number for the 0.24-Inch Zero-Caliber-Ogive in the 12-Inch Water Tunnel.

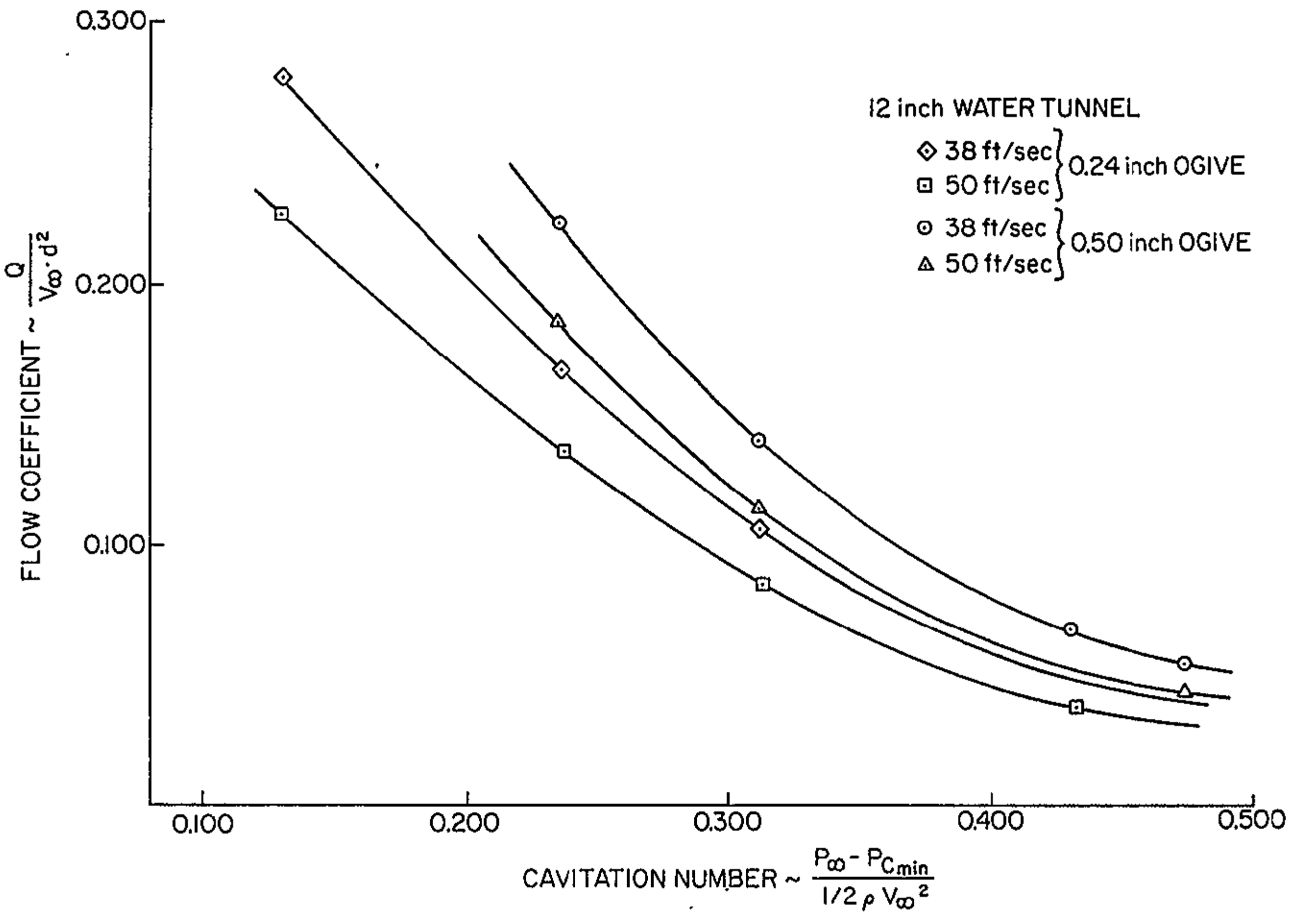

Figure 25 Flow Coefficient Versus Cavitation Number for Different Model Diameters

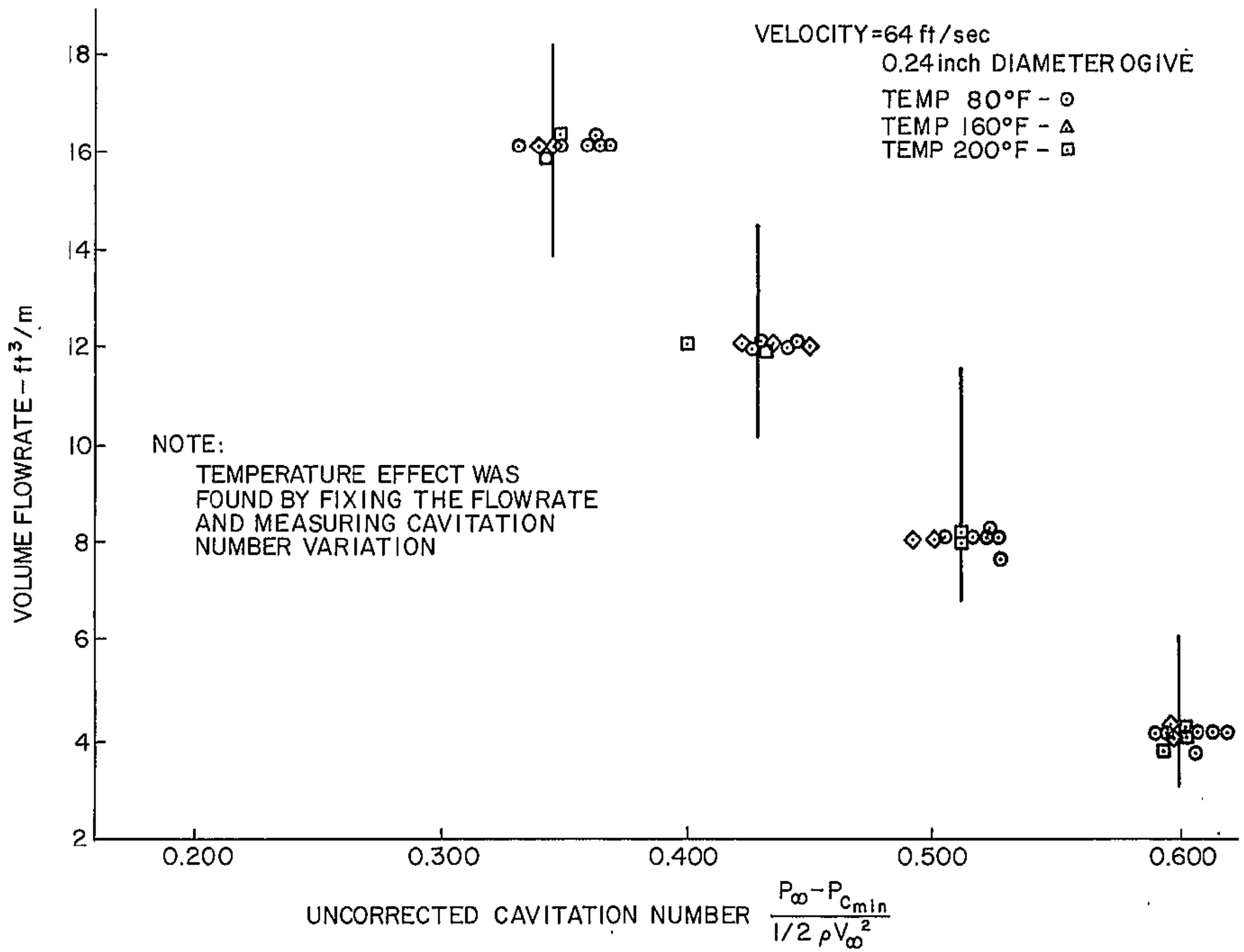

Figure 26 Entrained Volume Flowrate Versus Uncorrected Cavitation Number for Temperature Variations

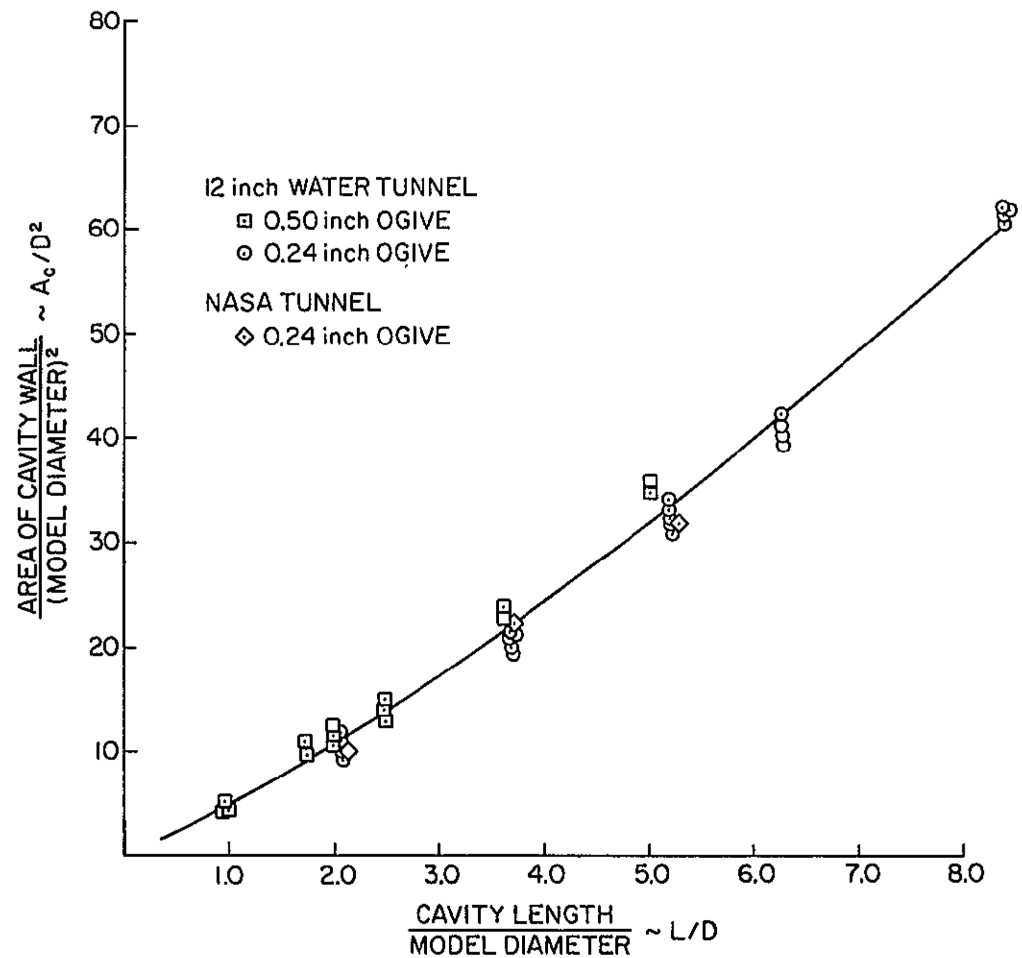

Figure 27 Ratio of Area of Cavity Wall to Model Diameter Squared Versus Ratio of Cavity Length to Model Diameter

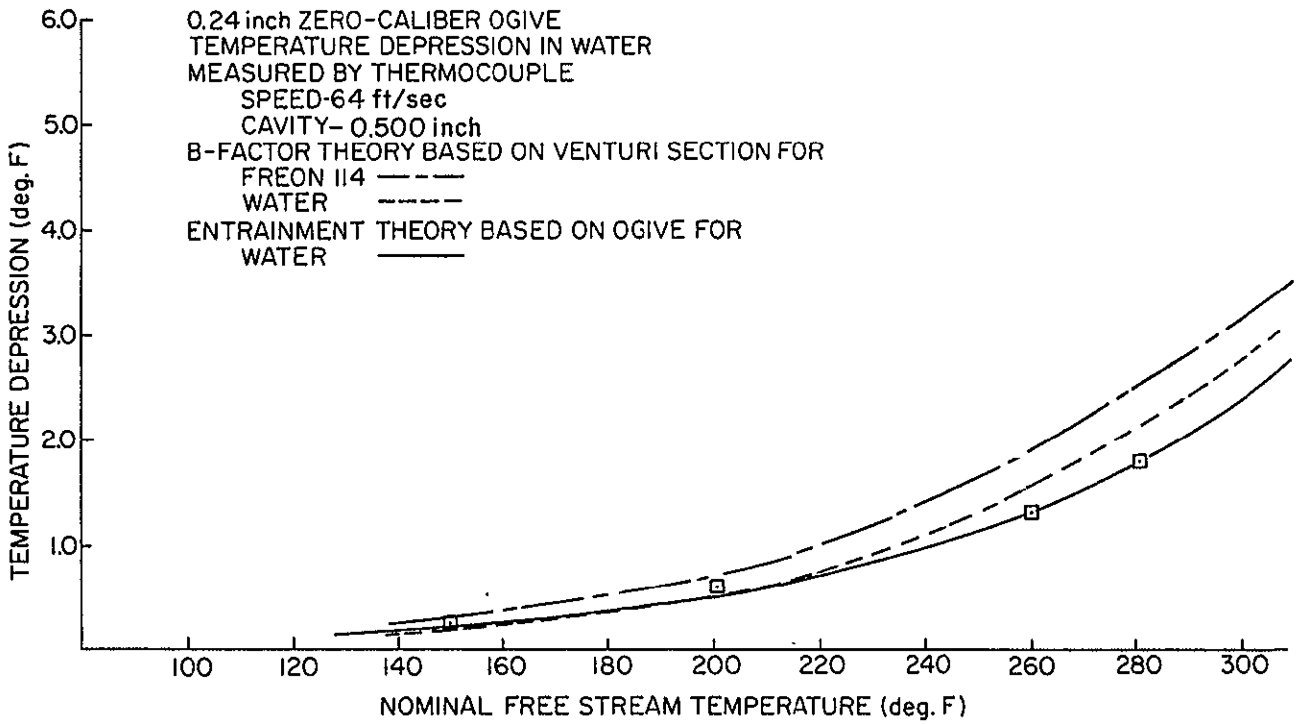

Figure 28 Cavity Temperature Depression Versus Temperature for Water; V = 64 ft/sec, L = 0.500 inch

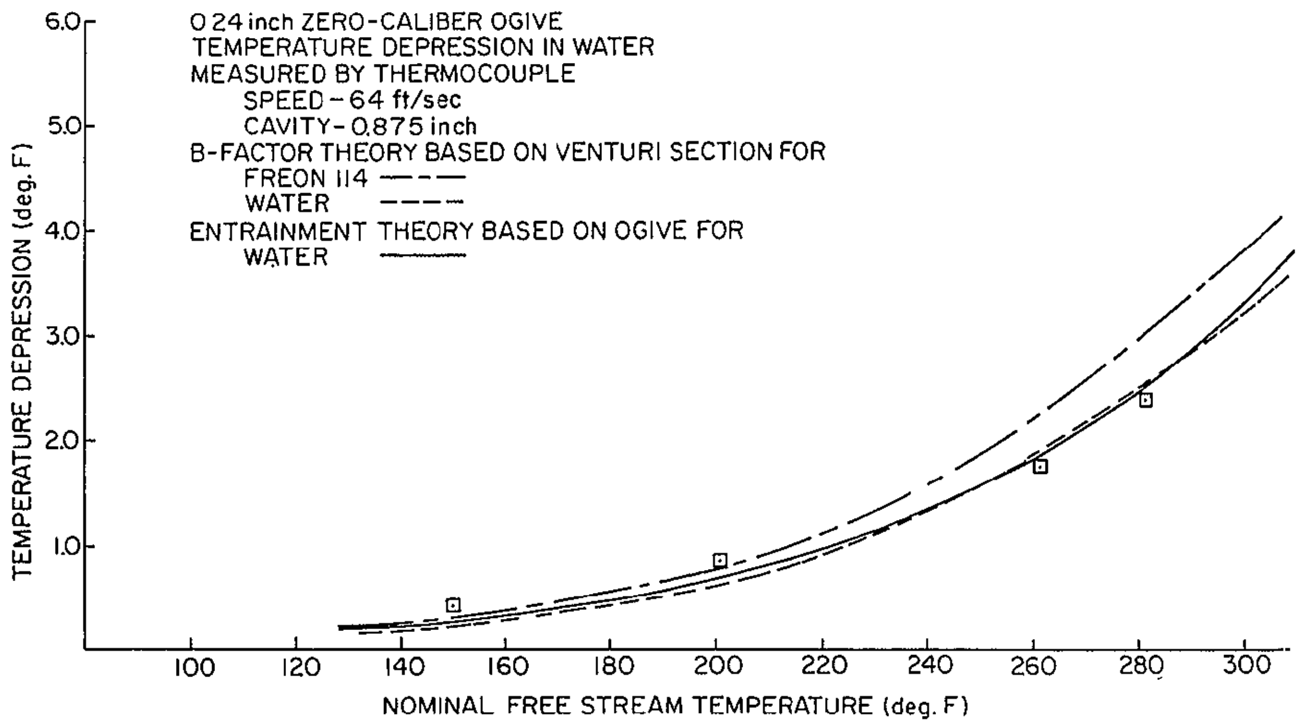

Figure 29 Cavity Temperature Depression Versus Temperature for Water; V = 64 ft/sec, L = 0.875 inch

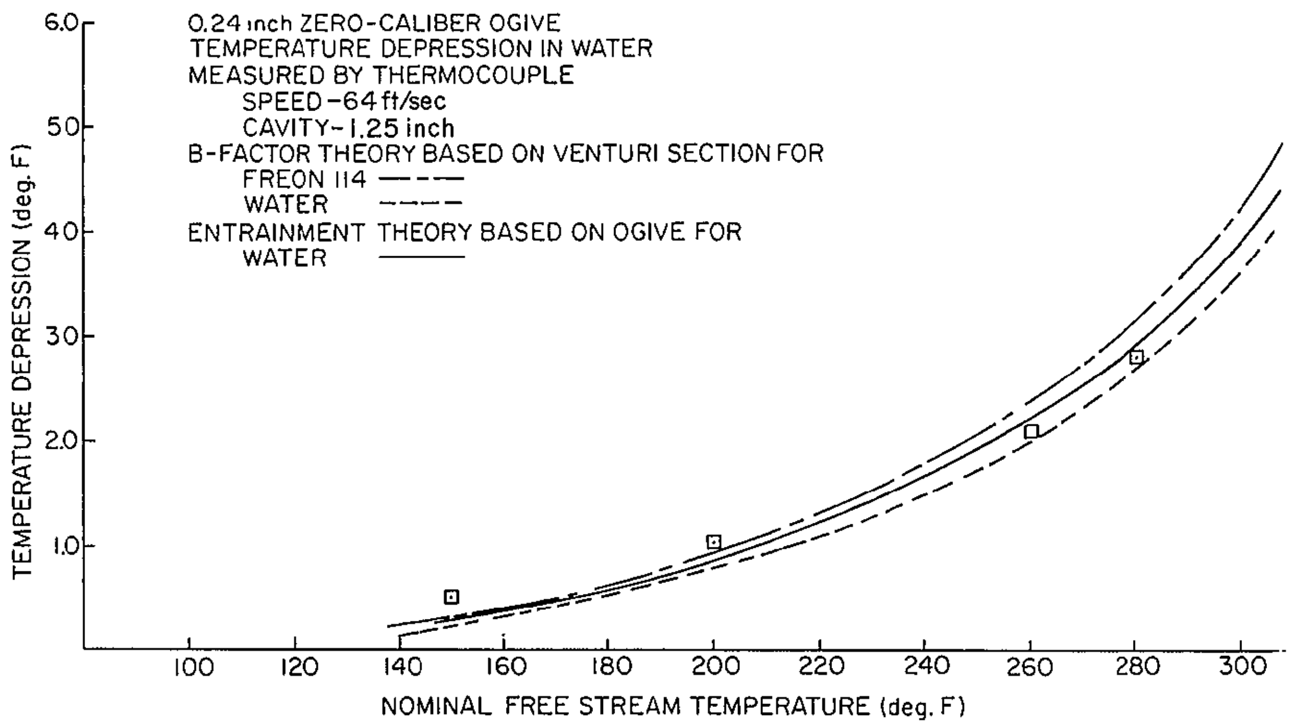

Figure 30 Cavity Temperature Depression Versus Temperature for Water;
V = 64 ft/sec, L = 1.25 inch

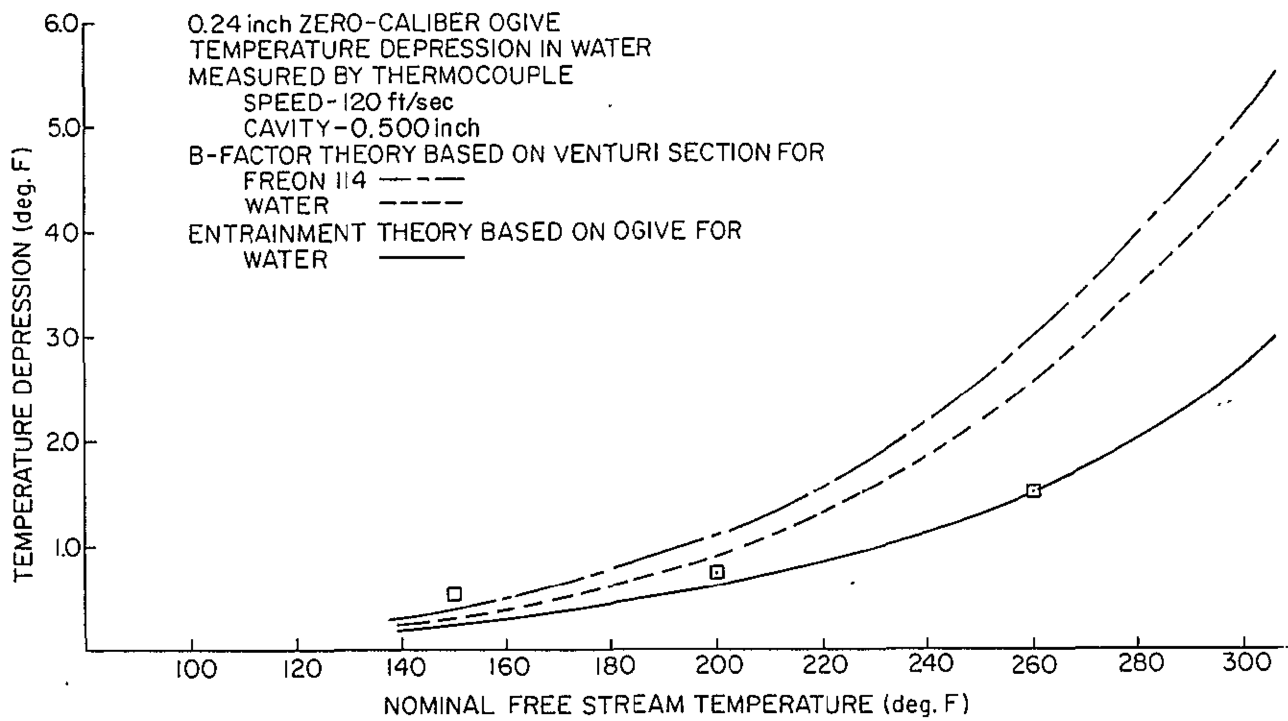

Figure 31 Cavity Temperature Depression Versus Temperature for Water; V = 120 ft/sec, L = 0.500 inch

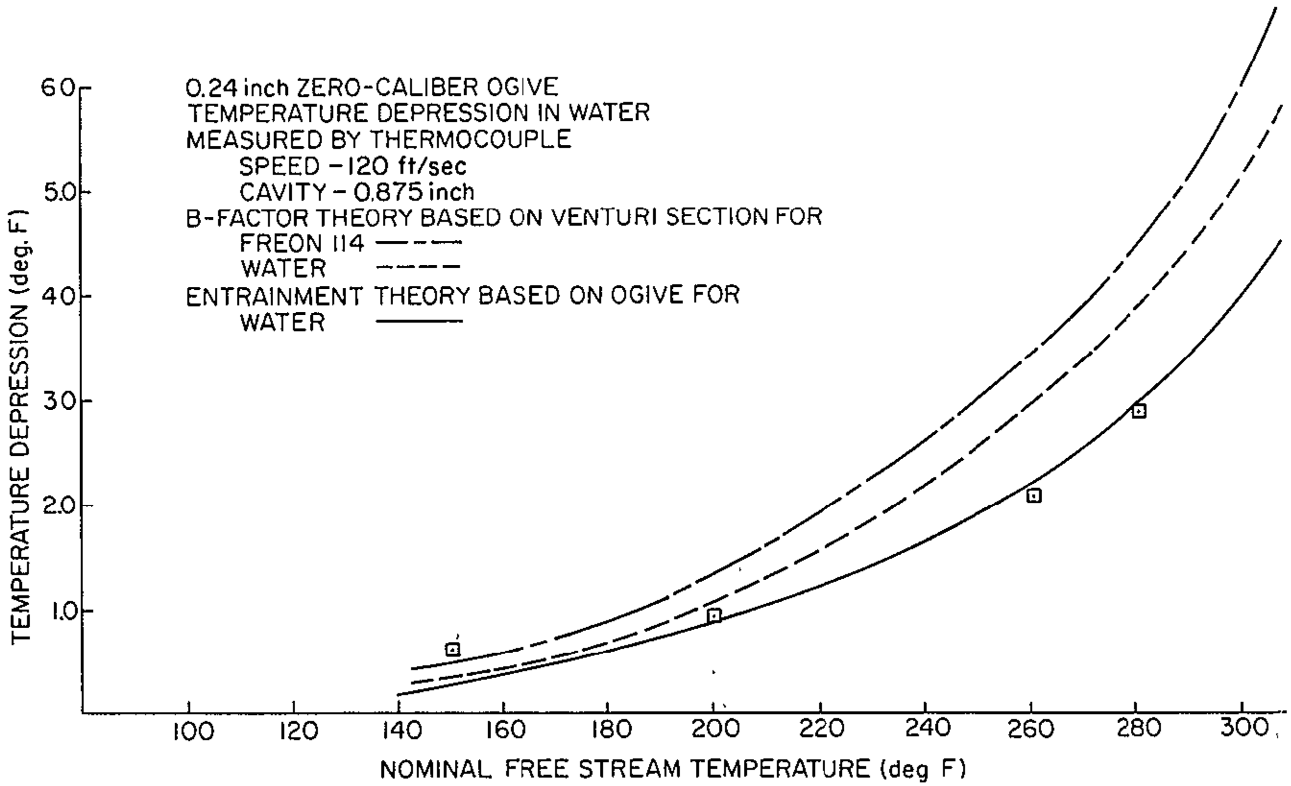

Figure 32 Cavity Temperature Depression Versus Temperature for Water; V = 120 ft/sec, L = 0.875 inch

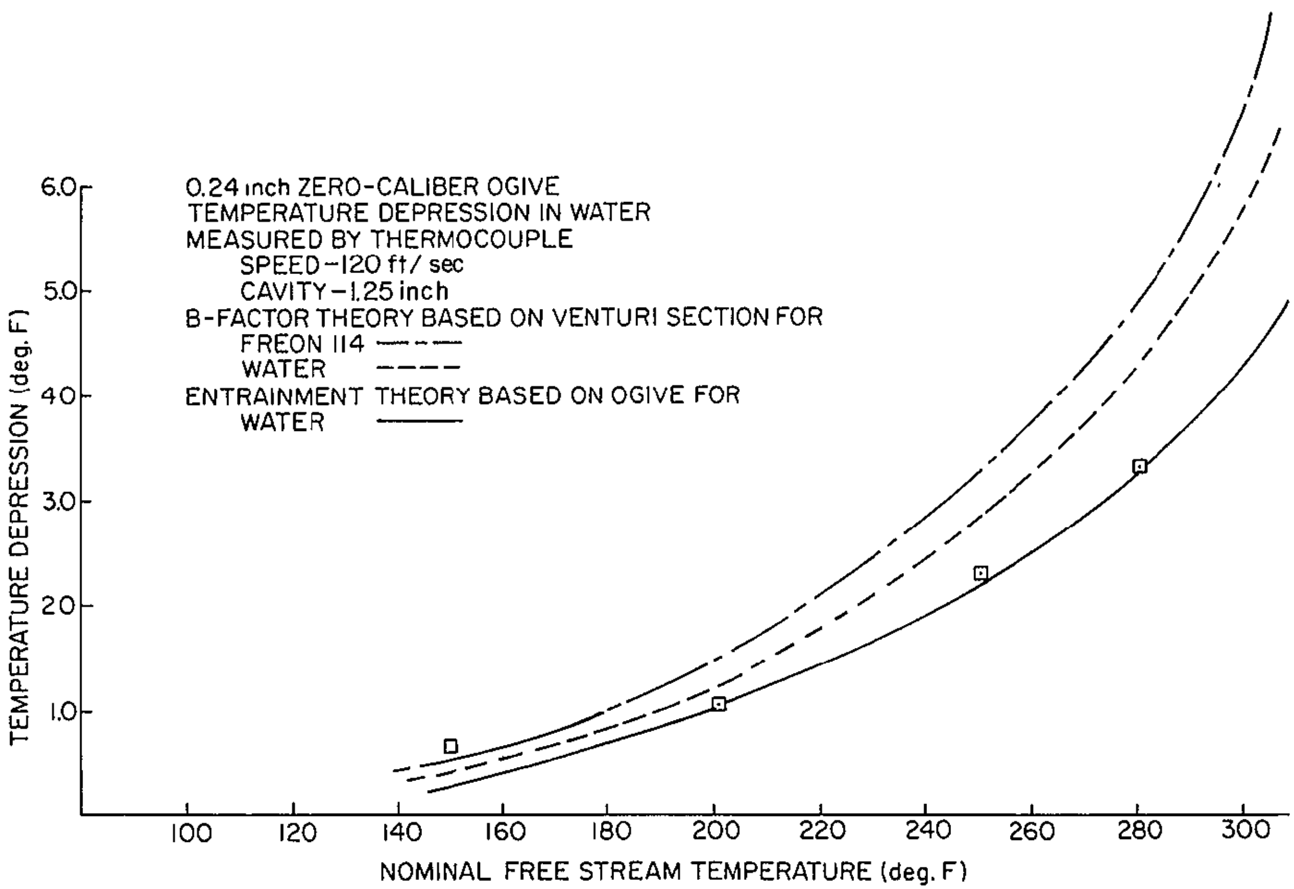

Figure 33 Cavity Temperature Depression Versus Temperature for Water; V = 120 ft/sec, L = 1.25 inch

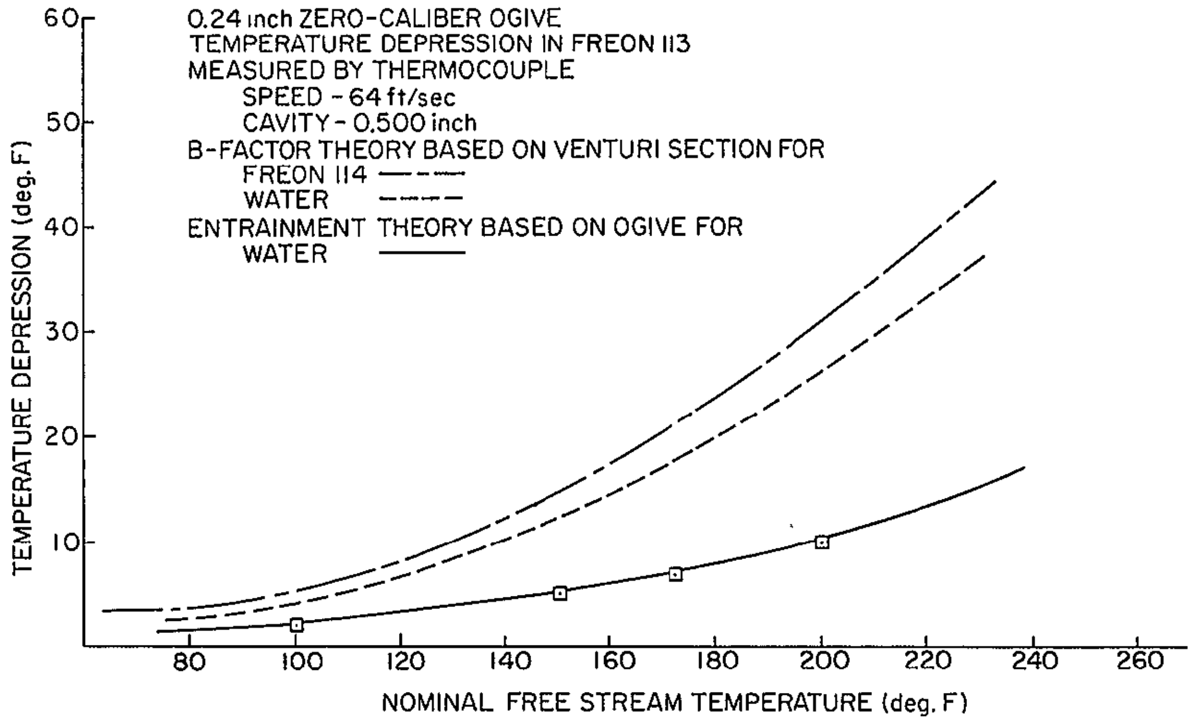

Figure 34 Cavity Temperature Depression Versus Temperature for Freon 113; V = 64 ft/sec, L = 0.500 inch

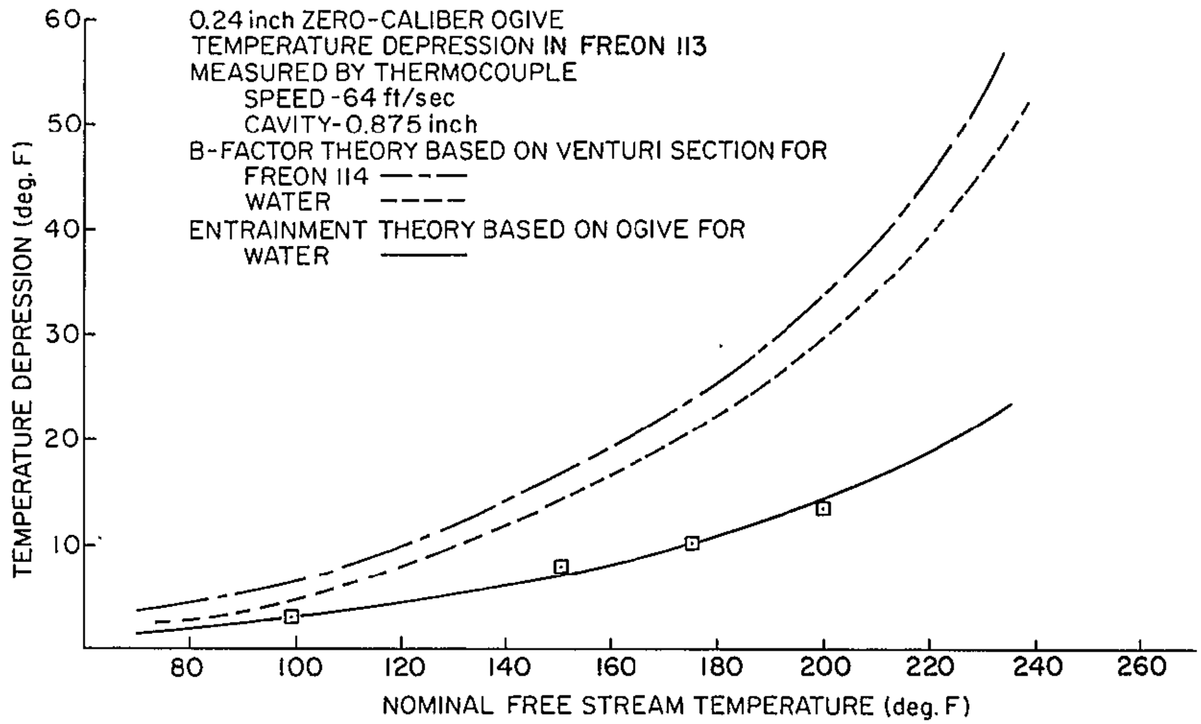

Figure 35 Cavity Temperature Depression Versus Temperature for Freon 113; V = 64 ft/sec, L = 0.875 inch

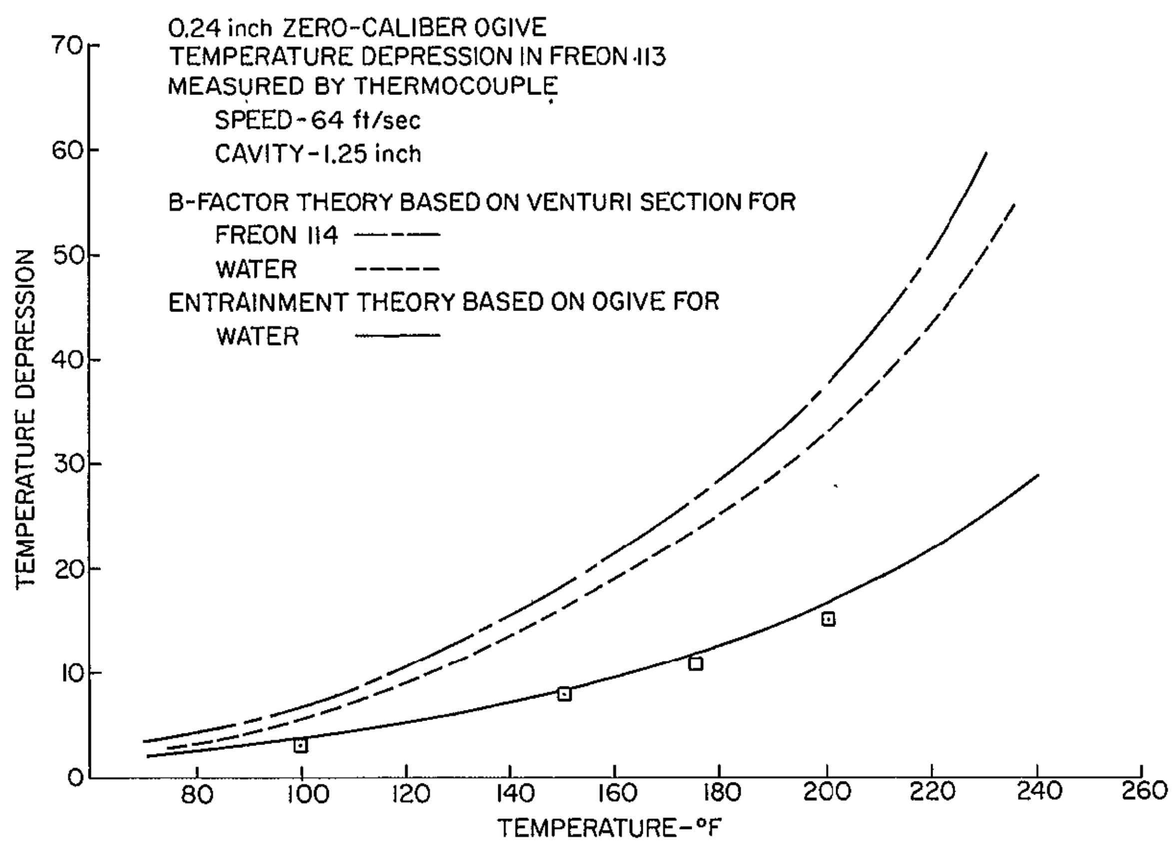

Figure 36 Cavity Temperature Depression Versus Temperature for Freon 113; V = 64 ft/sec, L = 1.25 inch

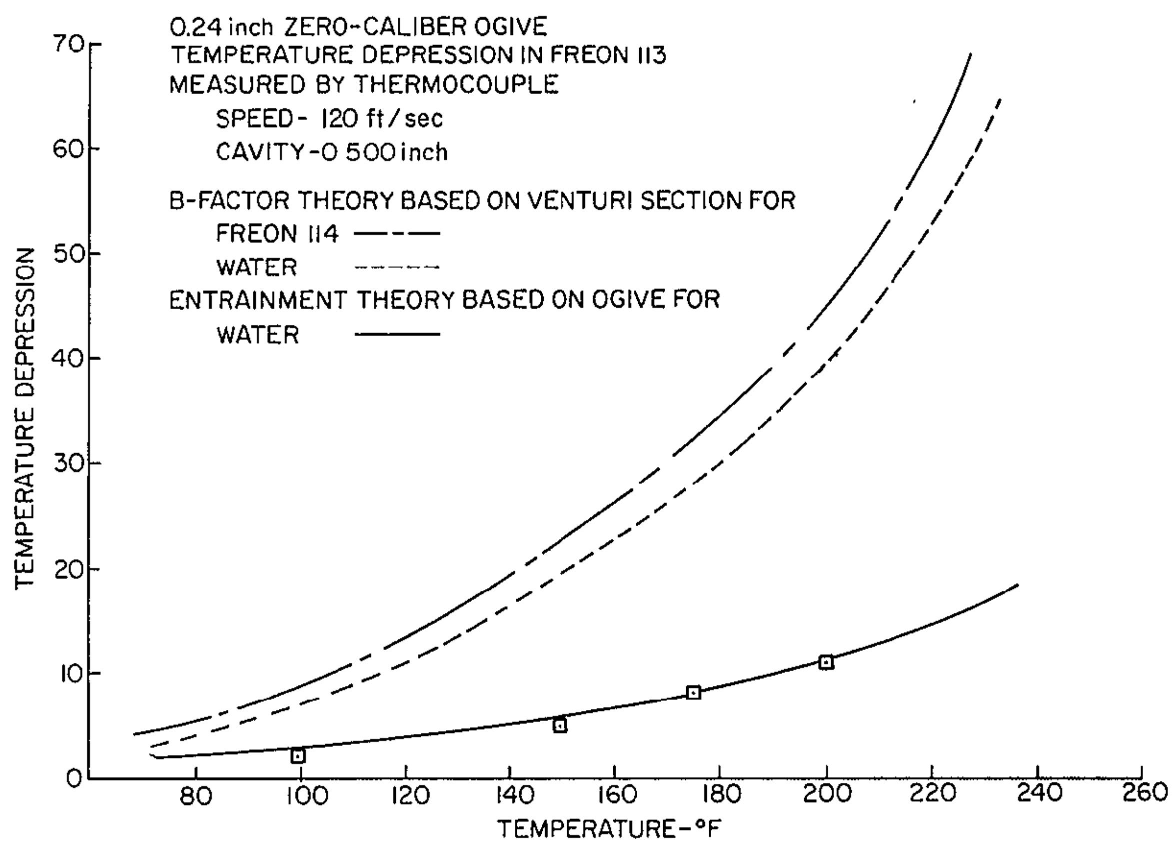

Figure 37 Cavity Temperature Depression Versus Temperature for Freon 113; V = 120 ft/sec, L = 0.500 inch

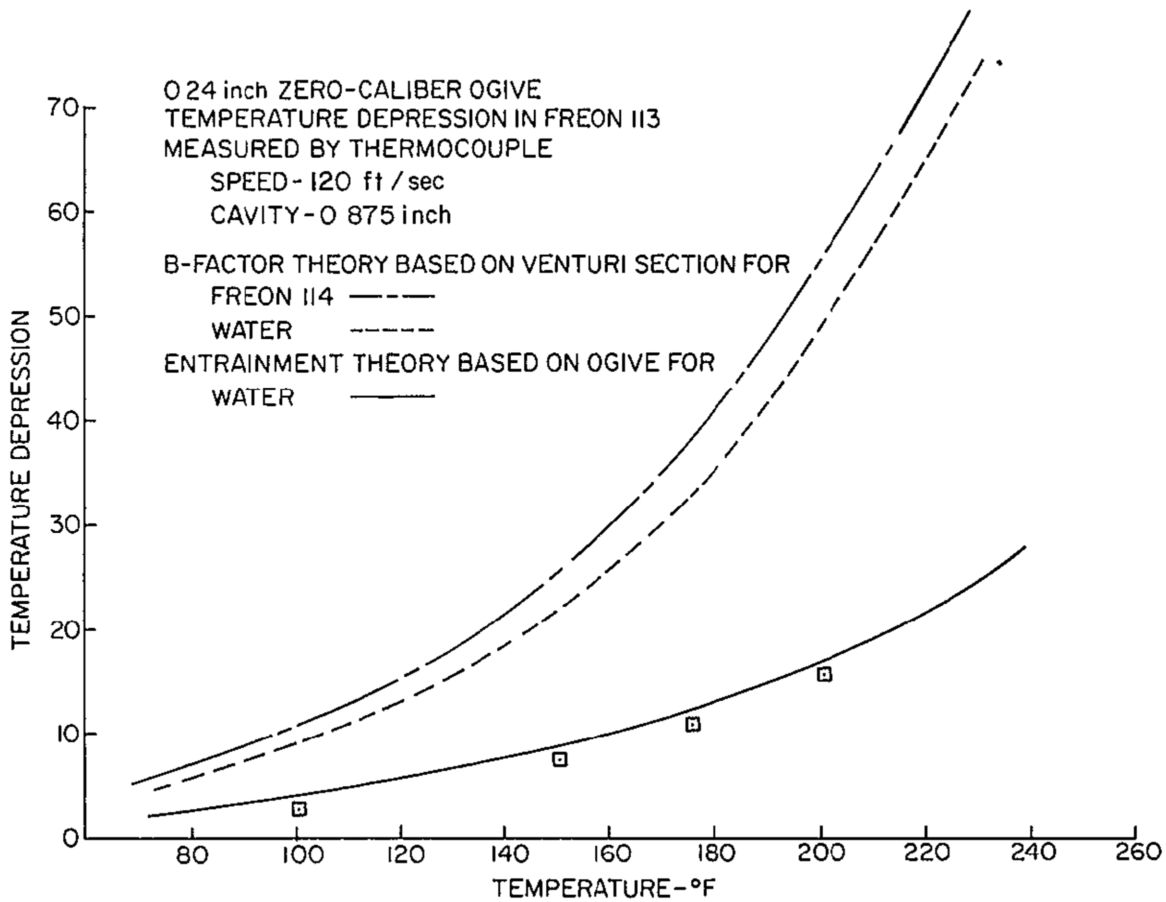

Figure 38 Cavity Temperature Depression Versus Temperature for Freon 113; V = 120 ft/sec, L = 0.875 inch

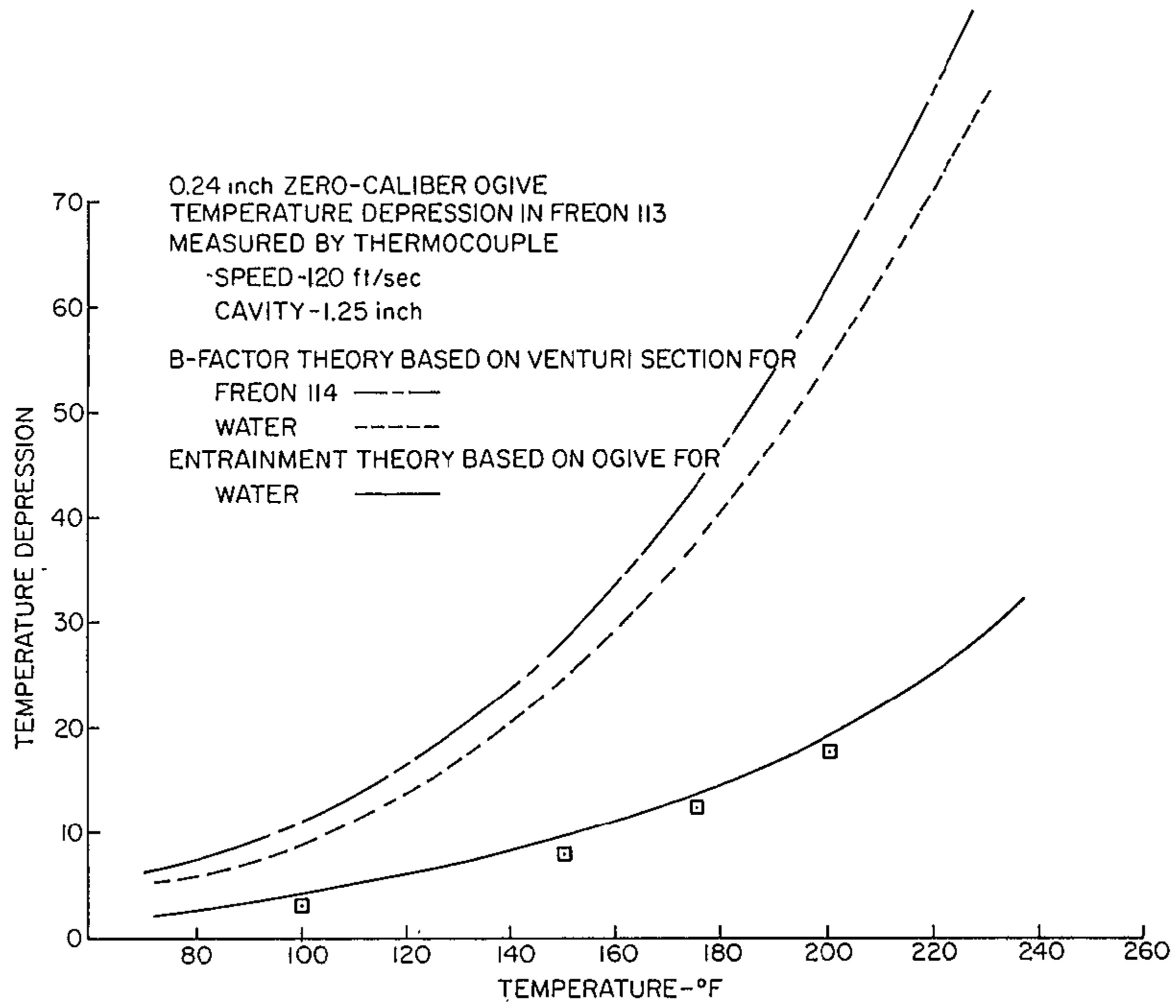

Figure 39 Cavity Temperature Depression Versus Temperature for Freon 113; V = 120 ft/sec, L = 1.25 inch

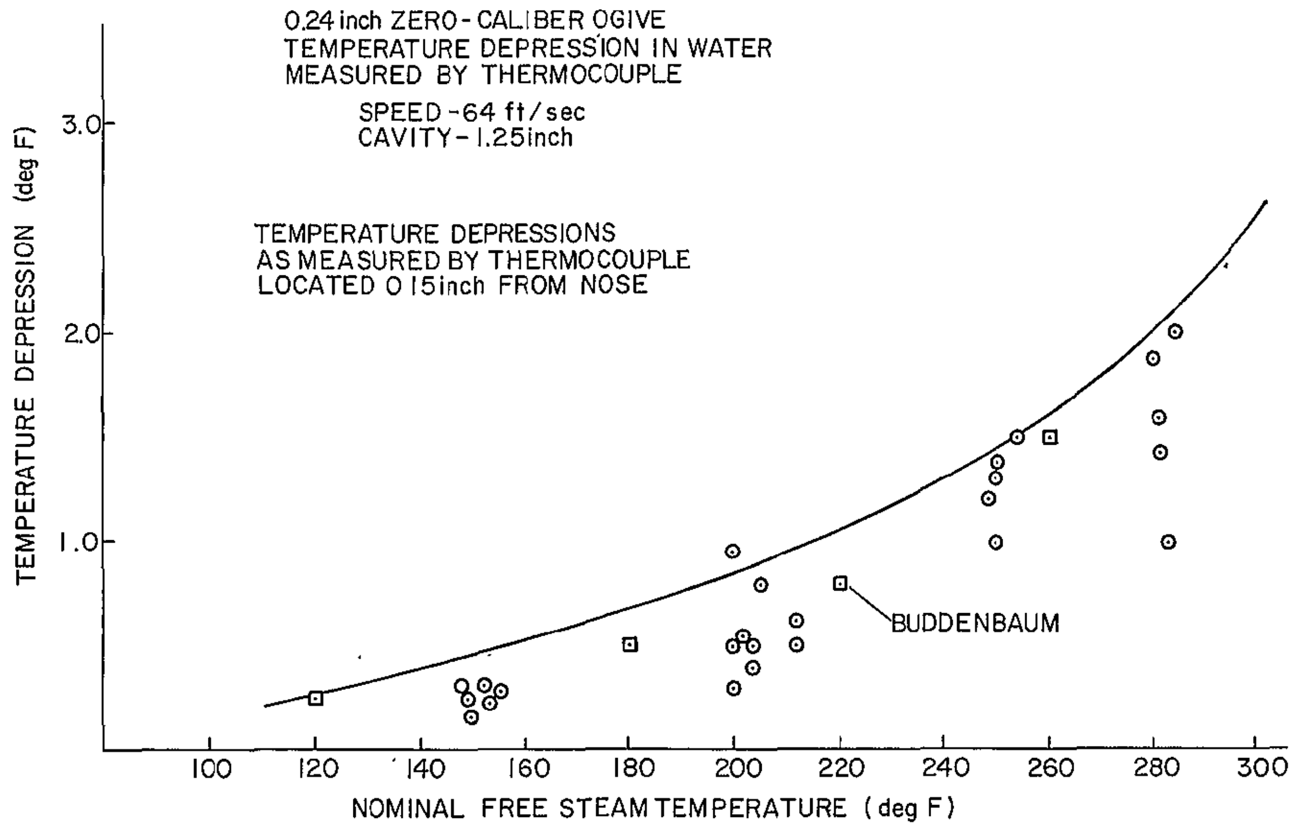

Figure 40 Cavity Temperature Depression Versus Temperature for Water; V = 64 ft/sec, L = 1.25 inch, Tap #1

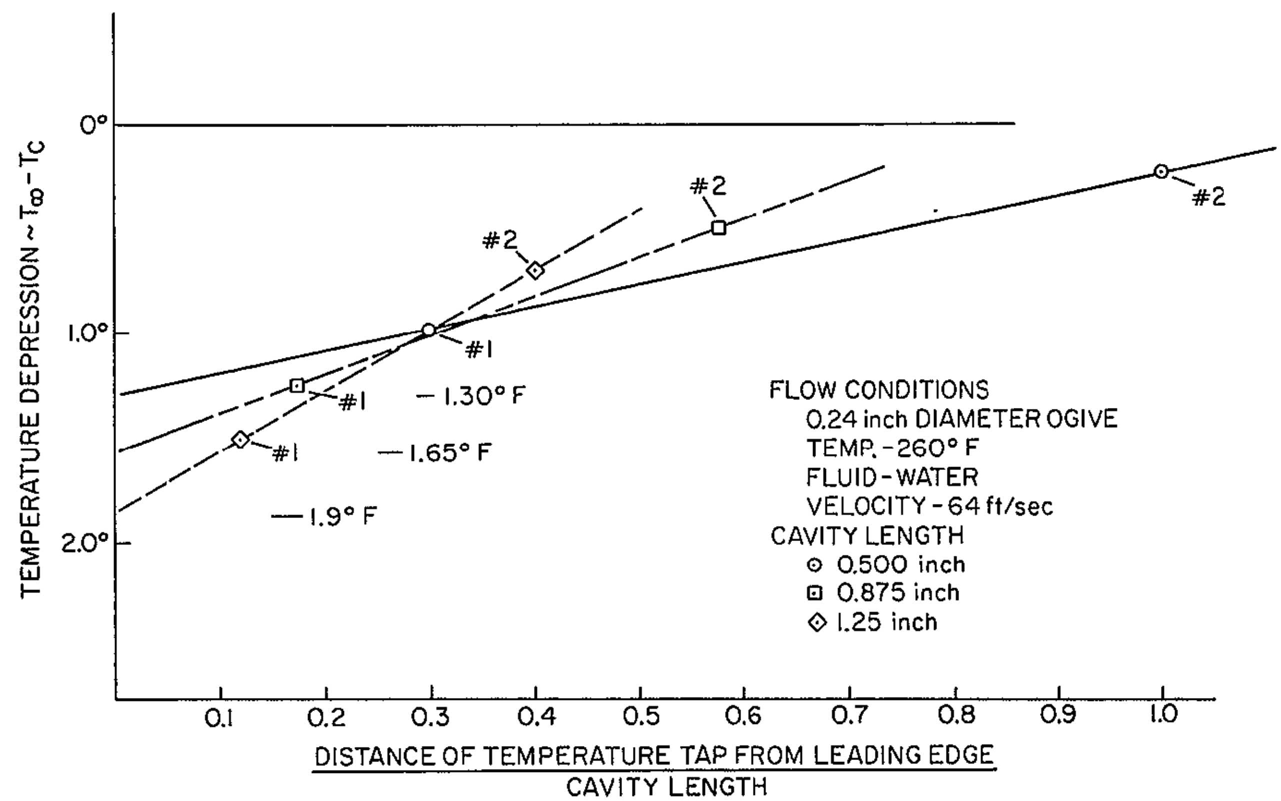

Figure 41 Cavity Temperature Depression Versus the Ratio of Length of Thermocouple Top From Nose to Cavity Length; Temperature = 260° F, Cavity Length = 0.500, 0.875, 1.25 inch

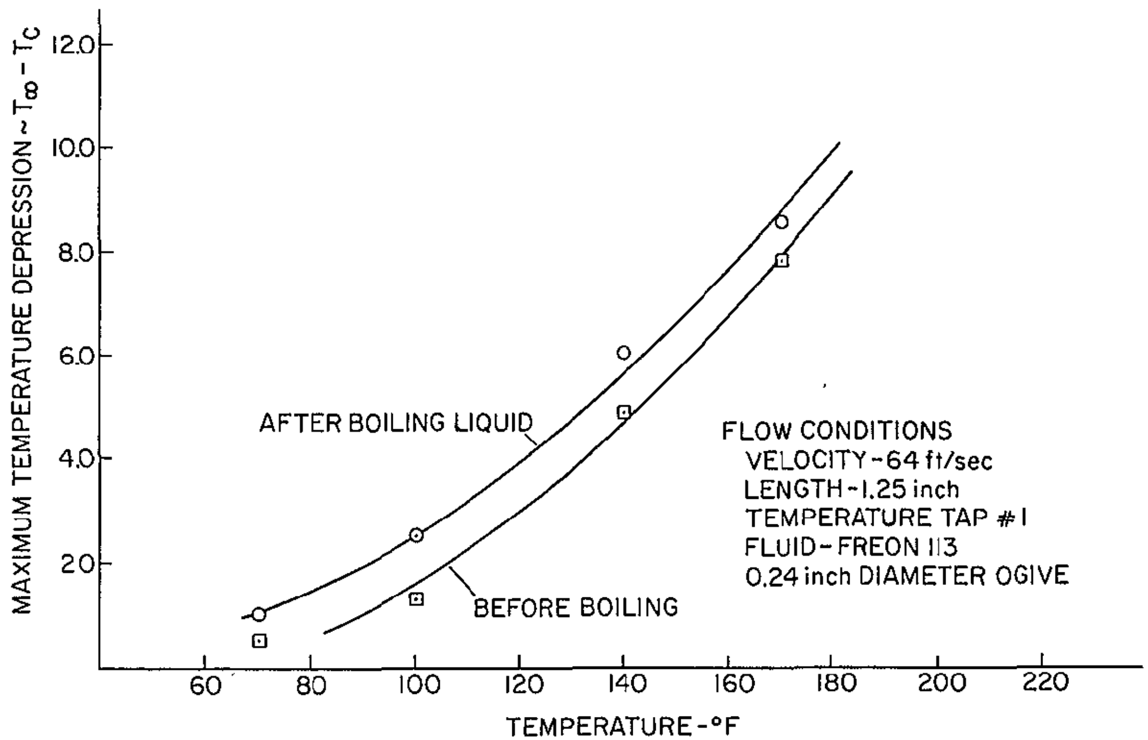

Figure 42 Cavity Temperature Depression Versus Temperature for Freon 113; V = 64 ft/sec, L = 1.25 inch, Two Different Air Contents

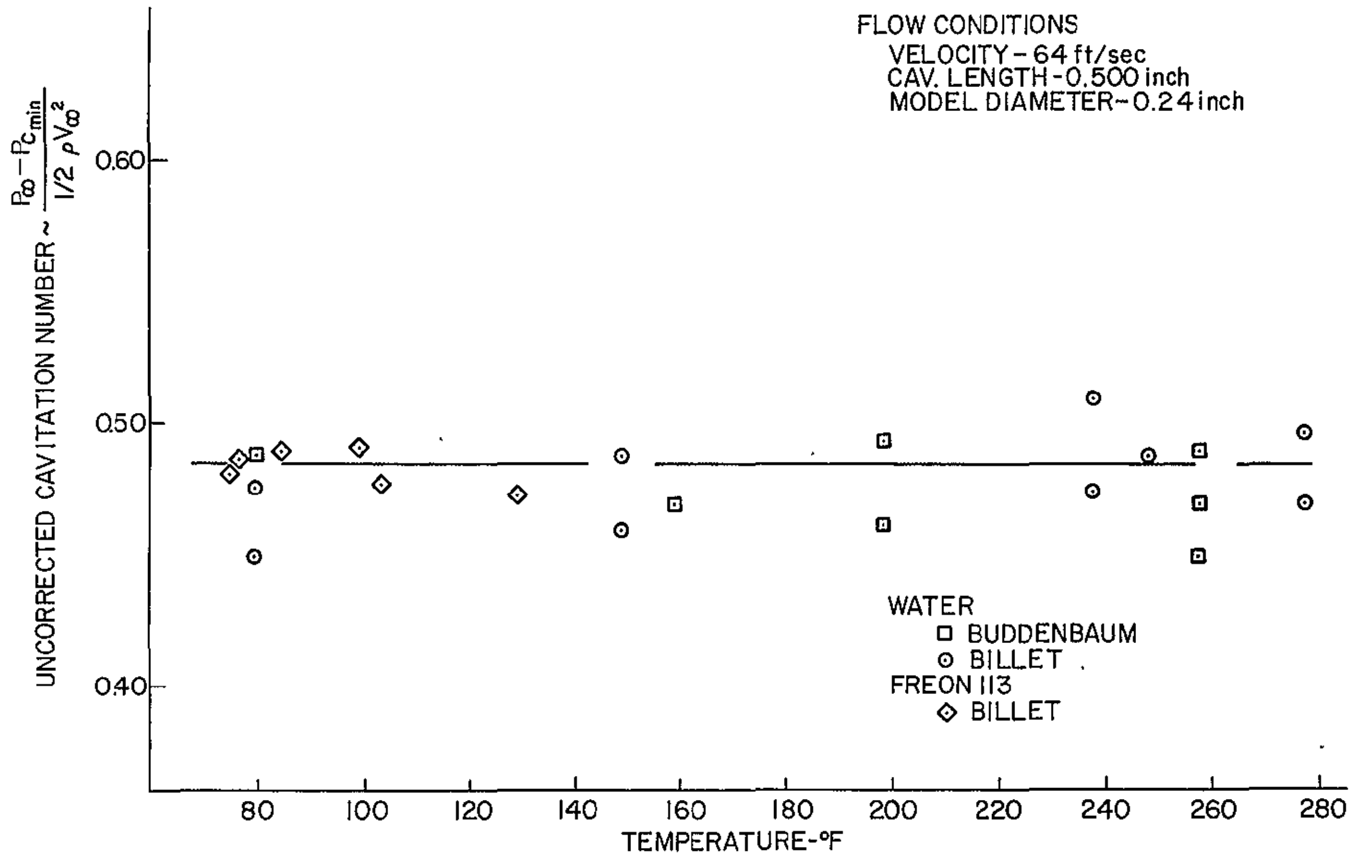

Figure 43 Uncorrected Cavitation Number Based on Minimum Cavity Pressure Versus Temperature; V = 64 ft/sec, L = 0.500 inch

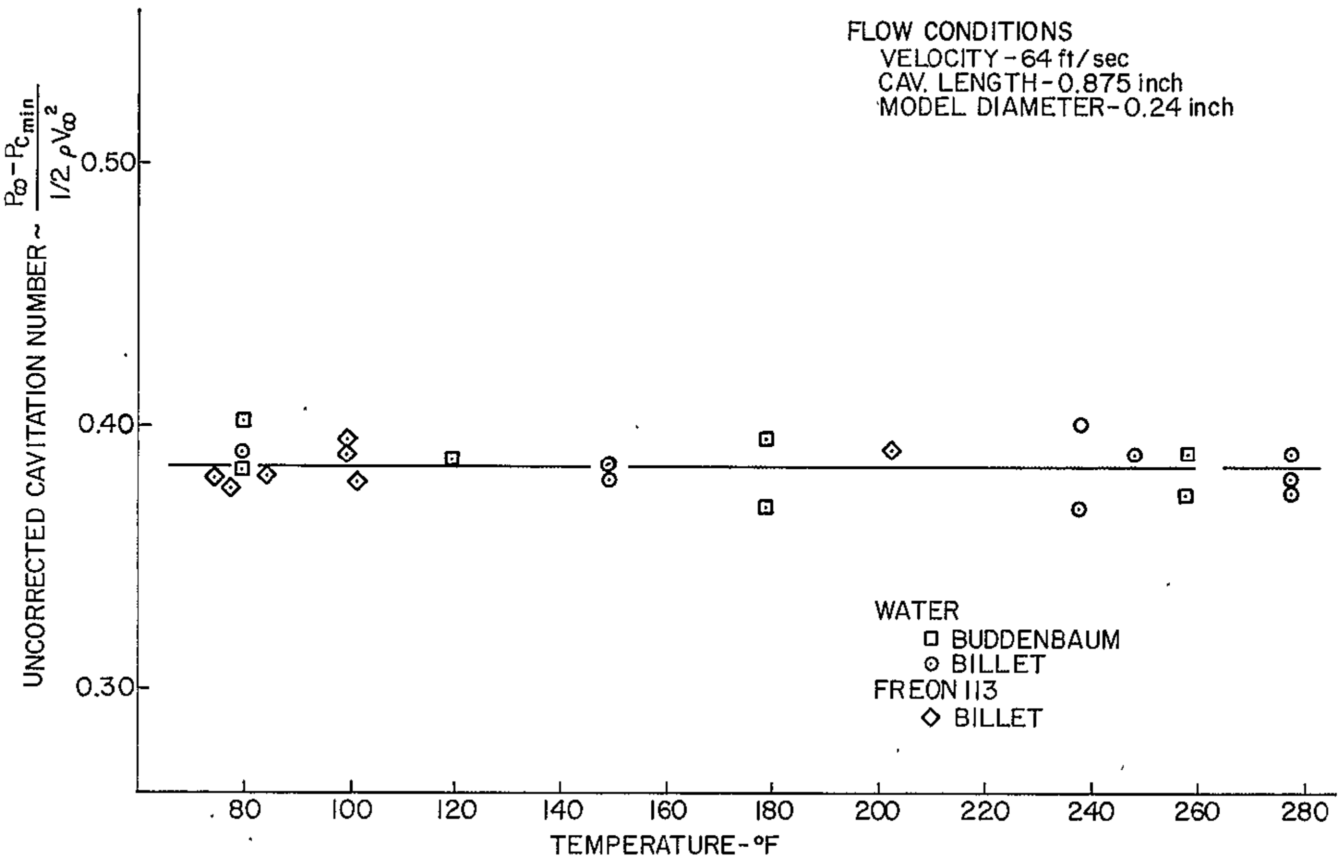

Figure 44 Uncorrected Cavitation Number Based on Minimum Cavity Pressure Versus Temperature; V = 64 ft/sec, L = 0.875 inch

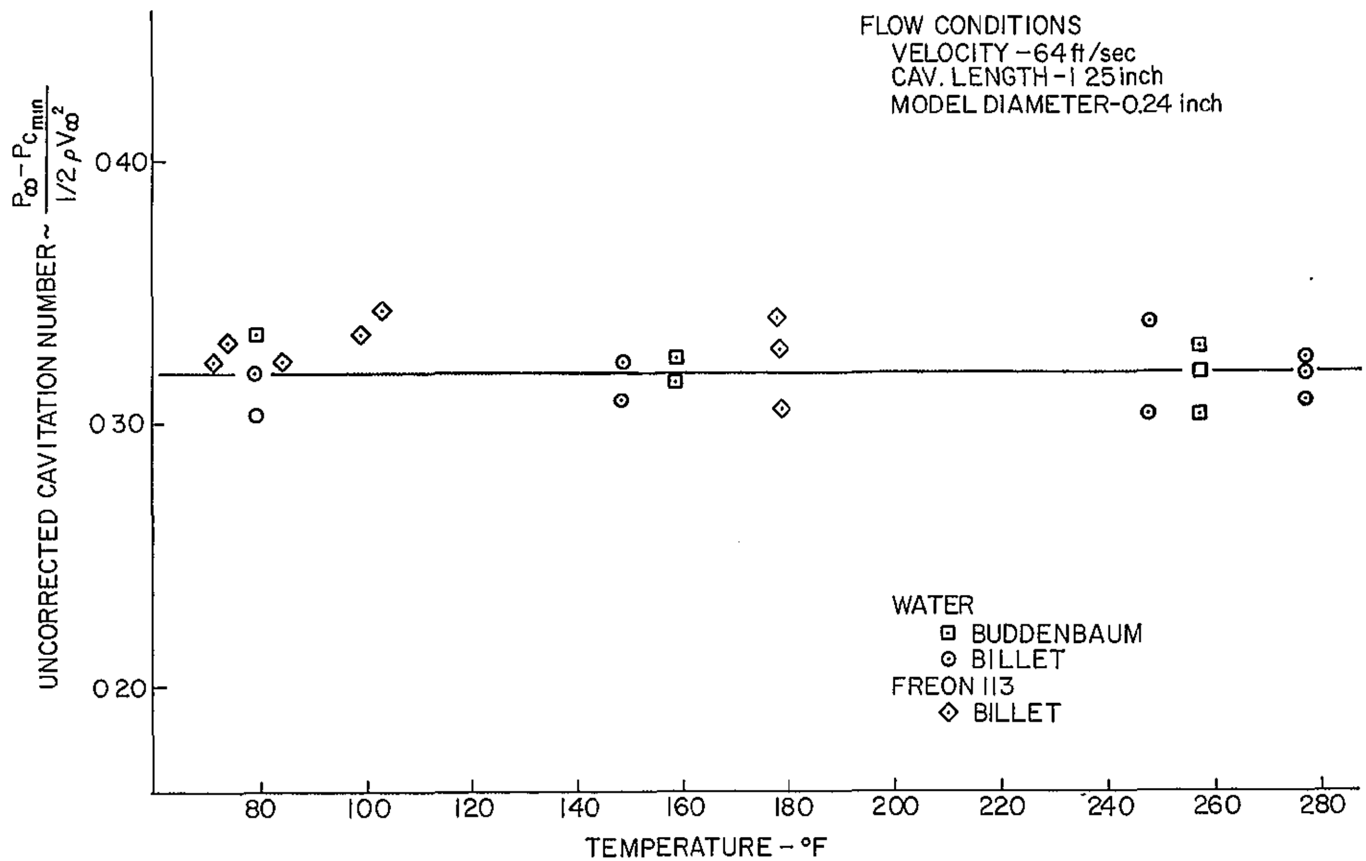

Figure 45 Uncorrected Cavitation Number Based on Minimum Cavity Pressure Versus Temperature; V = 64 ft/sec, L = 1.25 inch

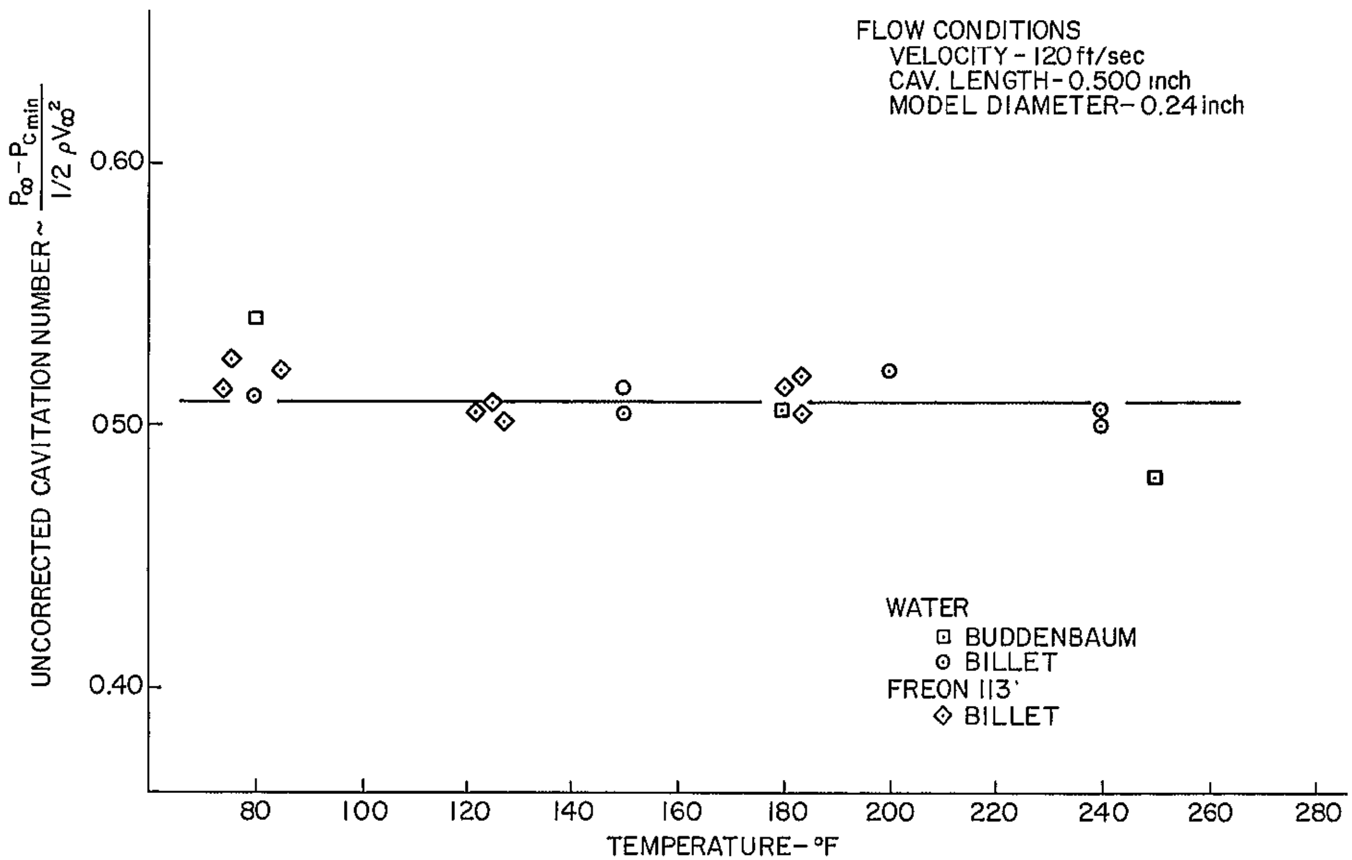

Figure 46 Uncorrected Cavitation Number Based on Minimum Cavity Pressure Versus Temperature; V = 120 ft/sec, L = 0.500 inch

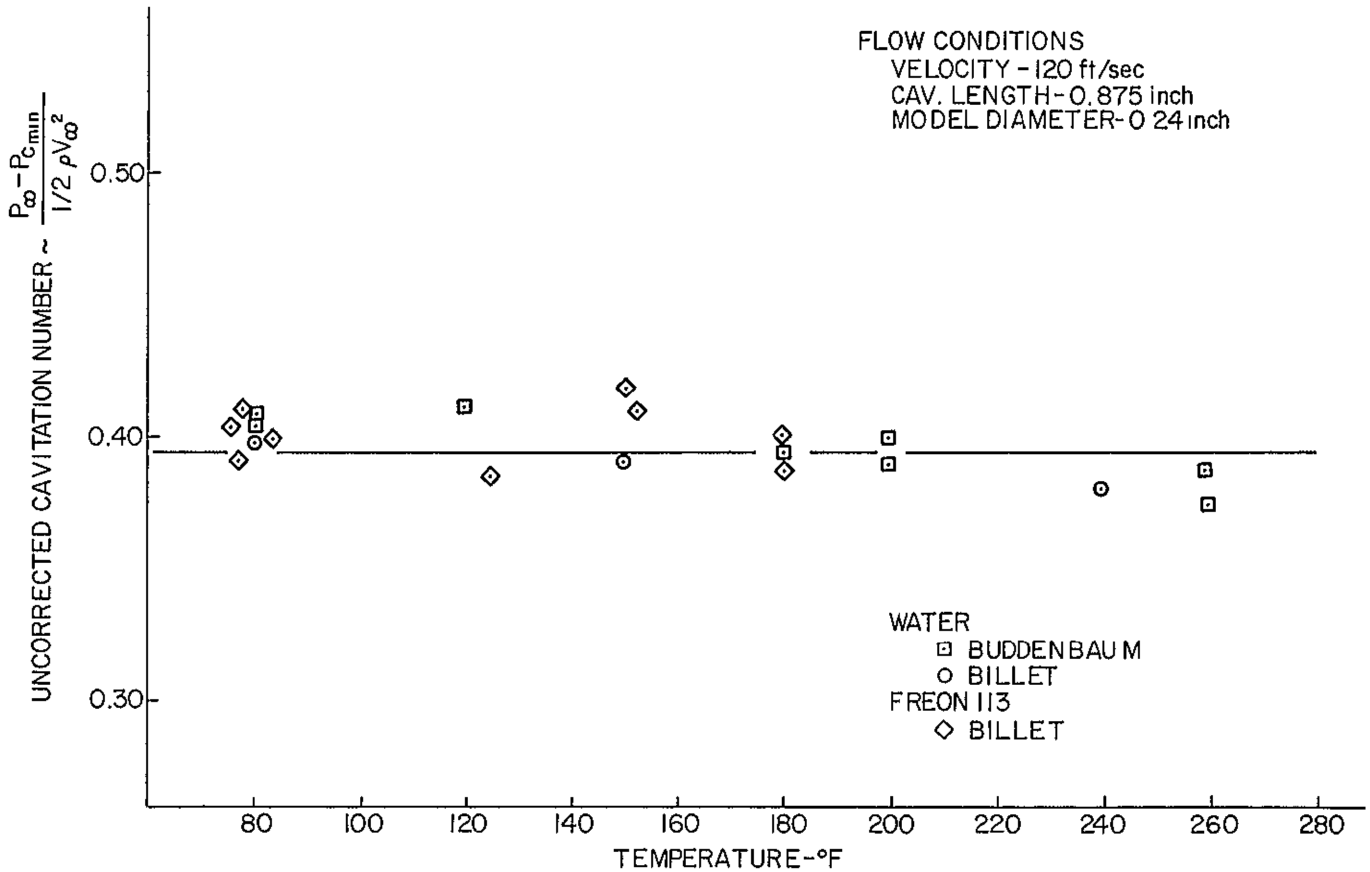

Figure 47 Uncorrected Cavitation Number Based on Minimum Cavity Pressure Versus Temperature; V = 120 ft/sec, L = 0.875 inch

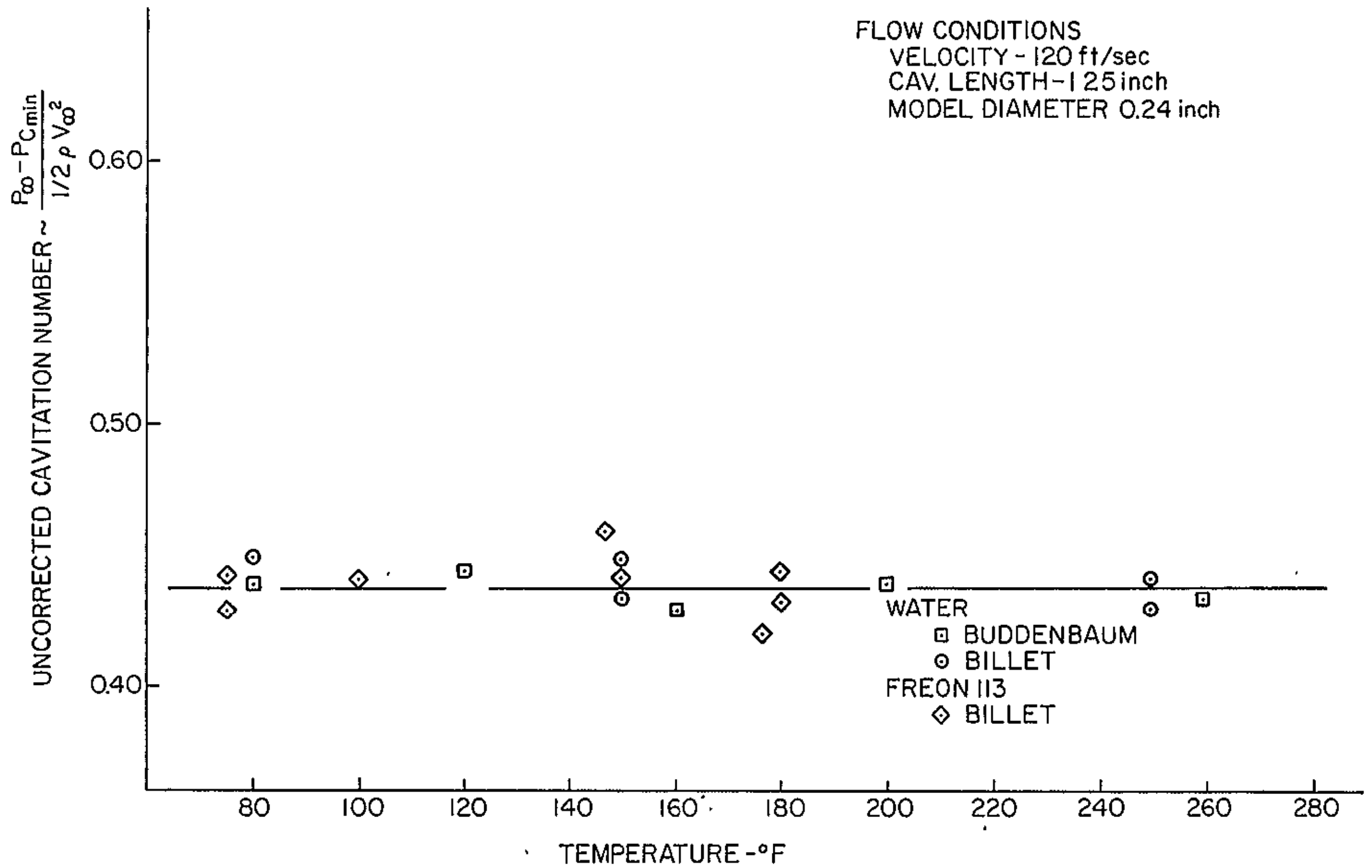

Figure 48 Uncorrected Cavitation Number Based on Minimum Cavity Pressure Versus Temperature; V = 1.20 ft/sec, L = 1.25 inch

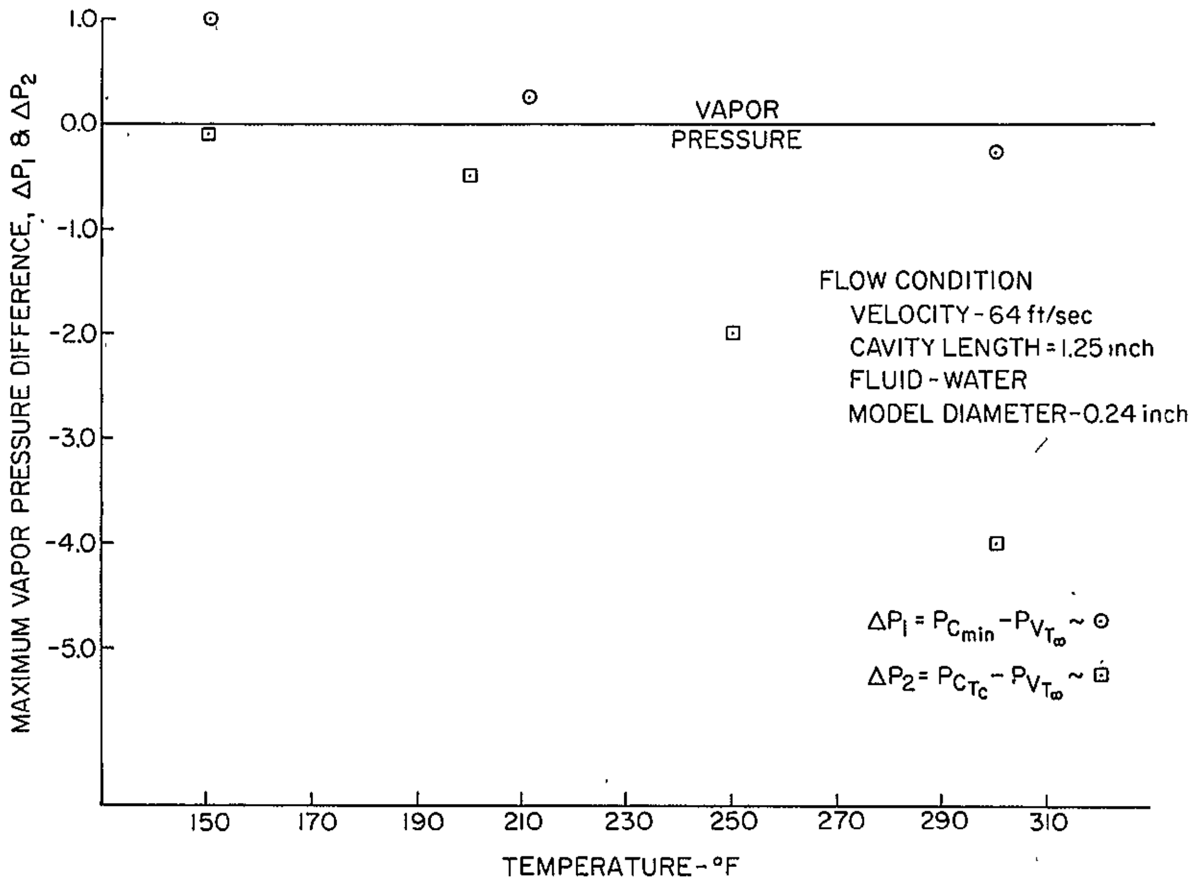

Figure 49 Vapor Pressure Difference Versus Temperature for Water; V = 64 ft/sec, L = 1.25 inch

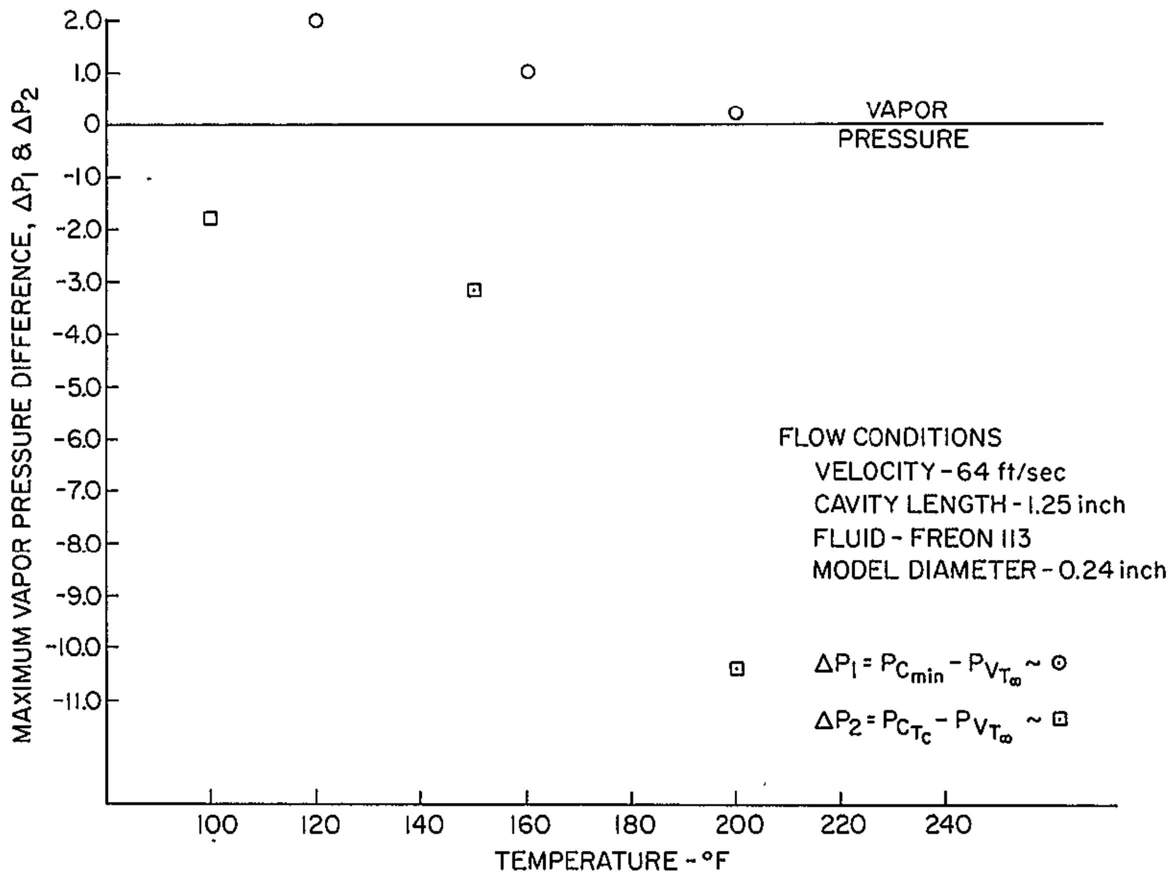

Figure 50 Vapor Pressure Difference Versus Temperature for Freon 113; V = 64 ft/sec, L = 1.25 inch

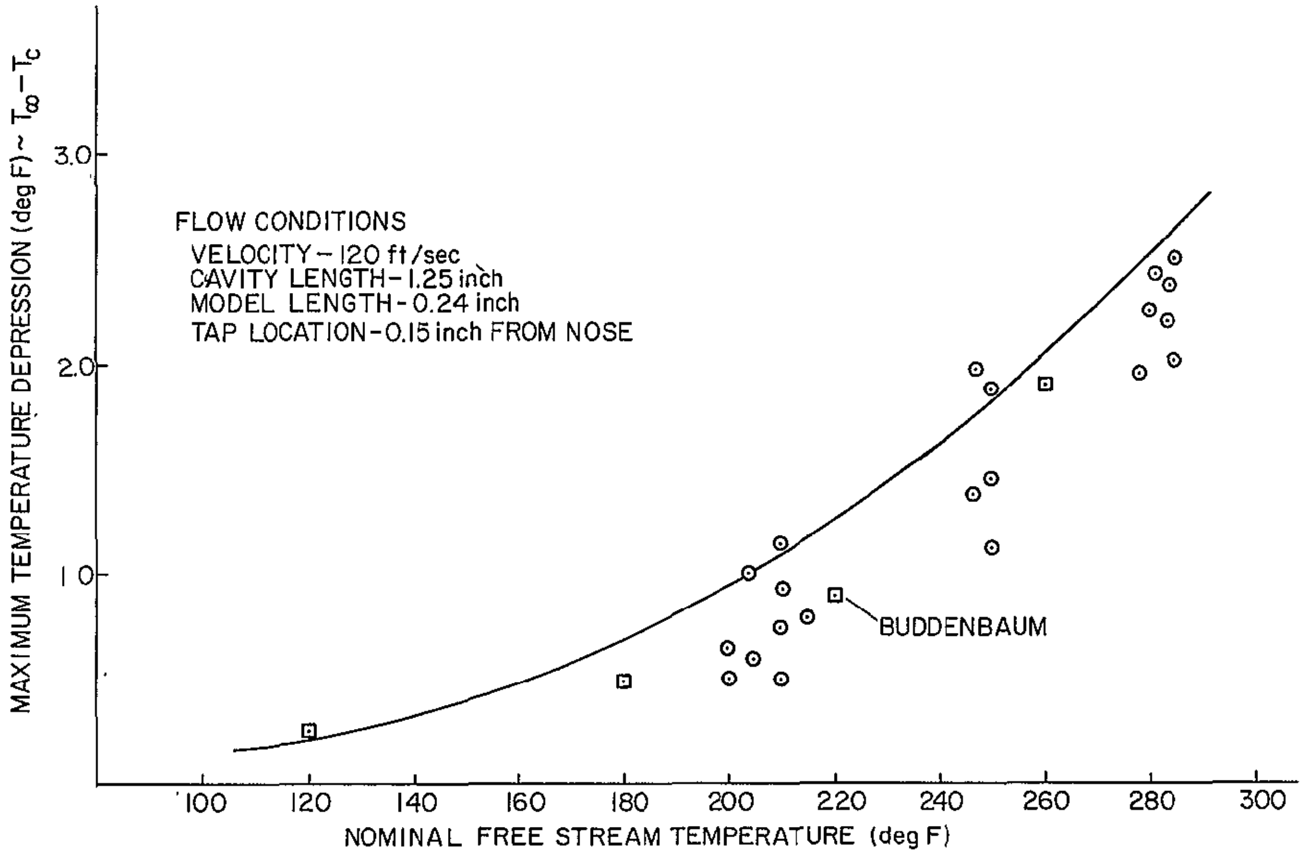

Figure 51 Cavity Temperature Depression Versus Temperature for Water; V = 120 ft/sec, L = 1.25 inch, Tap #1

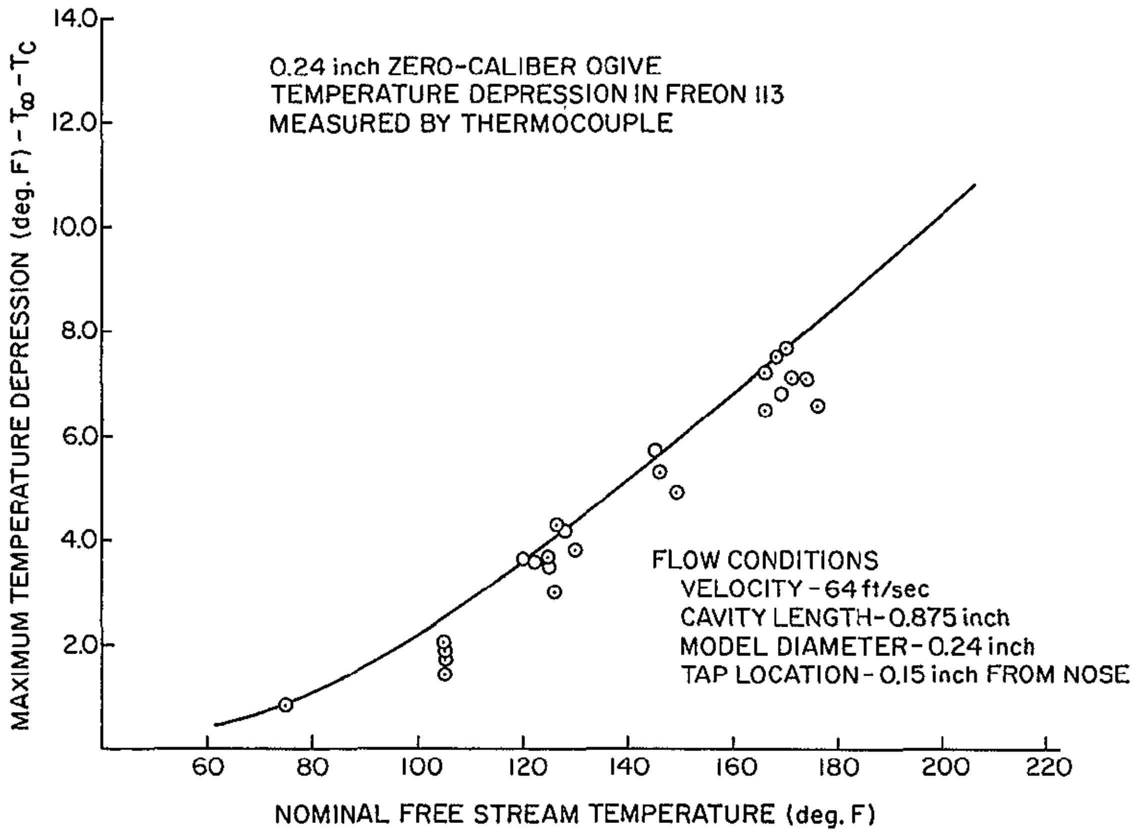

Figure 52 Cavity Temperature Depression Versus Temperature for Freon 113; V = 64 ft/sec, L = 0.875 inch, Tap #1

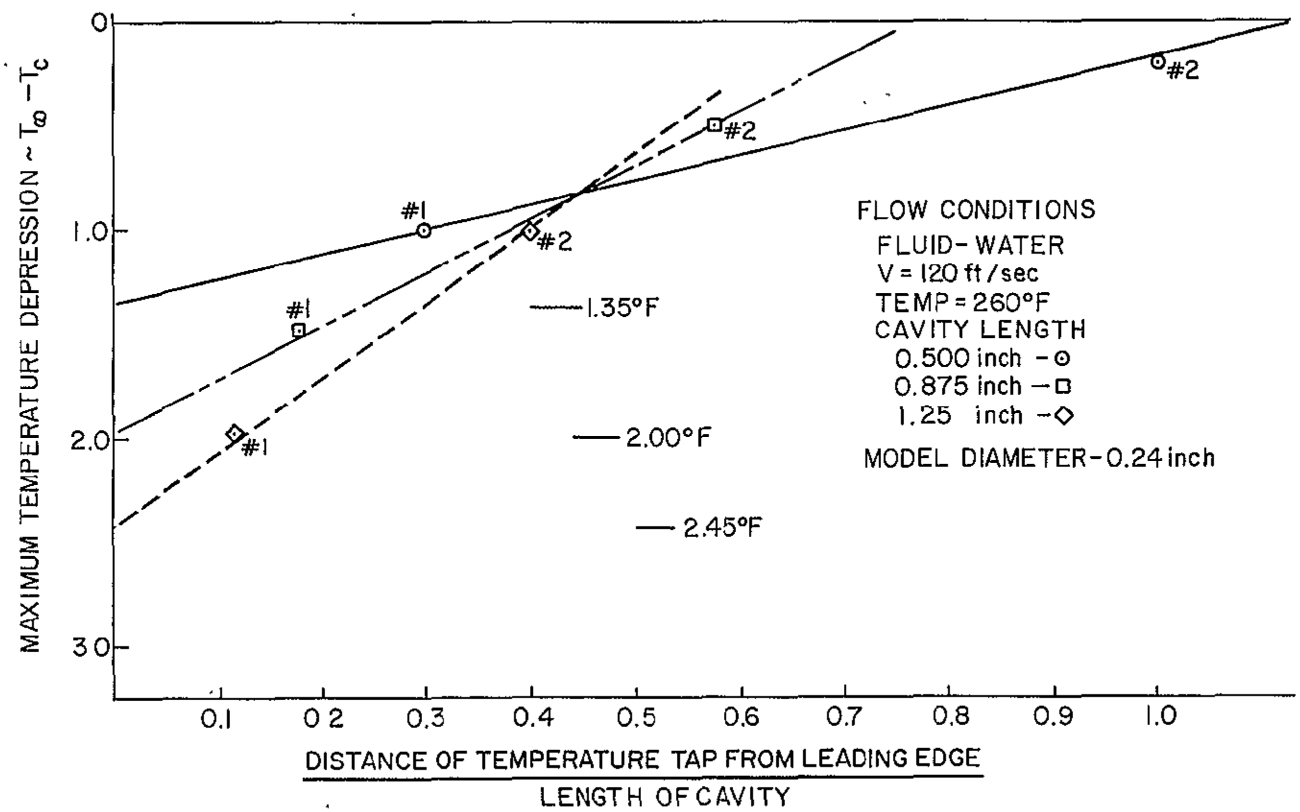

Figure 53 Maximum Temperature Depression Versus Cavity Tap Position for Water; Temp. = 260° F, L = 0.500, 0.875, 1.25 inch, V = 120 ft/sec

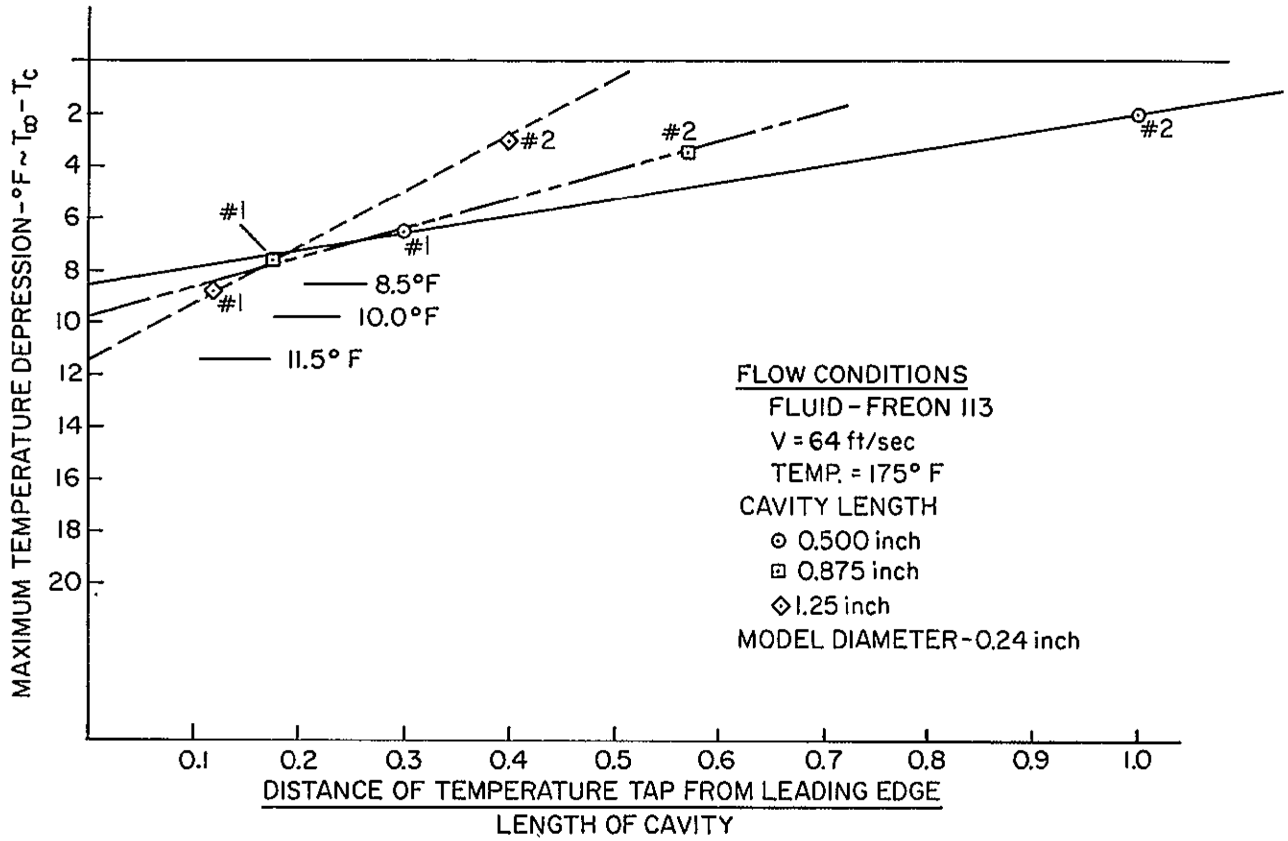

Figure 54 Maximum Temperature Depression Versus Cavity Tap Position for Freon 113; Temp. = 175° F, L = 0.500, 0.875, 1.25 inch, V $\doteq$ 64 ft/sec

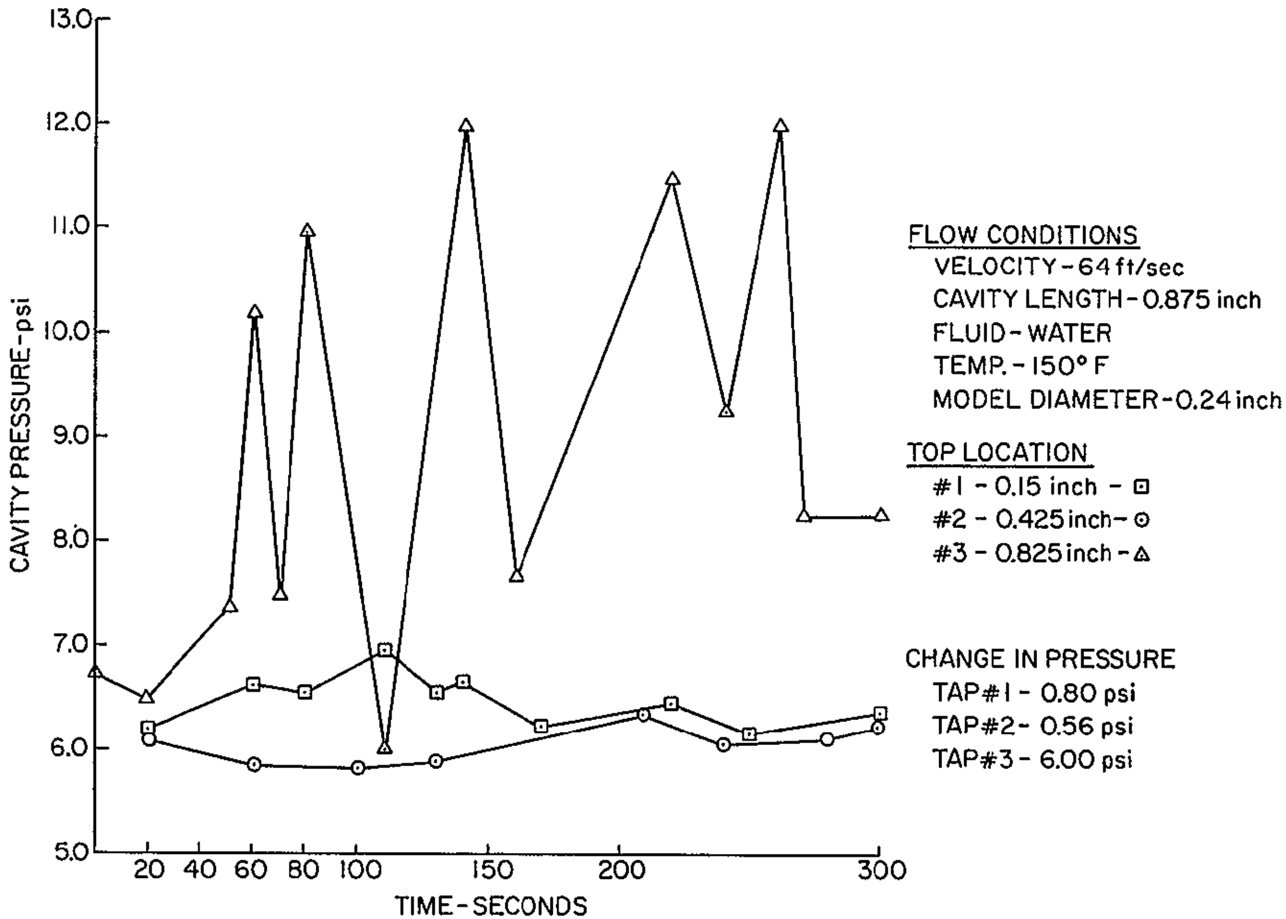

Figure 55 Cavity Tap Pressures Versus Time for Water; Temp. = 150° F, L = 0.875, V = 64 ft/sec

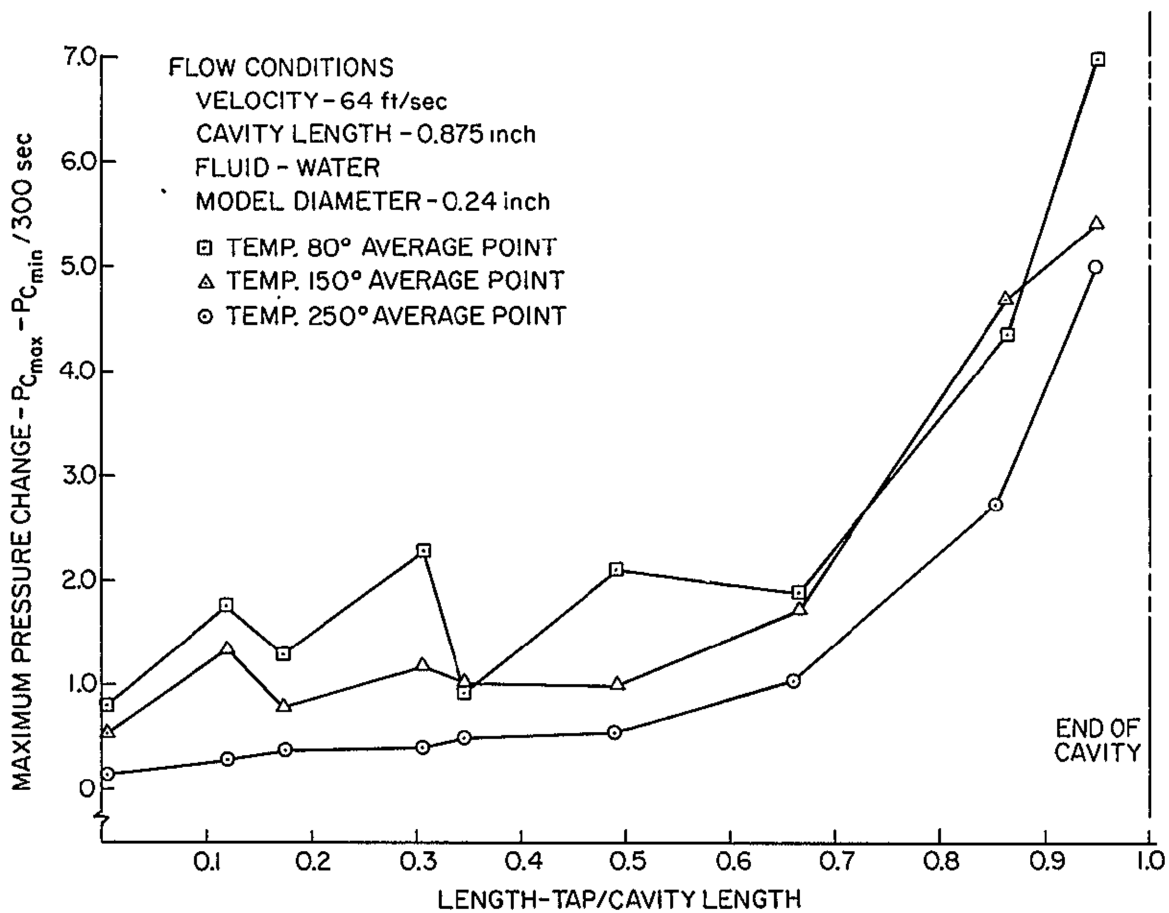

Figure 56 Maximum Pressure Change Versus Tap Location for Water at Various Temperatures

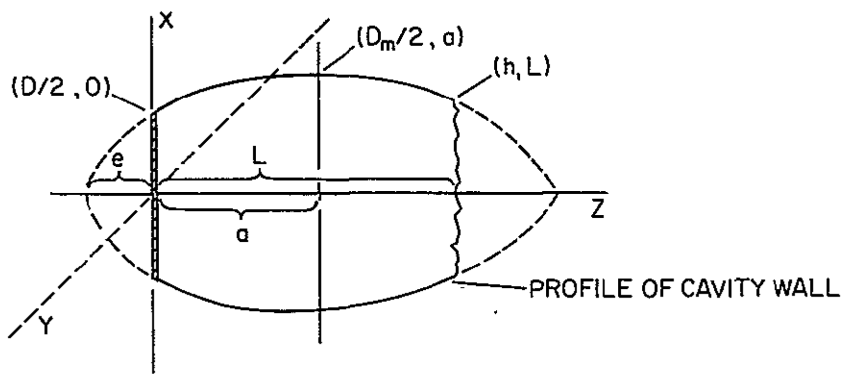

AND:
$D_m^2/4 = m^2$
$(a+e)^2 = n^2$

Figure 57 Orientation of Quasi-Elliptical Cavity

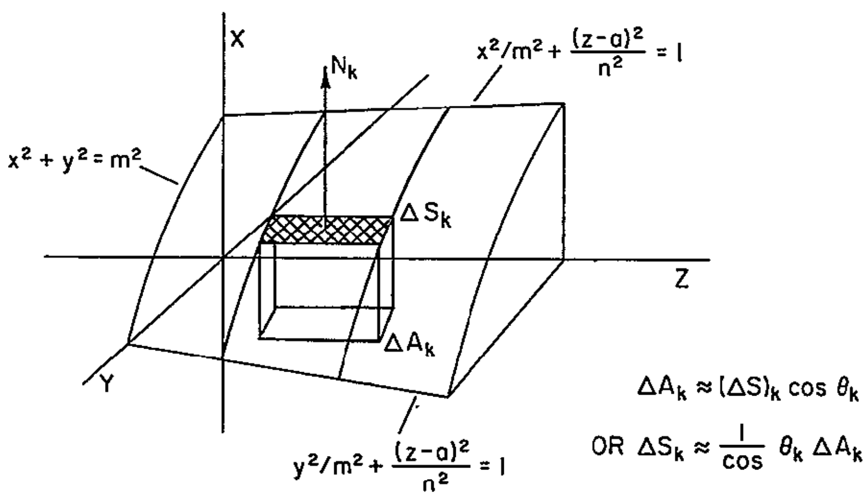

Figure 58 Diagram Showing Integration of Quasi-Elliptical Cavity